

INSTITUTE FOR SPACE STUDIES

THE STRUCTURE OF THE MARTIAN ATMOSPHERE

DUPLICATE PRICE \$ _____

REPRODUCTION PRICE(S) \$ _____

Hard copy (HC) 3.00

Microfiche (MF) _____

Joseph S. Hogan

Institute for Space Studies
Goddard Space Flight Center, NASA

and

New York University

N 68-34673

(ACCESSION NUMBER)

(THRU)

194
(PAGES)

(CODE)

TMX-61178
(NASA CR OR TMX OR AD NUMBER)

30
(CATEGORY)

FACILITY FORM 502



GODDARD SPACE FLIGHT CENTER
NATIONAL AERONAUTICS AND SPACE ADMINISTRATION

THE STRUCTURE OF THE MARTIAN ATMOSPHERE

Joseph S. Hogan

Institute for Space Studies
Goddard Space Flight Center, NASA

and

New York University

ABSTRACT

In order to obtain a better understanding of the results of the Mariner IV occultation experiment, a theoretical study of the structure of the neutral atmosphere and ionosphere on Mars has been made. The distribution of temperature in the lower atmosphere is obtained from a steady state solution of the equation of radiative transfer, allowing for vibrational relaxation of the radiating gas, and for the absorption of solar energy in the atmosphere. Possible relaxation of the vibration - rotation near infrared bands of CO_2 in which solar energy is absorbed is considered, and atmospheric transmission functions in the near and far infrared bands of CO_2 are calculated using a modified version of the Elsasser band model, taking both Lorentz and Doppler broadening of the spectral lines into account. The required input data are chosen from the most recent estimates of the surface parameters and atmospheric composition available at this time. Possible effects of CO_2 photochemistry on the atmospheric structure are estimated from a separate calculation of the photochemical equilibrium distribution of CO_2 and its dissociation products. Estimates of the solar heating produced by this photochemical activity are obtained simultaneously with the distribution of the gases. From consideration of the possible influence of turbulent mixing and molecular diffusion in altering the distribution of gases from

photochemical equilibrium conditions, upper and lower limits are derived for the neutral particle number density in the observed ionosphere. An ionospheric model consistent with the lower atmospheric structure is proposed.

The results of this study indicate that the run of atmospheric temperatures on Mars at the time and place of Mariner IV occultation was colder than had been estimated from previous thermal calculations which were used as a basis for an E-layer interpretation of the observed Martian ionosphere. At the same time, the thermal structures obtained here are considerably warmer than the heuristic models proposed to explain the observed ionosphere as a low-density, diffusion-controlled F2-peak, and demonstrate the unacceptability of this interpretation. For surface temperatures ranging from 175°K to 200°K, surface pressures ranging from 5 mb to 8 mb, and an atmospheric composition of 80% to 100% CO₂, the tropopause level is found between 2 km and 5 km above the surface of Mars. The convective layer is shallow (less than 5 km thick) in all cases considered, and it is estimated that at a ground temperature below ~ 140°K, no troposphere would develop. For surface temperature and pressure and composition within the above range, atmospheric temperatures decrease with altitude to values of 140°K - 150°K, 135°K - 145°K, and 130°K - 140°K at 50 km, 100 km and 125 km, respectively. The influence of the absorption of solar near infrared and ultraviolet energy on the atmospheric structure

below ionospheric levels is found to be small. On the basis of the calculated thermal models for the lower atmosphere, it is concluded that the neutral particle number density in the observed ionosphere was between 10^{10} mol/cm³ and 10^{11} mol/cm³, about 10^{10} mol/cm³ if mixing extends to near-ionospheric levels, and about 10^{11} mol/cm³ if the atmospheric gases are gravitationally separated above the region of maximum photochemical activity. Thus, the Martian ionosphere observed by Mariner IV is of the F1-type.

It is demonstrated that an F1-peak of O_2^+ ions in an atomic oxygen environment is unlikely, since the requirements for suppression of an F2-peak at higher levels can be met only by contradiction of a basic assumption. A peak composed of both CO_2^+ and O_2^+ ions in a CO_2 environment appears to be a more acceptable alternative, and suppression of an F2-peak can readily occur in this case if the O concentration at the F1-peak is less than one-tenth of the CO_2 concentration. It is thus suggested that the Martian atmosphere is mixed up to near-ionospheric levels, although at and above the observed ion maximum gravitational separation may be present. The neutral particle density at the observed peak is $\sim 2 \times 10^{10}$ mol/cm³, predominately CO_2 . A $CO_2^+ - O_2^+$ ion distribution consistent with the observed ion profile is calculated from basic ionospheric theory. The present ionospheric model allows for the development of a true thermospheric structure with a positive temperature gradient in the upper Martian atmosphere.

CONTENTS

	<u>Page</u>
ABSTRACT.	i
LIST OF FIGURES	vi
LIST OF TABLES.	viii
ACKNOWLEDGEMENTS.	ix
INTRODUCTION.	1
Formulation of the Problem	
Motivation and objective	
Scope of present study	
Earth-Based Observations of Mars	
Surface temperature	
Atmospheric composition and surface pressure	
Pre-Mariner IV Theoretical Investigations of Atmospheric Structure	
Lower atmosphere	
Upper atmosphere	
Mariner IV Occultation Experiment	
Experimental techniques	
Results and interpretation of experimenters	
Post-Mariner IV Atmospheric Models	
F2-layer interpretation	
E-layer interpretation	
F1-layer interpretation	
DETERMINATION OF ATMOSPHERIC STRUCTURE.	56
Evaluation of Model I of Prabhakara and Hogan (1965)	
Present Method	
Radiative transfer	
Convection	
Acceptability of method	
Photochemistry	
Numerical procedure	
Results and Discussion	
Lower atmosphere	
Ionosphere	
SUMMARY	121

(Continued)

CONTENTS (Continued)

	<u>Page</u>
APPENDIX A: THE EQUATION OF RADIATIVE TRANSFER.	125
APPENDIX B: VIBRATIONAL RELAXATION OF THE CARBON DIOXIDE MOLECULE.	130
APPENDIX C: RADIATIVE TRANSFER UNDER LTE AND NON-LTE CONDITIONS.	137
APPENDIX D: TRANSMISSION FUNCTIONS OF CARBON DIOXIDE. . .	143
Line shape and mean line absorption	
Band models	
Band parameters	
Numerical evaluation of CO ₂ transmission functions	
REFERENCES.	174

LIST OF FIGURES

<u>Figure</u>	<u>Page</u>
1. The surface temperature on Mars at the northern hemisphere winter solstice (After Mintz, 1961).	13
2. The CO ₂ bands at 1.60 and 1.57 μ in the Martian spectrum (After Kuiper, 1952).	15
3. Model I of Prabhakara and Hogan (1965).	25
4. Equilibrium temperature profiles calculated for Mars: radiative, radiative-convective and radiative-convective with solar heating (After Prabhakara and Hogan, 1965).	26
5. Thermospheric model of Chamberlain (1962) and Arking (1962) (After Rasool, 1963).	29
6. Mariner IV encounter sequence and trajectory (After Anderson, 1965).	32
7. Relation of total phase change to time. Abscissa is UT, 15 July (After Kliore, <u>et al.</u> , 1965).	38
8. Electron density profile for Mars (After Fjeldbo, <u>et al.</u> , 1966a).	43
9. Schematic diagram.	67
10. Comparison of calculated temperatures with observations at Ft. Churchill and White Sands. I: $\lambda_0 = 10^{-6}$ sec; II: $\lambda_0 = 5 \times 10^{-5}$ sec; III: $\lambda_0 = 1.5 \times 10^{-5}$ sec. (After Prabhakara and Hogan, 1966).	73
11. Martian lower atmosphere: Models I thru IV (100% CO ₂). J: Johnson (1965); P&H: Prabhakara and Hogan (1965).	86
12. Martian lower atmosphere: Models V thru VII (80% CO ₂ - 20% N ₂). J: Johnson (1965); P&H: Prabhakara and Hogan (1965).	87

(Continued)

LIST OF FIGURES (Continued)

<u>Figure</u>	<u>Page</u>	
13.	Martian lower atmosphere: Models VIII (100% CO ₂), IX (80% CO ₂ - 20% N ₂), and IX A. J: Johnson ² (1965); P&H: Prabhakara and Hogan (1965).	88
14.	Martian lower atmosphere: Models II, II A and II B.	95
15.	Photochemical equilibrium distribution of gases corresponding to thermal model IX.	103
D.I	Near infrared absorption spectrum of CO ₂ (After Stull, <u>et al.</u> , 1963).	152
D.II	$f_1(\beta, x)$ vs $\beta^2 x$ for constant values of β and constant values of βx . Also $f_2(\beta, x)$ vs $\beta^2 x$	154
D.III	$f_1(\beta, x)$ vs βx for constant values of β . Also $f_3(\beta, x)$ vs βx	156
D.IV	\bar{A} vs $u p^*$ for constant values of p^* and constant values of u for spectral interval $720 \pm 10 \text{cm}^{-1}$ (From transmission tables of Stull, <u>et al.</u> , 1963).	157
D.V	\bar{A} vs u for constant values of p^* for spectral interval $720 \pm 10 \text{cm}^{-1}$ (From transmission tables of Stull, <u>et al.</u> , 1963).	158
D.VI	Comparison of present calculations of fractional absorption with Stull, <u>et al.</u> (1963).	168
D.VII	Absorption by mixed Doppler and Lorentz lines in the 15μ CO ₂ band. The abscissa $2\pi\alpha x = Su/\alpha_D$, and $\bar{d}/\alpha_D = 2.46 \times 10^3$	169

LIST OF TABLES

<u>Table</u>	<u>Page</u>
I	Temperature of the Martian Surface (After Rasool, 1963). 12
II	Summary of Occultation Experiment (After Kliore, et al., 1965.. . . . 40
III	Basic Characteristics of Model Martian Atmospheres.. . . . 85
IV	Temperature, Pressure and Number Density at 100 km.. . . . 92
V	Estimated Range of Neutral Number Density at Ionospheric Level. 111
VI	Ionospheric Model. 119
D.I	Band Parameters C_1 and C_2 for Near and Far Infrared CO_2 Bands. 160
D.II	Band parameters S , d and Γ for Infrared CO_2 Bands.. . . . 163

ACKNOWLEDGEMENTS

I am deeply indebted to Dr. Cuddapah Prabhakara of the Goddard Institute for Space Studies for his great encouragement and interest in my work. Our many discussions of the problem proved invaluable to me.

Many thanks to Professor James E. Miller of New York University and Drs. S. Ichtiaq Rasool and Albert Arking of the Institute for Space Studies for their helpful advice and criticism, and to Dr. Robert Jastrow for making the facilities of the Institute available to me during the course of this research.

I am also most grateful to Mr. Ludwig Umscheid of Computer Applications, Inc. for his expert programming of the problem and advice on numerical techniques.

Thanks also to Mr. Robert Rabinoff of Columbia University for his programming help with some aspects of the problem.

This research was supported by the National Aeronautics and Space Administration under Grant Number Ns G - 499 to New York University.

INTRODUCTION

Formulation of the Problem

The principal problem treated in this paper is the determination of a model vertical structure of the Martian atmosphere which is both physically sound and consistent with the most recent observational findings. The basic vertical structure is obtained from solution of the equation of radiative transfer in the presence of energy sources and sinks, allowing for vibrational relaxation of the infrared-active constituent.

Motivation and objective.

The brilliant success of the Mariner IV occultation experiment resulted in significant new estimates of the surface parameters and vertical structure of the lower Martian atmosphere, as well as the first observational evidence of the existence of a Martian ionosphere. The occultation data clearly indicate that the atmospheric pressure, density and scale height near the surface of Mars are all considerably lower than had previously been supposed. They also indicate that the ionosphere is located nearer the surface and has a far smaller electron density than had been predicted on the basis of classical ionospheric theory. Although free from the terrestrial interference which has limited the precision

of Earth-based observations of Mars, the Mariner IV data have, nevertheless, not fully resolved the problem of the Martian atmosphere, and have left room for a variety of interpretations. However, the basic indications of the Mariner IV occultation experiment are indisputable and must serve as a guidepost for further theoretical and experimental investigations of the Martian atmosphere.

Principal discussion in the literature of the Mariner IV findings has been with regard to the identification of the type of the Martian ionosphere observed in the occultation phase-shift data. The relative importance of the various processes responsible for the formation of an ionosphere depends principally on the number of neutral particles present locally. Thus the type of ionosphere observed by Mariner IV depends upon the molecular number density at ionospheric height (~ 125 km). The molecular number density at this level cannot be derived from the occultation data and must be estimated from theoretical modelling. Hence, a knowledge of the vertical structure of the lower Martian atmosphere is essential to an understanding of the Martian ionosphere.

Meaningful models of the vertical structure of a planetary atmosphere can be obtained from consideration of basic physical principles when certain characteristics of the planet and its atmosphere are known. These characteristics include the surface pressure and temperature, the type and amount of infrared-active constituents present, and the spectral distribution of

solar energy incident at the top of the atmosphere. By specifying these quantities and by considering in detail the internal sources and sinks of energy together with the mechanisms of vertical energy transport and the important photochemical reactions, an equilibrium height-distribution of temperature, density and chemical composition can be determined for the planetary atmosphere. Then, from this vertical structure, a better understanding of the ionosphere of the planet can be achieved.

Previous theoretical studies of the atmospheric structure on Mars are of limited practical value for two basic reasons. Firstly, they have dealt with simplified models and neglected physical processes which could be important such as solar heating, photochemistry, and non-local thermodynamic equilibrium effects. Secondly, they have been based upon assumptions of surface pressure and atmospheric composition which are no longer realistic in view of the most recent estimates of these parameters.

The primary objective of the present study is the determination of an equilibrium distribution of temperature, density and chemical composition for the Martian atmosphere in accord with the latest observations, considering all processes important in the energy balance of the atmosphere.

Scope of present study.

From our understanding of the basic physical processes which govern the vertical temperature distribution in the Earth's atmosphere, some insight into the energetics of the Martian atmosphere may be gained.

Near the surface of Mars, convective energy transport will be large, due to the discontinuous nature of the lower boundary, and a troposphere will be established, extending upward to the level at which the lapse rate of temperature becomes stable against convection. Since surface temperatures on Mars are generally lower than are found on Earth, and the primary constituent of the Martian atmosphere, CO_2 , is a strongly radiating gas, one would expect the Martian convective layer to be thinner than the Earth's troposphere.

Above the convective layer, radiative transfer by the large amounts of CO_2 present on Mars will largely control the temperature structure. At levels in a planetary atmosphere where temperatures are moderate and where there is an abundance of polyatomic molecules, radiative fluxes will determine the distribution of temperature. The radiative transfer process in the Earth's atmosphere is complicated by the presence of three infrared-active gases (CO_2 , O_3 and H_2O) with overlapping absorption spectra. Furthermore, a sizable temperature maximum is produced in the middle atmosphere of the Earth by the large amount of solar energy absorbed in the dissociation of O_2 and photochemically produced O_3 . On Mars,

however, the problem of radiative transfer is considerably simplified, since observations indicate that the Martian atmosphere is composed primarily of CO_2 . In the presence of large amounts of CO_2 and moderate pressures ($> 10^{-2}$ mb), the absorption of solar energy would probably have little effect on the local temperature, due to the very large radiative fluxes of planetary origin. One expects, therefore, no temperature maximum of any consequence in the middle atmosphere of Mars, with the temperature structure largely determined by radiative transfer in the $15\ \mu$ CO_2 band.

At higher levels in the Martian atmosphere where pressure is low ($< 10^{-2}$ mb), the absorption of solar energy may exert a stronger effect on the local temperature, even if CO_2 is present in abundant quantities. The transfer of energy between the molecular kinetic mode and the radiative field via the vibrationally excited states of CO_2 will be inhibited at higher levels, where the radiative lifetime of these excited states becomes shorter than the collisional deactivation or "relaxation" lifetime. At these levels, with the linkage between matter and radiative field broken by "relaxation", any external source supplying energy directly to the kinetic mode might considerably alter the temperature structure. In the Earth's atmosphere, vibrational relaxation in the $15\ \mu$ CO_2 band occurs between 75 km and 85 km. The vibrational relaxation level on Mars should be found at a lower altitude, however, due to the lower surface pressure and colder atmospheric temperatures anticipated.

The photodissociation of CO_2 and that of photochemically produced O_2 and O_3 will result in the deposition of solar ultraviolet energy in the region of the Martian atmosphere where vibrational relaxation is occurring. Because of the relative magnitudes of the lifetimes for the collisional and radiative processes involved, this energy will pass into the kinetic mode with an efficiency less than but of the order of 1. In addition, CO_2 absorbs strongly in the $1\mu - 6\mu$ near infrared bands where the solar flux is strong also. However, most of this energy should be scattered at higher levels in the Martian atmosphere where these bands also relax, and passage of the solar near infrared energy into the kinetic mode should be minimized. Still, since the amount of energy in the near infrared solar spectrum is much greater than that found in the ultraviolet spectral regions, it is possible that the absorption of near infrared energy would exert a larger influence on the temperature at higher levels than would the ultraviolet absorption.

In higher regions of the Martian atmosphere, turbulent mixing must become insignificant and the constituent gases must separate diffusively in the gravitational field of the planet. In the terrestrial atmosphere, the transition between homogeneous and inhomogeneous atmospheric regions is rather abrupt, due to the highly stable conditions which result from the sharp rise in temperature above the Earth's mesopause. It is improbable that a region of such high stability is present

in the upper atmosphere of Mars, as temperature gradients should be relatively small; therefore no level can be set with any definition for the turbopause on Mars.

In the upper Martian atmosphere, as in the Earth's upper atmosphere, where the vertical temperature gradient becomes significant as the temperature rises to its thermospheric values, the heat conduction process will begin to play an important role in the vertical transport of energy. At altitudes where CO_2 is largely dissociated, radiative loss by forbidden transitions of O atoms and vibrational-rotational transitions of CO molecules must be considered. In this region, equilibrium can be assumed to exist between the photoionizing solar energy absorbed, the divergence of the conductive flux and the loss of radiant energy by O or CO emission. Here the temperature structure must be obtained from a solution of the heat conduction equation with radiative sources and sinks. It is unlikely, however, that temperature gradients below the level of the Martian ionosphere would be large enough to make the divergence of the conductive heat flux comparable in magnitude to the heating and cooling in the 15μ CO_2 band, even if CO_2 undergoes moderate dissociation below the ionospheric level.

By a proper synthesizing treatment of the various aspects of the atmospheric problem outlined above, a totally self-consistent solution for an equilibrium structure of the Martian atmosphere will be obtained numerically by an iterative solution

of the energy balance equation. Not only will the resulting distributions of temperature, density and composition be self-consistent, but, furthermore, they will be consistent with the boundary conditions suggested by the most recent observations of Mars.

Earth-Based Observations of Mars

Since the turn of the century, numerous experiments have been performed to determine the surface and atmospheric conditions on Mars. Radiometric, photometric, polarimetric and spectroscopic methods have all been employed and a sizable body of observational data has been amassed. In addition, the observations have been clarified and supplemented by many theoretical works.

Estimates of the surface temperature on Mars can be readily obtained from infrared and microwave radiometry, and, consequently, this parameter has been fairly well established for several decades. Interpretation of photometric, polarimetric and spectroscopic measurements is far more difficult, and no clear picture of the surface pressure or atmospheric composition on Mars emerged from any of these techniques until quite recently. Knowledge of the vertical structure of the Martian atmosphere cannot be gained from observations made from the surface of the Earth. Since the major infrared-active constituent of the atmosphere of Mars is also an important component of the terrestrial atmosphere, interpretation of observed spectra of Mars to obtain a vertical temperature distribution is not practicable.

Those Earth-based observations of greatest historical importance and relevance to the problem are briefly reviewed here.

Surface temperature.

The first infrared radiometric measurements of the Martian surface were made by Coblentz and Lampland (1923, 1927) at Lowell Observatory and by Pettit and Nicholson (1924) at Mount Wilson during the oppositions of 1922, 1924 and 1926. Using various filtering techniques and lunar calibration, these experimenters made latitudinal and longitudinal scans of the planetary disk to determine the diurnal and seasonal variations of temperature as a function of latitude. An extension of this work was carried on by Lampland in a systematic program of Martian radiometry at Lowell Observatory between 1926 and 1943. A summary of all measurements of surface temperatures on Mars prior to 1952 has been given by de Vaucouleurs (1954), along with a detailed discussion of experimental methods, the interpretation of measurements and the problems encountered in making observations of this type.

Hess (1950) constructed an isotherm map for Mars during northern hemisphere winter from measurements made along the noon meridian by Coblentz and Lampland (1927). Gifford (1956) analyzed the much larger body of data obtained over the years by Lampland, and determined the average diurnal temperature variation near the Martian equator, the average temperature variation along the noon meridian for the four seasons, and seasonal noon meridian isotherm maps for southern hemisphere summer, winter and fall. His southern hemisphere summer map agrees in general with the map of Hess (1950).

. During several weeks following the 1954 opposition, Sinton and Strong (1960) obtained drift curve measurements of surface temperature on Mars at the Mount Palomar Observatory. Their results agree quite well with the earlier observations and are summarized in Table I (Rasool, 1963).

Determinations of the microwave brightness temperature of the Martian disk by Mayer, et al. (1958) and Giordmaine, et al. (1959) resulted in somewhat lower values of surface temperature than those obtained from infrared radiometry. Mayer (1961) has explained this discrepancy as a consequence of the microwave radiation originating a few centimeters beneath the surface of the planet, where, on the sunlit side, the temperature is lower than that of the surface itself.

Making use of the observations of Sinton and Strong (1960) and Giordmaine, et al. (1959) as well as the results of Gifford (1956), Mintz (1961) has derived the latitudinal variation of surface temperature on Mars. Figure 1, from Mintz (1961), shows the variation of daily mean, maximum (noontime) and minimum (sunrise) temperatures with latitude at northern hemisphere winter solstice. Although based on a subjective synthesis of observational evidence, Figure 1 must depict the variation of surface temperature on Mars with reasonable accuracy.

Atmospheric composition and surface pressure.

In 1947 at McDonald Observatory, the 1.57μ and 1.60μ vibration-rotation bands of CO_2 were observed in the spectrum

TABLE I

TEMPERATURE OF THE MARTIAN SURFACE

(After Rasool, 1963)

Maximum temperature at equator	~ 300°K
Mean amplitude of diurnal variation	
Noon to sunset	~ 60°K
On Earth in desert	~ 30°K
Night side temperature cannot be measured but probably can be estimated at the equator	~ 200°K
Day side temperature at poles	~ 220°K
Mean temperature of day side	~ 260°K
Mean temperature of whole planet	~ 230°K

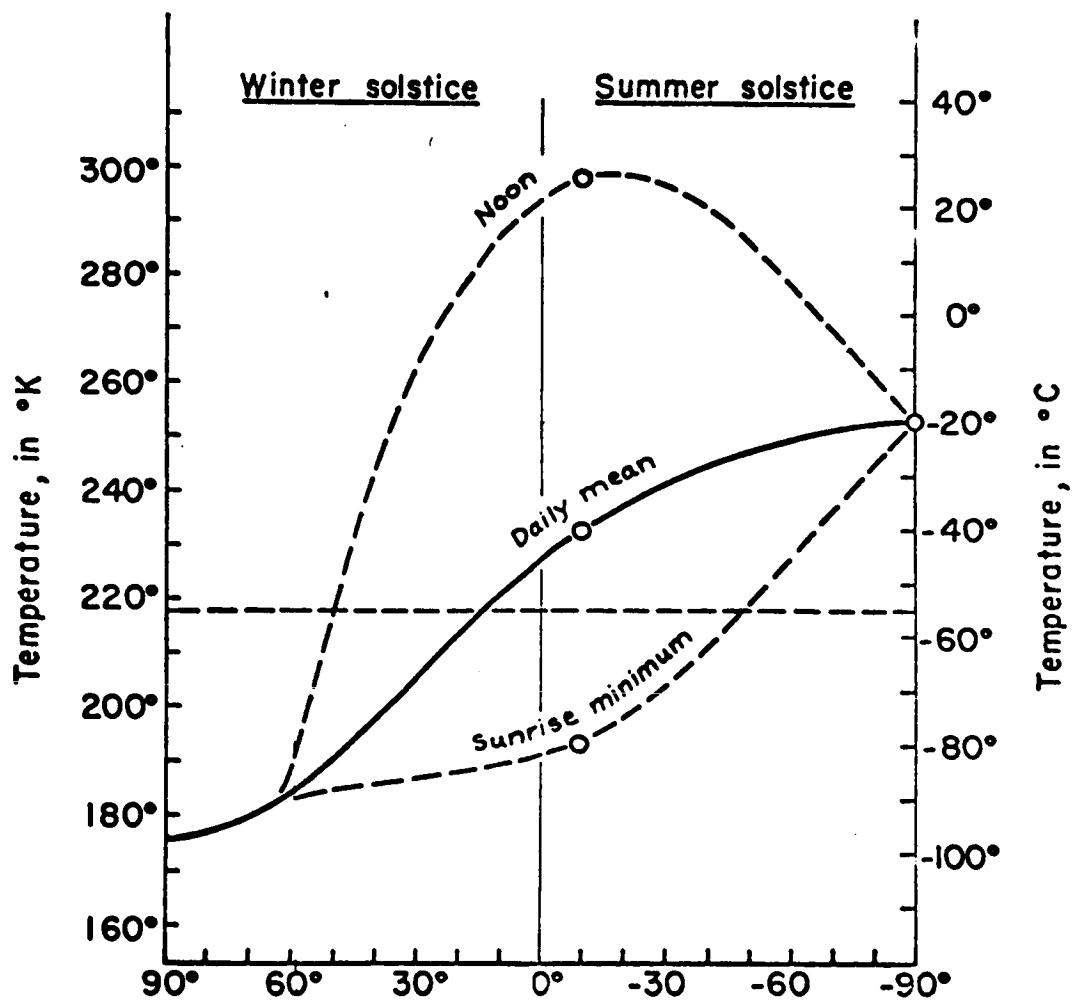


Figure 1. The surface temperature on Mars at the northern hemisphere winter solstice (After Mintz, 1961).

of Mars by Kuiper (1952) (See Figure 2.). This observation was confirmed by Kuiper in the following year when he detected three additional CO₂ bands at 1.96 μ , 2.01 μ and 2.06 μ . By comparing the intensity of the bands observed in the Martian spectrum with those observed in the spectrum of the sun, he estimated the amount of CO₂ present in the atmosphere of Mars to be ~ 4.4 m-atm, about twice the amount found in the Earth's atmosphere (Kuiper, 1952).

Grandjean and Goody (1955) redetermined the concentration of CO₂ in the Martian atmosphere from Kuiper's observations, taking into account the fine structure of the band and the shape of the rotation lines. They found that for a surface pressure of 100 mb, the total amount of CO₂ on Mars would be thirteen times greater than the amount present in the atmosphere of the Earth, or about 30 m-atm.

In 1963, using high-resolution spectroscopy, Kaplan, Münch and Spinrad (1964) at Mount Wilson detected the rotational lines of CO₂ in a weak band near 8700 Å, and, from laboratory determinations of the line strengths, estimated the amount of CO₂ in the Martian atmosphere to be 55 ± 20 m-atm.

Early attempts to detect H₂O in the atmosphere of Mars (Adams and Dunham, 1937; Adams, 1941) were unsuccessful and an upper limit of 10^{-3} g/cm² precipitable water was set by the investigators (Dunham, 1952). Later negative observations by Kiess, et al. (1957) had resulted in a larger estimate (8×10^{-3} g/cm² precipitable water) for the amount of H₂O which could be

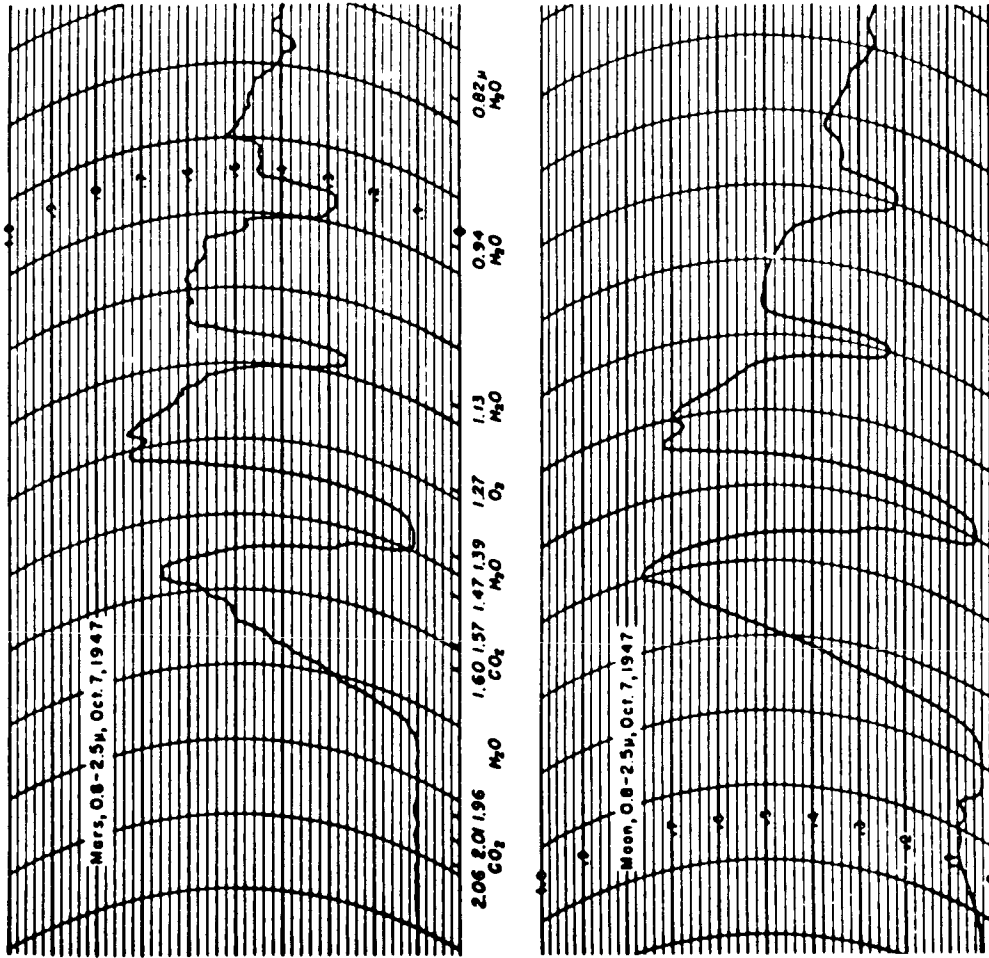


Figure 2. The CO₂ bands at 1.60 and 1.57μ in the Martian spectrum (After Kuiper, 1952).

present on Mars and yet remain undetected. Finally, in 1963, several independent observations positively verified the presence of H_2O in the Martian atmosphere. Dollfus (1963) detected H_2O bands near 1.4μ using a polarizing photometric method and estimated the amount of precipitable water on Mars at $2 \times 10^{-2} \text{ g/cm}^2$. Danielson, et al. (1964), from their spectroscopic measurements in the 2.7μ band, suggested that less than $4 \times 10^{-3} \text{ g/cm}^2$ precipitable water is present, while Kaplan, Münch and Spinrad (1964) arrived at an amount of $(1.4 \pm .7) \times 10^{-3} \text{ g/cm}^2$ from their observation of the rotational lines of H_2O near 8300 \AA .

Spectroscopic observations at Mount Wilson during 1933 and 1934 by Adams and Dunham, rediscussed by Dunham (1952), failed to detect any evidence of O_2 in the Martian spectrum, and it was concluded, therefore, that the amount of O_2 present could not exceed 2.4 m-atm. Richardson (1957) and Kiess, et al. (1957) confirmed this negative result for O_2 , and Kaplan, Münch and Spinrad (1964), from the absence of O_2 in their spectra, derived an upper limit of 70 cm-atm for this gas on Mars, a limit lower by a factor of three than that suggested by Dunham (1952).

To date, examinations of the spectra of Mars for evidence of various other gases (Kuiper, 1952; Sinton, 1961) have had only negative results, and upper limits have been given for the amounts of these gases. (See Rasool (1963) for a summary of the possible abundances of gases in the Martian atmosphere.)

From measurements of the polarization of sunlight scattered by the planet, Lyot (1929) estimated the total pressure of the atmosphere on Mars to be less than 25 mb. This estimate was superseded by that of Dollfus (1957) who, at the Pic du Midi Observatory, made polarimetric measurements across the Martian disk at different phase angles and in different colors. By several methods of data reduction, Dollfus obtained a value of about 85 mb for the surface pressure. De Vaucouleurs (1954), from visual observation of the brightness of Martian markings at the Peridier Observatory in 1939, deduced a value of 80 ± 13 mb, while photometric determinations of atmospheric density (Sytinskaya, 1962) have given surface pressures ranging between about 60 mb and 110 mb. Kaplan, Münch and Spinrad (1964), by combining their estimate of CO₂ abundance with spectroscopic observations by Kuiper (1963) and Sinton (1963) of the strong Martian bands near 2μ , estimated the total atmospheric pressure on Mars to be 25 ± 15 mb. This pressure estimate suggested the possibility that CO₂ is a major constituent of the Martian atmosphere.

In reviewing the various techniques which have been used to estimate the surface pressure and atmospheric composition on Mars, Chamberlain and Hunten (1965) concluded that both polarimetric and photometric methods of pressure determination are unreliable. Because both techniques would actually measure scattering by any submicron particles present in addition to molecular scattering, they may be worthless for determining atmospheric pressure.

According to Chamberlain and Hunten, spectroscopic observations are, in principle, capable of yielding both atmospheric pressure and composition. In their view, however, observations made prior to 1965 are not refined enough to estimate either parameter with great accuracy. They underlined the need for an improved determination of CO_2 abundance from a weak band.

Belton and Hunten (1966) observed the weak 1.05μ band of CO_2 in the spectrum of Mars at Kitt Peak National Observatory in 1965 and derived an atmospheric abundance of 68 ± 26 m-atm for CO_2 , corresponding to a partial pressure of 5 ± 2 mb. They have coupled this result with Gray's (1966) analysis of Kuiper's (1963) data for the strong 2μ bands to obtain a surface pressure in the range of 5 mb to 13 mb, with a preferred value of 6 mb. Thus, their results indicate that CO_2 is the dominant constituent of the Martian atmosphere.

Pre - Mariner IV Theoretical Investigations
of Atmospheric Structure

Lower atmosphere.

A number of theoretical models for the lower Martian atmosphere have been constructed from radiative transfer considerations. Most of the models, however, are physically oversimplified and based upon earlier estimates of surface pressure and atmospheric composition which are now known to be unrealistic.

Goody (1957) computed the vertical distribution of temperature in the Martian atmosphere taking both convective and radiative energy transport into account. Assuming a ground temperature of 270°K suggested for noontime equatorial regions by Hess (1950), a surface pressure of 85 mb suggested by the polarization measurements of Dollfus (1957) and a tropospheric lapse rate of 3.7°K/km suggested by the small value of the acceleration due to gravity on Mars, Goody obtained the temperature structure for two different compositions. For one model he chose CO₂ as the only infrared-active constituent, with a concentration suggested by the observations of Kuiper (1952) and the analysis of Grandjean and Goody (1955). For the other model he chose H₂O as the only infrared absorber with a total amount of 10⁻² cm precipitable water. In the case of CO₂ alone, the tropopause was found near 8.5 km at a temperature of ~ 240°K, with temperatures falling off with height to an approximately constant value of 134°K above 90 km. Since the temperature gradient in the region above the tropopause is only just stable

in this model, the exact tropopause height is somewhat indefinite. In the case of H_2O alone, a 25 km tropopause height was obtained, with a tropopause temperature of $\sim 178^\circ K$. At higher levels in this model the atmosphere is more nearly isothermal, with temperatures approaching a constant value of $153^\circ K$. Goody also found that decreasing the H_2O concentration in this model would cause the stratosphere to warm, but that the maximum value of tropopause temperature that could be achieved was $\sim 227^\circ K$, with the tropopause at 11.6 km.

Arking (1962) examined the effects of three assumptions commonly used in treating the problem of vertical heat transfer in planetary atmospheres. These assumptions are (1) that the atmosphere is infinite in extent, (2) that absorption and emission are grey and (3) that no convection is present. He assumed that the atmosphere is completely transparent to solar radiation and that conditions of local thermodynamic equilibrium exist at all levels. He found that when the atmosphere is optically thick (optical depth 3 or 4), the temperatures remain within 1% or 2% of the results for an infinite atmosphere (the Milne problem), but that for optically thin atmospheres (optical depth ~ 1 or less) the temperature deviations may be greater than 10%. He also found that the effect of a spectral window on the cooling of the planetary surface cannot be offset by a band of equal strength elsewhere in the spectrum; raising the absorption coefficient somewhere in the spectrum has a much smaller effect than lowering it, and this non-grey cooling

effect becomes much more important the thicker the atmosphere is. In calculating a grey-convective model designed to approximate conditions in the Martian atmosphere, Arking assumed an effective planetary temperature of 217°K , a total optical thickness of 0.5 and the decrease of opacity with height with an "absorption scale height" of 17 km. He found a tropopause at the 8 km level, a surface temperature of 235°K and a temperature of $\sim 188^{\circ}\text{K}$ at an altitude of 30 km.

Ohring (1963) computed the vertical run of atmospheric temperatures on Mars assuming a surface temperature of 230°K and a surface pressure of 85 mb, with a tropospheric lapse rate of $3.7^{\circ}\text{K}/\text{km}$ and a CO_2 concentration of 2% by volume. He obtained a tropopause height and temperature of 9 km and 196°K , respectively. Above the tropopause the temperature decreases at a rate only slightly less than adiabatic to the rather low value of about 90°K near 42 km. Ohring comments that at this temperature CO_2 would condense and that this condensation phenomenon might have some connection with the blue haze observed in the Martian atmosphere.

More meaningful models of the atmospheric structure on Mars were developed by Prabhakara and Hogan (1965), who were motivated by the fact that none of the earlier models described above had taken the absorption of solar energy in the atmosphere into account, as well as the fact that the input values of the parameters employed in these models had become outdated. Prabhakara and Hogan reexamined the radiative equilibrium temperature

structure of the Martian atmosphere, including the absorption of solar ultraviolet and visible energy by oxygen and ozone and solar near infrared energy by CO_2 in the $1\mu - 6\mu$ bands in the calculation of atmospheric heating. They theoretically calculated the transmission functions of CO_2 , making use of the strong line approximation to the "statistical" model to simulate band absorption, and used these transmission functions to evaluate the absorption of solar energy in the near infrared and to investigate the radiative transfer in the far infrared. For various spectral intervals in the near and far infrared, they derived the theoretical band parameters involving the line intensity and mean ratio of line half-width to line spacing from the transmittance tables of CO_2 presented by Stull, et al. (1963).

Prabhakara and Hogan used the basic photochemical theory of O_3 production to determine a vertical distribution of O_3 consistent with the computed radiative equilibrium temperature structure. They integrated the equation of radiative transfer numerically to obtain the temperature distribution, avoiding use of the empirical relationships commonly involved in the pressure dependence of CO_2 absorption, and also calculated the infrared flux transmittance without any simplifying assumptions. Instead of a "time marching" approach to the radiative transfer problem, in which a final solution requires the rate of heating to become vanishingly small, they used a steady state approach, requiring equality between absorbed and emitted energies for

all levels at each step. They considered both radiative and convective energy transport in their solution of the radiative transfer equation; whenever the calculated lapse rate tended to be superadiabatic it was replaced by the adiabatic lapse rate.

In their study, Prabhakara and Hogan calculated radiative equilibrium temperatures from the surface of Mars to the 100 km level for six models with surface temperatures ranging from 230°K to 270°K, surface pressures from 10 mb to 50 mb and CO₂ concentrations from 4% to 44% by volume. In all of their models, they found the tropopause at levels below 10 km, with the temperature above the tropopause steadily decreasing to a value of about 155°K in the upper layers. Their results indicated definitely that no temperature maximum is produced in the Martian atmosphere by the absorption of solar energy in the ultraviolet and visible by O₂ and O₃ or in the near infrared by CO₂. The maximum O₃ number density occurred at the surface of Mars with a gradual decrease with altitude, and the total amount of ozone present was found to be about one-tenth of the amount found in the Earth's atmosphere (~ 0.3 cm-atm). The total ultraviolet energy absorbed in the Martian atmosphere by O₂ and O₃ was found to be comparable to the near infrared energy absorbed by CO₂. However, the vertical distribution of absorbed energy showed that below ~ 20 km, O₂ and O₃ absorption is comparable to CO₂ absorption, while above this level CO₂ absorption becomes much larger.

Of the six models presented by Prabhakara and Hogan, their Model I most closely approximates conditions in the lower atmosphere of Mars as revealed by Mariner IV. This model was widely referred to in post-Mariner IV studies of the Martian atmosphere, being directly adopted as a lower atmospheric model by some (Chamberlain and McElroy, 1966) and conveniently ignored by others (Johnson, 1965; Fjeldbo, et al., 1966) in constructing ionospheric models. In Model I of Prabhakara and Hogan, considered an extreme case at the time, a 10 mb surface pressure was adopted along with a ground temperature of 230°K and a CO₂ concentration of 44% by volume. The remainder of the atmosphere was assumed to be N₂. The complete vertical structure of the atmosphere resulting in this case is shown in Figure 3. The tropopause appeared near the 3 - 4 km level at a temperature of $\sim 212^\circ\text{K}$, with a decrease in temperature above this level to a constant value of 158.5°K at the top of the model. The pressure obtained at the 100 km level was $\sim 1.2 \times 10^{-3}$ mb, and a number density of $\sim 5 \times 10^{13}$ mol/cm³ at this level resulted.

Another result of the study of Prabhakara and Hogan indicated that solar heating in the near infrared bands of CO₂ might warm the Martian atmosphere at some levels by $\sim 20^\circ\text{K}$ above its radiative - convective equilibrium temperature structure. This effect is illustrated in Figure 4 (an amended version from Prabhakara and Hogan (1965)), for a case of 30 mb surface pressure and 9% by volume CO₂ concentration. In this particular case, excluding the absorption of solar energy lowers the temper-

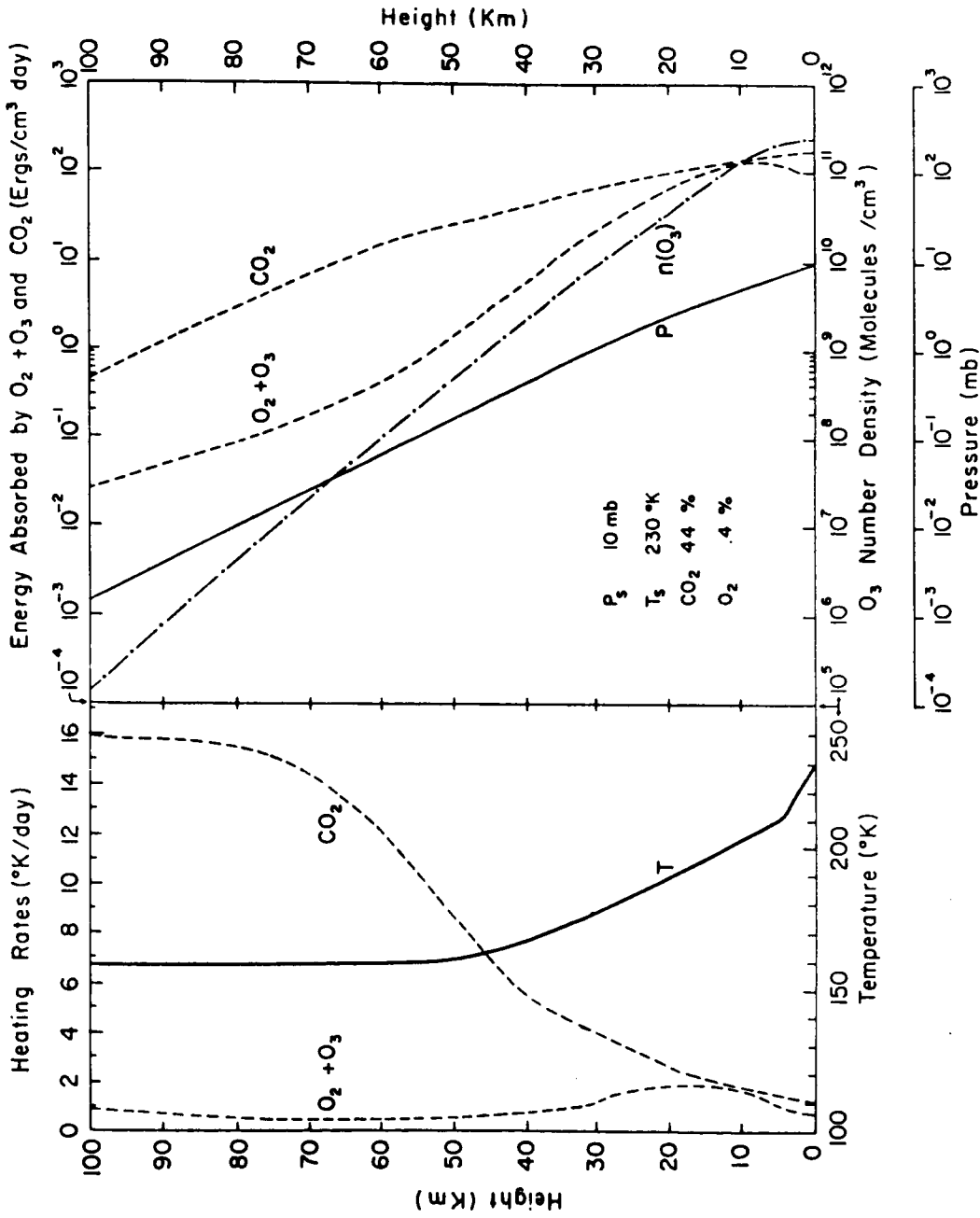


Figure 3. Model I of Prabhakara and Hogan (1965).

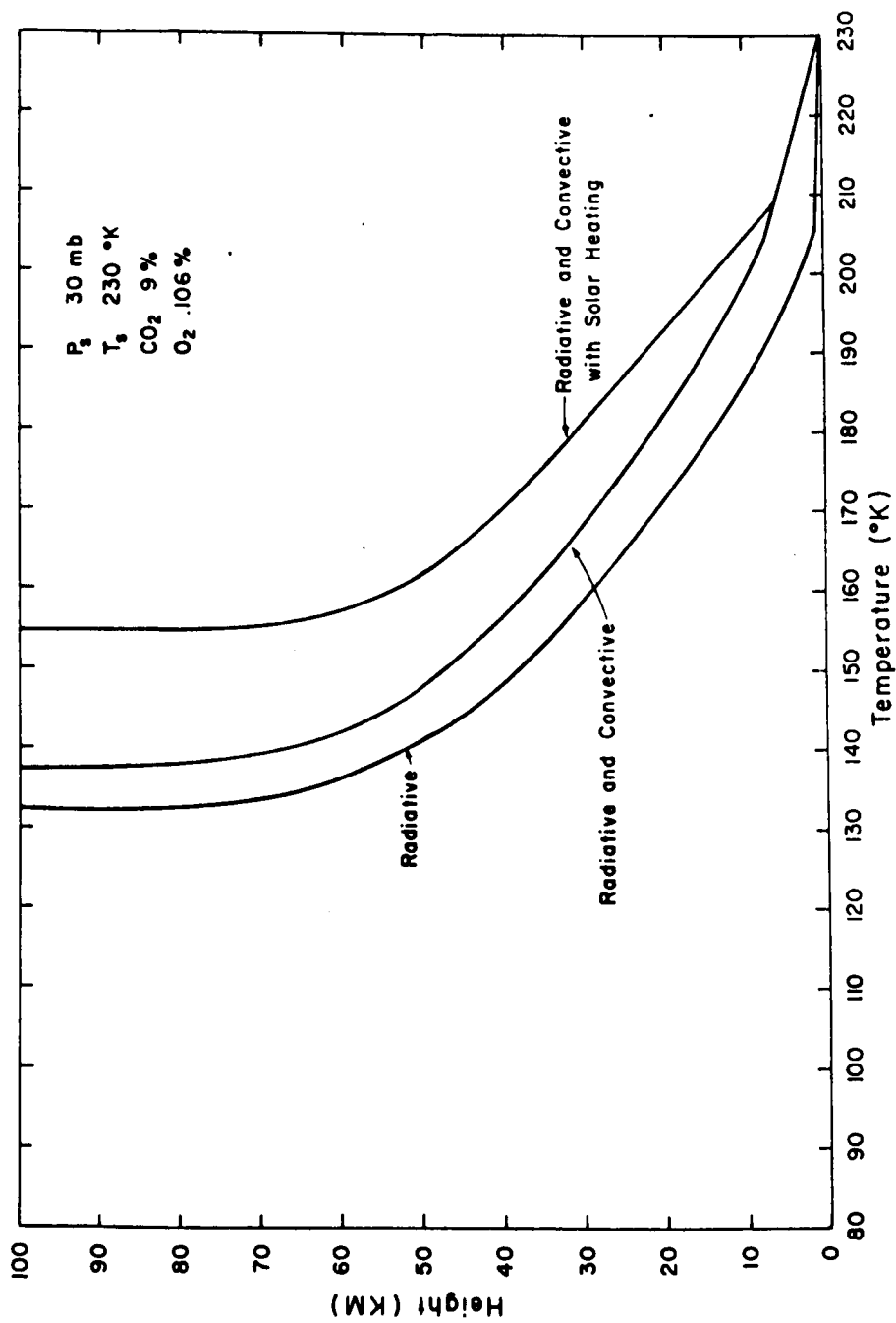


Figure 4. Equilibrium temperature profiles calculated for Mars: radiative, radiative-convective and radiative-convective with solar heating (After Prabhakara and Hogan, 1965).

ature considerably, and the cumulative effect of the lower temperatures causes a significant reduction in number density at the 100 km level. In the work of Prabhakara and Hogan (1965) the existence of local thermodynamic equilibrium conditions throughout the atmosphere was implicitly assumed, both in the near and far infrared bands of CO_2 . Also, in their calculations they did not give consideration to the Doppler broadening of the spectral lines or photodissociation of CO_2 . Well aware of these limitations, they set a limit to the region of validity of their results. In the case of Model I, their results are admittedly of questionable accuracy above ~ 65 km altitude.

Upper atmosphere.

No observational evidence of the characteristics of the upper atmosphere of Mars was available prior to the Mariner IV occultation experiment. Upper atmospheric models had been proposed, however, from Earth-analogy and energy balance considerations involving the solution of the radiative transfer and heat conduction equations.

Adopting a lower atmospheric model from Goody (1957), Chamberlain (1962) derived a temperature structure for the Martian mesosphere and thermosphere taking into account the various heating and cooling and energy transport processes involved. He concluded that the CO, present in the upper atmosphere as a result of CO_2 photodissociation, has a large

thermostatic effect, keeping thermospheric temperatures on Mars from exceeding $\sim 1100^\circ\text{K}$, so that Mars might retain O .

Chamberlain obtained a pronounced temperature minimum of $\sim 76^\circ\text{K}$ at the Martian mesopause near ~ 130 km altitude, due to large radiative cooling by CO_2 in this region, and he suggested a possible link between this low temperature (at which CO_2 would freeze out) and the Martian blue haze. He estimated that the solar energy absorbed in molecular photodissociation is readily radiated away by CO_2 and that the thermosphere is produced entirely by photoionization energy. This photoionization energy is lost by a downward flux of heat by conduction, coupled with CO radiative losses near 4.6μ from excited vibrational states, so that an equilibrium temperature distribution results. The thermospheric model obtained by Chamberlain is shown in Figure 5, from Rasool (1963). (In this figure, the temperature structure in the lower atmosphere (insert) is basically that computed by Arking (1962).)

Chamberlain also speculated on the structure of the Martian ionosphere, estimating smaller ionization densities than are found in the Earth's ionosphere. He suggested an E region consisting of two distinct portions, X-rays forming an E2 maximum at 200 km, and ultraviolet radiation forming an E1 maximum near the mesopause at 130 km. He also anticipated an F1 ionospheric region near 320 km, with a noontime electron number density of $\sim 10^5$ electrons/cm³. He concluded that an F2 region on Mars would not develop to the extent that it does on Earth and all ionospheric regions might disappear during the night.

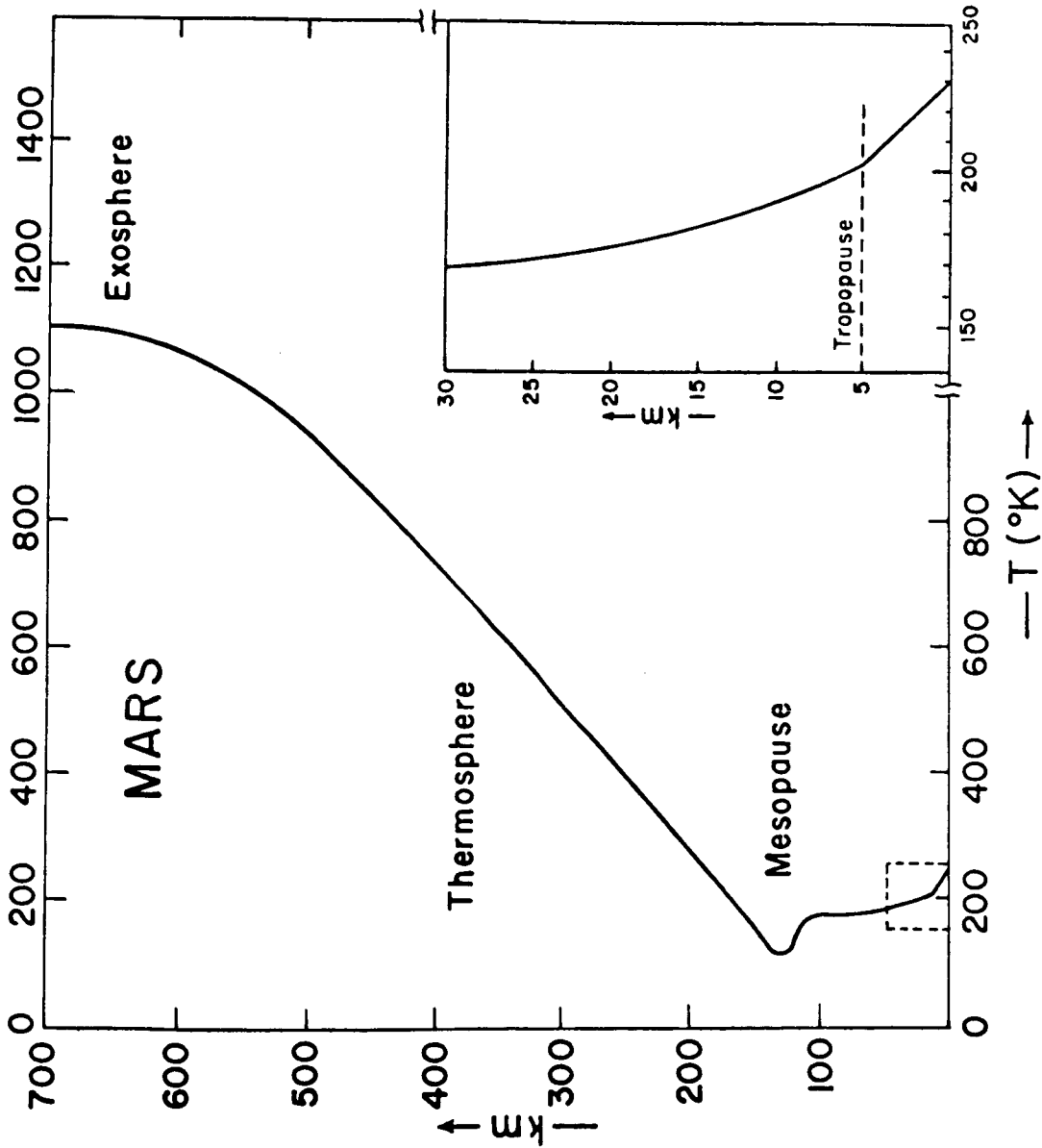


Figure 5. Thermospheric model of Chamberlain (1962) and Arking (1962) (After Rasool, 1963).

McElroy, et al. (1965) also examined the structure of the upper Martian atmosphere, constructing a number of models with various constants and boundary conditions in the heat conduction equation. They found that CO vibrational cooling is not as important as had been suggested by Chamberlain, but that the rotational levels of CO and the fine structure levels of the ground state of O may cause appreciable radiative loss. They also found that changing the composition at the mesopause level only moderately affects the temperature structure as does increasing the total number density at the mesopause level. Exospheric temperatures ranged between $\sim 725^{\circ}\text{K}$ and $\sim 950^{\circ}\text{K}$ in the three models illustrated. McElroy, et al. also found that it appears to be a good approximation to neglect radiative losses to space at optical depths greater than unity.

Mariner IV Occultation Experiment

The highly successful mission of Mariner IV provided interesting new information on the physical properties of the planet Mars. On November 28, 1964, the Mariner IV spacecraft was launched into orbit about the sun on a trajectory which would result in rendezvous with Mars and occultation of the spacecraft by Mars as viewed from Earth. On July 15, 1965, with data acquiring systems operating at their maximum capability, Mariner IV approached to within 6118 miles of the Martian surface, passed behind the planet and reappeared again on the opposite limb. The encounter sequence and spacecraft trajectory near encounter are depicted in Figure 6, after Anderson (1965). At the time of the encounter Mars was 2.16×10^8 km from the Earth and 2.32×10^8 km from the sun with an Earth - sun - Mars angle of 64° . The subpolar point at encounter was 15.3° N of the Martian equator.

Magnetometer and high and low energy particle detector measurements in the vicinity of Mars all indicated that only a very weak magnetic field ($< 10^{-3}$ gauss) can be present (Smith, et al., 1965; O'Gallagher and Simpson, 1965; Van Allen, et al., 1965), and photography of the planet revealed that the Martian surface, like that of the moon, is heavily cratered (Leighton, et al., 1965). Of particular relevance to the present study is the Mariner IV occultation experiment (Kliore, et al., 1965)

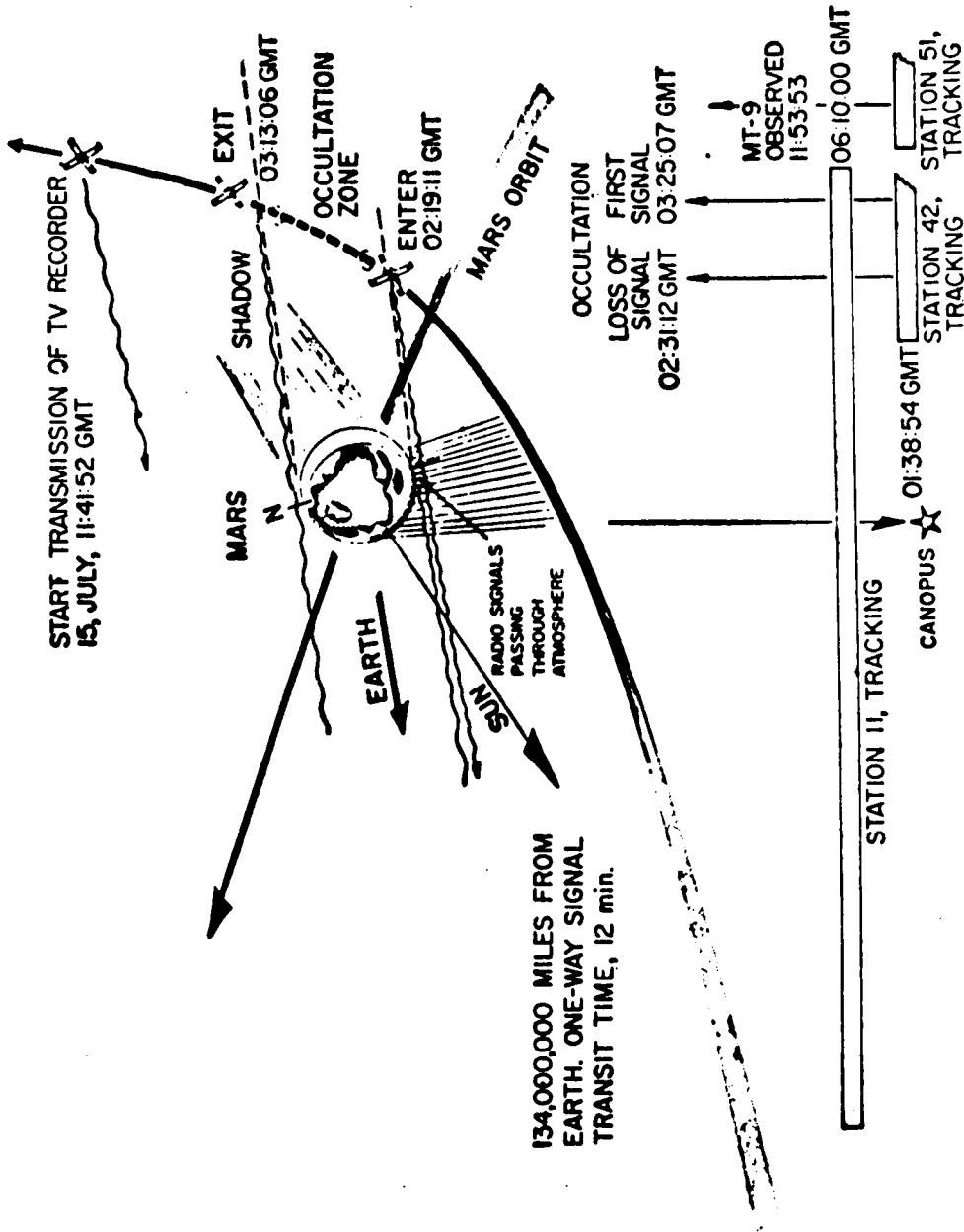


Figure 6. Mariner IV encounter sequence and trajectory (After Anderson, 1965).

which resulted in estimates of the gross properties of the lower atmosphere of Mars, and clearly indicated the presence of an ionosphere.

Experimental techniques.

The possibility of using the radio waves propagated between the Earth and a spacecraft whose trajectory passes behind a planet to obtain certain properties of the planetary atmosphere has been discussed by Fjeldbo and Eshleman (1965) and Fjeldbo, et al. (1965). As the spacecraft approaches the limb of a planet, the phase path, frequency and amplitude of the telemetry signal will be altered by the presence of a planetary atmosphere and/or ionosphere. The local index of refraction in the neutral atmosphere and ionosphere varies from unity, so that in these regions, the phase and group velocities will depart from their free space values. In addition, the mean refractive index along the ray path varies with the distance of the path from the planetary limb, and bending of the rays from a straight line will occur, along with focusing and defocusing of the signal. The changes in the phase path, frequency and amplitude of the radio signal are thus a function of the distribution of the index of refraction in the planetary atmosphere, and if these changes are carefully monitored as the spacecraft passes behind the planet, the distribution of the index of refraction can be inferred.

The observed alteration in the characteristics of the signal will in general be due to the combined effects of the neutral atmosphere and ionosphere of the planet. Since the contribution of the neutral atmosphere to the phase path change is directly proportional to the integrated atmospheric density along the ray path, this contribution will be largest when the spacecraft is close to the limb of the planet. On the other hand, the effects of the ionosphere on the phase path change are proportional to the integrated ion content along the ray path, so that these effects will predominate when the spacecraft lies at a distance from the limb approximately equal to the height of the ionosphere above the surface of the planet. Since it is reasonable to expect some separation in height between the neutral and ionized regions causing significant changes in the phase path of the signal, it should be possible to obtain information about both atmospheric regions, using a single radio frequency.

The phase changes due to the presence of the planetary atmosphere can be obtained by subtracting all predictable phase shifts due to light transit time, spacecraft motion, Earth rotation, etc., from the total phase change during the period of the experiment. Extreme accuracy is necessary here; in the case of the Mariner IV occultation experiment, the total phase change due to all causes other than the planetary atmosphere had to be known to 1 part in 10^{11} (Kliore, et al., 1965). Of prime importance is an exact knowledge of the

spacecraft trajectory and range rate. If this accuracy is achieved, the residual phase changes can be used to estimate the properties of the atmosphere and ionosphere by model fitting, or alternately, by integral inversion.

It is obvious, that no unique spatial distribution of refractive index corresponds to a given distribution of residual phase change as a function of distance from the planetary limb. Reason, therefore, must govern the choice of an atmospheric model. Fjeldbo, et al. (1965) point out that an assumption of a spherically symmetric atmosphere permits use of the numerical integral inversion technique in the derivation of the refractivity distribution. As is well known, however, an ionosphere is not spherically symmetric, with maximum electron-ion number densities being found near the subsolar point. A test of the validity of the symmetric ionosphere assumption was made by Fjeldbo (1964) and a similar test was performed in the present study. Both examinations indicate that the non-spherical nature of an ionosphere affects the integrated refractive index along a ray path only slightly, and that at high latitudes in winter, where the solar zenith angle is quite large and varies only over a small range during the day, the effects of non-sphericity are negligible.

Fjeldbo, et al. (1965) also found that changes in phase path due to the variation of the electron density in the Earth's atmosphere during the short time period of the experiment should be of no consequence and can be excluded from consideration.

Results and interpretation of experimenters.

The estimates of the atmospheric properties on Mars which resulted from the Mariner IV occultation experiment were surprisingly unlike those which had been given on the basis of earlier theoretical and experimental work. The Martian atmosphere was found to be colder, more rarified and composed of heavier molecules than had been predicted, and the ionosphere was discovered to be under-developed and located at a lower altitude than had been anticipated. These basic atmospheric features were well established by Mariner IV. Various atmospheric models have since been proposed, however, to clarify the Mariner observations and to give further understanding of the Martian atmosphere and ionosphere. These are treated in the next section.

At Mariner IV entry into occultation, the point of tangency of the Earth-spacecraft line on the surface of Mars was located at 55° S latitude and 177° E longitude, while at exit, the point of tangency was at 60° N latitude and 34° W longitude. At the entry point, local time was afternoon (13:30 h) in winter, and the solar zenith angle was $\sim 70^{\circ}$; at the exit point, local time was near midnight in summer, and the solar zenith angle was $\sim 106^{\circ}$. During entry into and exit from occultation, phase, frequency and amplitude measurements of the S band (2300 Mcy) Mariner IV telemetry signal were made at four receiving stations, two (Pioneer

and Echo) at Goldstone, California and two in Australia at Tibinbilla and Woomera. Entry data were obtained with the frequency reference of the Mariner IV transmitter provided by a frequency standard on Earth, while some of the exit data were taken with a crystal oscillator on board the spacecraft providing the frequency reference. The phase measurements made during exit using the oscillator as a frequency reference lacked precision, and, consequently, emphasis was placed on the data obtained during entry into occultation by Kliore, et al. (1965). The effects due to the neutral atmosphere and ionosphere can clearly be distinguished in Figure 7 from Kliore, et al. (1965). In this figure, which represents the total phase change on entry into occultation as a function of time (from the Goldstone-Pioneer data), the maximum ionospheric effect of $\nu - 10$ cycles appears at about 2:30:10 UT and the final upswing caused by the neutral atmosphere begins at about 2:30:50 UT and reaches a maximum of $\nu + 30$ cycles at signal extinction (2:31:11.2 UT).

By relating the maximum phase change (29 ± 2 cy), maximum frequency change (5.5 ± 0.5 cy/sec) and refractive gain at the time of signal extinction (1.5 db to 2.0 db) to the surface refractivity and scale height of a model atmosphere where density decreases exponentially with height, Kliore, et al. (1965) obtained values of 3.6 ± 0.2 N units for the surface refractivity and 9 ± 1 km for the scale height in

PHASE DIFFERENCE (RESIDUAL SUM)
DSIF II

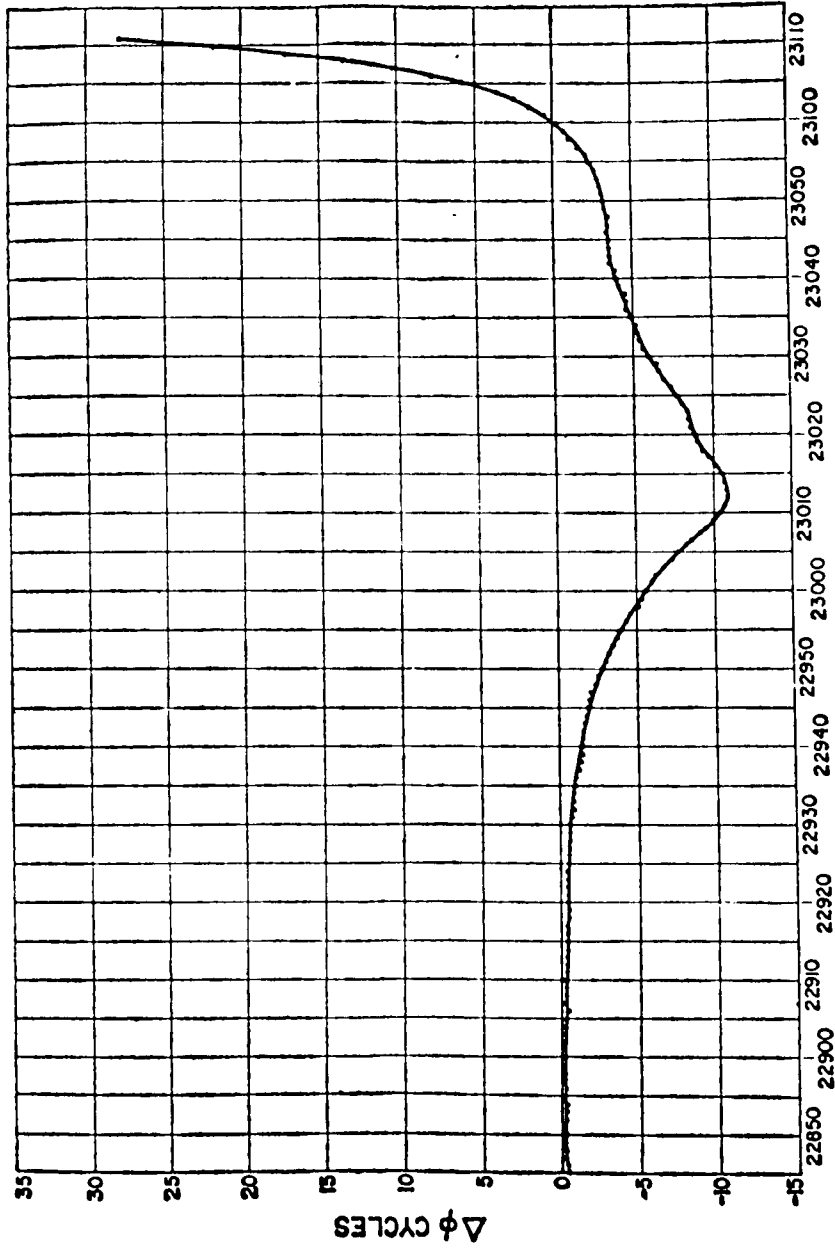


Figure 7. Relation of total phase change to time. Abscissa is UT, 15 July (After Kliore, et al., 1965).

the lower 30 km of the Martian atmosphere near the entry point of tangency. Kliore, et al. (1965) suggest that the final ray paths may have grazed an elevated surface feature, so that the mean surface refractivity may be slightly larger than the above value.

The inference of density and pressure from the refractivity and scale height estimates involves the assumption of an atmospheric composition, since the density - refractivity relationship depends upon the type of molecules making up the gas. Spectroscopic evidence, coupled with the low scale height measured by Mariner IV, indicates that the Martian atmosphere consists primarily of CO₂. Kliore, et al. (1965) obtained estimates of mass density corresponding to a surface refractivity of 3.6 ± 0.2 N units for three atmospheric models differing somewhat in composition but all having CO₂ as a major constituent. Temperatures near the surface of Mars were derived from the assumed composition (mean molecular weight) and the measured scale height of 9 ± 1 km. From the values of mass density and temperature near the Martian surface so derived, estimates of surface pressure were obtained using the equation of state. The surface pressure estimates of Kliore, et al. (1965) lie within the range of 4.0 mb to 7.0 mb, in good agreement with the values obtained spectroscopically by Belton and Hunten (1966). Table II from Kliore, et al. (1965) contains the values for surface temperature, number and mass density

TABLE II

SUMMARY OF OCCULTATION EXPERIMENT

(After Kliore, et al., 1965)

<u>Atmosphere</u>	
Surface refractivity	3.6 ± 0.2 N units
Scale height	8 to 10 km
Surface number density	
100% CO ₂	$1.9 \pm 0.1 \times 10^{17}$ mol/cm ³
Up to 20% A or N ₂ , or a mixture	$2.1 \pm 0.2 \times 10^{17}$ mol/cm ³
50% A	$2.5 \pm 0.15 \times 10^{17}$ mol/cm ³
Surface mass density	
100% CO ₂	$1.43 \pm 0.1 \times 10^{-5}$ g/cm ³
Up to 20% A or N ₂ , or a mixture	$1.5 \pm 0.15 \times 10^{-5}$ g/cm ³
50% A	$1.75 \pm 0.10 \times 10^{-5}$ g/cm ³
Temperature	
100% CO ₂	$180 \pm 20^\circ$ K
Up to 20% A or N ₂ , or a mixture	$175 \pm 25^\circ$ K
50% A	$170 \pm 20^\circ$ K
Surface pressure	
100% CO ₂	4.1 to 5.7 mb
Up to 20% A or N ₂ , or a mixture	4.1 to 6.2 mb
50% A	5.0 to 7.0 mb

Ionosphere

Maximum electron density ($\theta = 70^\circ$)	$9 \pm 1.0 \times 10^4$ el/cm ³
Altitude of maximum	120 to 125 km
Electron scale height above maximum	20 to 25 km
Temperature	$< 200^\circ$ K at 120 to 200 km

and pressure for each of the three models considered by the experimenters.

Measurements made after emersion from occultation indicate a surface pressure higher by 50% than the values obtained from the entry data (Fjeldbo, et al., 1966a). This discrepancy may be due to the presence of local surface features on Mars or due to the departure of the mean surface of the planet from a geopotential surface. The temperature and lapse rate inferred from the exit data are also higher (Fjeldbo, et al., 1966a) as might be expected since the emersion point is located in the summer hemisphere.

Inversion of the ionospheric phase path data obtained during entry into occultation indicate a peak electron number density of $\sim 9 \times 10^4$ electrons per cm^3 at about 125 km above the Martian surface, with an electron scale height above this peak of 20 - 25 km. Kliore, et al. (1965) concluded from the low altitude of the electron peak and the small electron scale height above the peak, that the Martian atmosphere is considerably cooler than had been previously anticipated. From the absence of a detectable ionospheric phase change in the exit data, Kliore, et al. (1965) set an upper limit on the nighttime ion density in the region probed by the signal at 20 times less than the daytime number density observed, or $\sim 4.5 \times 10^3$ electrons/ cm^3 . A minor ion peak near 95 km altitude was suggested by the entry data, which also show

evidence of asymmetry in the ion distribution below the peak at 125 km. Kliore, et al. (1965) have stated that their estimate of electron number density at the peak is correct to within 10%. The ionospheric data derived from the occultation experiment are presented in Table II. A profile of electron number density vs. height deduced from the occultation data by Fjeldbo, et al. (1966a) is illustrated in Figure 8.

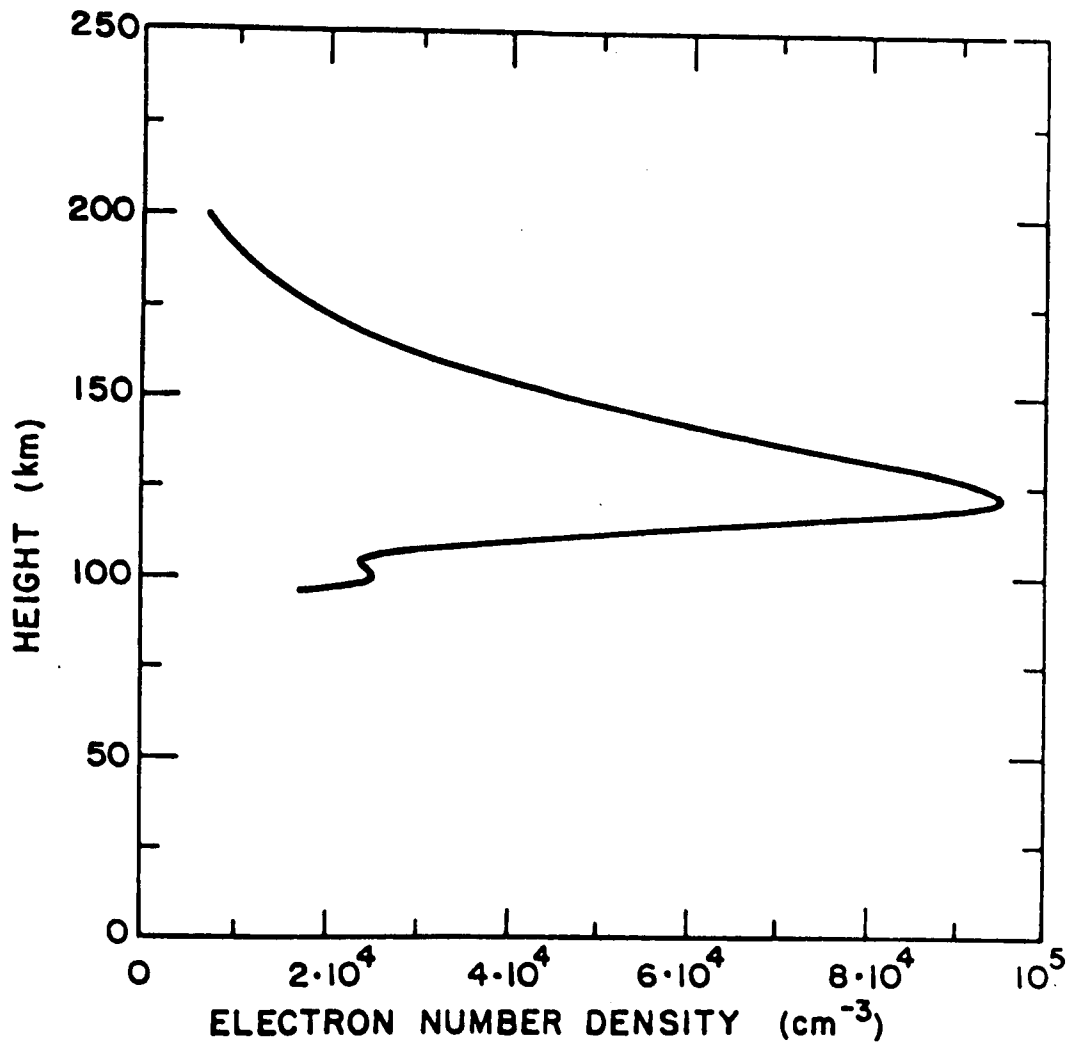


Figure 8. Electron density profile for Mars
(After Fjeldbo, et al., 1966a).

Post - Mariner IV Atmospheric Models

The nature of the ionospheric layer detected by Mariner IV is the principal problem which has emerged from the results of the occultation experiment, and various interpretations have been forthcoming in explanation. Closely related to the ionospheric problem is the question of the structure of the atmosphere below. Some of the proposed ionospheric interpretations place severe restrictions on lower atmospheric conditions and necessitate the adoption of atmospheric models which appear to be unreasonable on physical grounds. Other interpretations have been based upon lower atmospheric models with considerable physical backing, and these would seem to be, in general, more acceptable.

In all of the proposed explanations of the Martian ionosphere, analogy with the different regions of the terrestrial ionosphere has been widely used. Since the regions of the Earth's ionosphere can be classified in various ways, some basic convention must be employed to avoid confusion. Such a convention has been suggested by Hunten (1967) who formally proposed categorizing the ionospheric regions according to the physical processes governing ion production, redistribution and loss. His suggested definitions are: E-layer: A region ionized by radiation with an "effective" cross-section (i.e. weighted by the fractional abundance of the absorber) of $\sim 10^{-19} \text{ cm}^2$,

where the loss rate is limited by the dissociative recombination of molecular ions. F1-layer: A region ionized by radiation with an effective cross-section of $\sim 10^{-17} \text{ cm}^2$, where loss may be limited either by dissociative recombination or by charge transfer. F2-layer: A region of atomic oxygen ions forming a peak of electron density above the F1 maximum of production rate. Here, recombination is limited by the rate of charge transfer to molecular ions; as this rate decreases with altitude, diffusion of ions becomes more important and an ion peak is formed. Atomic oxygen is the most abundant constituent in this region. As each of the published models may be placed in one of these three categories, these general definitions will be adhered to in the present discussion.

F2-layer interpretation.

It was found necessary by Johnson (1965) and Fjeldbo, et al. (1966a), from analogy with the terrestrial ionosphere, to identify the ionospheric layer observed by Mariner IV as an F2 ion peak. Rishbeth and Barron (1960), in their study of the relative importance of recombination and diffusion, demonstrated that an F2-type peak occurs very close to the level where the loss rate β and the diffusion rate (D/H^2) are equal, $\beta = D/H^2$, where D is the ambipolar diffusion coefficient for electrons and ions in atomic oxygen and H is the scale height of atomic oxygen, the medium of diffusion. Above the F2 peak, the plasma

can be assumed to be in diffusive equilibrium and the plasma scale height related to the temperature, if appropriate assumptions are made. By applying the relationships derived by Rishbeth and Baron (1960), Johnson (1965) and Fjeldbo, et al. (1966a) concluded that the neutral number density at the ionospheric (F2) peak on Mars must be close to $\sim 10^9$ particles/cm³. Since a number density of $\sim 10^{17}$ particles/cm³ at the surface of Mars is indicated by the occultation experiment (Table II), a decrease of eight orders of magnitude in particle number density within 125 km is implied by the F2 assumption. Thus, the mean scale height below the ionosphere on Mars could be no greater than ~ 6.5 km, and the lower Martian atmosphere would have to be very cold. Even if, for example, the mean molecular weight of the atmosphere were as large as that of CO₂, the mean temperature would still have to be $\leq 130^\circ\text{K}$.

By assuming that the atmosphere at ionospheric levels is composed almost entirely of O atoms, Johnson (1965) and Fjeldbo, et al. (1966a) obtained atmospheric temperatures of 85°K and 80°K respectively at ionospheric height from the plasma scale height indicated by Mariner IV (Table II). Since the plasma scale height was announced by Kliore, et al. (1965) to be fairly constant up to ~ 200 km, Johnson (1965) and Fjeldbo, et al. (1966a) concluded that the 80°K - 85°K temperature also applied up to the 200 km altitude. They found, therefore, that the upper atmosphere of Mars is very

cold and nearly isothermal.

The two thermal structures obtained may be described as follows: Johnson (1965) assumed a surface temperature of 210°K with a convective layer 14 km thick adjacent to the ground. The tropopause temperature in his model is 140°K ; above the tropopause the temperature decreases along the vapor pressure curve for dry ice to a value of 85°K at 100 km. Above this altitude the atmosphere is isothermal. Fjeldbo, et al. (1966a) assumed a surface temperature of 180°K with temperature falling gradually with height to the low value of $\sim 50^{\circ}\text{K}$ near 100 km. Higher up, the temperature rises again, and the atmosphere becomes isothermal at $\sim 80^{\circ}\text{K}$ near 135 km.

There are numerous objections to the two models described above, the most serious of which is with regard to the extremely cold atmospheric temperatures they require. It has been shown convincingly by Prabhakara and Hogan (1965) that radiative transfer in the Martian atmosphere is sufficiently strong to maintain atmospheric temperatures well above the values proposed by Johnson (1965) and Fjeldbo, et al. (1966a). The radiative transfer process has been completely neglected in the construction of the above models, which constitute, in essence, interpolation between the surface and ionosphere. Moreover, careful studies of the Martian thermosphere by Chamberlain (1962) and McElroy, et al. (1965) have resulted in positive temperature gradients in the upper atmosphere in every case considered, with exospheric temperatures nearly an order of magnitude higher than those proposed by Johnson (1965)

or Fjeldbo, et al. (1966a). (Hunten (1967) has argued that the thermal calculations of Fjeldbo, et al. (1966b), which resulted in an exospheric temperature of $\sim 130^\circ\text{K}$, were performed using an unstable method, and are meaningless.) Therefore, on physical grounds, the F2 interpretation is questionable, because of the unrealistically low temperatures demanded throughout the atmosphere.

Gross, et al. (1966), in proposing an F2 model ionosphere, have pointed out that higher temperatures in the Martian upper atmosphere are consistent with the Mariner IV observations if a positive temperature gradient is present. In the presence of such a gradient, the actual scale height can be much larger than the isothermal scale height. They obtain an exospheric temperature of $550 \pm 150^\circ\text{K}$, the large uncertainty due to the uncertainties in the heating efficiency and extreme ultraviolet solar flux. However, Chamberlain and McElroy (1966) have brought attention to an internal inconsistency in the model of Gross, et al. (1966), arising from the fact that for the atmospheric structure given by this model, the F2 layer would be formed well above 125 km.

In constructing their atmospheric models, it was implicitly assumed by Johnson (1965), Fjeldbo, et al. (1966a, 1966b) and Gross, et al. (1966) that the electron and ion temperatures are equal to each other, and that both are equal to the neutral gas temperature. However, as pointed out by McElroy (1967) and Stewart (1967), it is well established by both observations

and theory, that the electron temperature in the Earth's ionosphere exceeds the ion temperature by a factor of 2 or 3 during the sunlit part of the day, and that at high enough levels both exceed the neutral gas temperature. Thus, the neutral gas temperatures derived from the observed plasma scale height by Johnson (1965), Fjeldbo, et al. (1966) and Gross, et al. (1966) are probably all too high. Therefore, even harsher conditions would be required by the F2 interpretation if allowances were made for elevated electron temperatures.

Finally, a point which would affect the F2 interpretation has been raised by Hunten (1967), who contends that double differentiation of the phase path data to obtain the variation of electron scale height with altitude involves accentuation of small random and systematic errors. As a result, he finds that the observed phase path changes, which were interpreted by Kliore, et al. (1965) as implying a constant electron scale height above the electron peak, are actually consistent with a scale height gradient as large as 0.8 km/km. Thus, his analysis indicates that rather large scale heights could be present some distance above the peak, at an altitude of ~ 200 km.

These many difficulties with this interpretation appear to rule out explanation of the Martian ionosphere as an F2 region. The fundamental objection to this interpretation is that there is no sound physical basis to any of the models proposed, and that the low temperatures required to produce

an F2 layer at 125 km are impossible to achieve on physical grounds. An implication of the unacceptability of the F2 ionospheric model is that the derivation of a temperature from the ion distribution above the peak is meaningless, since the ion distribution must be governed by local production and loss mechanisms, rather than diffusion.

E-layer interpretation.

A sounder approach to the problem of the Martian ionosphere was made by Chamberlain and McElroy (1966) who combined an existing model of the lower atmosphere with their own calculations of the thermospheric structure to obtain the neutral particle density at the ionospheric level. As a lower atmospheric structure, Chamberlain and McElroy (1966) adopted Model I of Prabhakara and Hogan (1965) (shown in Figure 3) up to an altitude of ~ 50 km. They extrapolated this model to ionospheric levels, and constructed a model thermosphere upon it, treating the various terms involved in the energy balance of the higher atmosphere in the manner developed previously by Chamberlain (1962) and McElroy, et al. (1965). Strong dissociation of CO_2 had been assumed in these earlier studies, with thermospheric cooling by O and CO being important factors in establishing the thermal structure of this region. However, Chamberlain and McElroy (1966) argue that, in order to maintain the generally cool thermosphere indicated by Mariner IV, CO_2 cannot be strongly dissociated, but must exert a strong

thermostatic effect, with CO_2 radiative losses keeping the overall temperature at higher levels low. In addition, they argue that due to the long photodissociation lifetime (~ 1 month) of CO_2 in the upper Martian atmosphere, mixing should control the distribution of gases, so that large quantities of CO_2 must be present at high levels.

In spite of the assumptions that CO_2 is only slightly dissociated and that the entire atmosphere is thoroughly mixed, both of which have a tendency to produce lower temperatures in the upper atmosphere from the radiative cooling of CO_2 , Chamberlain and McElroy (1966) nevertheless find a buildup of temperature with height. As a result of the balance between solar ionizing the dissociating radiation on the one hand, and infrared radiative losses coupled with downward transport of heat by conduction on the other, they obtain a true thermosphere in which temperatures increase to a value of 400°K or more in the exosphere.

Extrapolating Model I of Prabhakara and Hogan (1965), Chamberlain and McElroy (1966) obtain the same number density at the 100 km level ($\sim 5 \times 10^{13}$ particles/cm³) as was obtained by those authors. At the ionospheric level (125 km), they obtain a number density of $\sim 5 \times 10^{12}$ particles/cm³, and therefore interpret the observed layer of ionization as a Chapman type E-region produced by X-rays at the level where the optical depth in the ionizing frequency is unity. Since the sun was at a zenith angle of $\sim 70^\circ$ at the time of the observation and since the scale height at the level of the

ionosphere must be of the order of 10 km, a neutral particle number density of $\sim 5 \times 10^{12}$ particles/cm³ in the ionosphere implies a mean ionization cross-section of the order of 10^{-19} cm². Thus, according to the definitions suggested by Hunten (1967), the ionosphere must be of the E type. For an estimated X-ray photon flux of $\sim 5 \times 10^8$ photons/cm²sec, and a peak electron density of 10^5 electrons/cm³, the effective recombination coefficient must be $\sim 2.5 \times 10^{-8}$ cm³/sec, a reasonable value for an ionospheric region in which dissociative recombination limits electron loss. Chamberlain and McElroy (1966) argue that although ionization of all constituents occurs, various ionic reactions would likely result in most of the ionization appearing in the form of NO⁺ or O₂⁺, since these species have the lowest ionization potentials of all the constituents which could be present locally in significant amounts.

If the Martian ionosphere is an E region, then somehow, suppression of F1 and F2 regions must be explained. Chamberlain and McElroy (1966) point out that three conditions must be met for suppression of an F1 region at higher levels: 1) the effective recombination coefficient of CO₂⁺ must be at least 10^{-6} cm³/sec, 2) there cannot be a fast reaction transforming CO₂⁺ into another ion which has a slower recombination rate, and 3) O/CO₂ and O₂/CO₂ abundance ratios must each be less than $\sim 10\%$, so that O₂⁺ does not become the dominant ion. To satisfy the last condition, there must be little CO₂ dissociation above 100 km and little diffusive separation at the F1 level (~ 190 km). Chamberlain and McElroy (1966) reason

that with the small O/CO_2 ratio required to explain the absence of a detectable F1 region, it is unlikely that O^+ could become the dominant ion below the level at which diffusion becomes the main process for ion removal. Thus, no F2 region will appear at higher levels.

Additional thermal calculations for the lower and upper atmosphere of Mars have been performed by McElroy (1967) who obtains essentially the same atmospheric structure as was obtained from the Prabhakara and Hogan (1965) - Chamberlain and McElroy (1966) model. A neutral particle number density of $\sim 5 \times 10^{12}$ particles/cm³ at the ionospheric level results here also, and the E-layer interpretation is adopted. Furthermore, the same conditions for suppression of F1 and F2 layers as outlined by Chamberlain and McElroy (1966) are required.

Since physically significant model atmospheric structures were adopted in these studies, it would appear that the E-layer interpretation of the Martian ionosphere is basically correct. One piece of experimental evidence, however, raises serious questions with this explanation. The coefficient for dissociative recombination of CO_2^+ ions with electrons has been recently measured at $(3.8 \pm 0.5) \times 10^{-7}$ cm³/sec at a temperature of 300°K and appears to be of the same size at a temperature of $\sim 210^\circ K$ (Weller and Biondi, 1967). This value is substantially smaller than the minimum value of 10^{-6} cm³/sec required by the E-layer interpretation for suppression of other ionospheric features and, thus, the need for considerable modification of

the ionospheric models of Chamberlain and McElroy (1966) and McElroy (1967) is evident.

F1-layer interpretation.

Donahue (1966) suggests the possibility that the ionospheric layer observed on Mars is an F1 region. Assuming that the thermal structure above 50 km obtained by Chamberlain and McElroy (1966) is accurate, Donahue (1966) points out that, if the lower atmosphere of Mars consists primarily of CO₂ rather than the 44% CO₂ - 56% N₂ mixture considered by Prabhakara and Hogan (1965), the smaller scale heights in the lower atmosphere could result in a gas density of $\sim 10^{11}$ particles/cm³ near 125 km. In this case, he finds that the maximum photionization rate would occur when the sun is $\sim 20^\circ$ above the horizon, as it was during the occultation experiment. For a characteristic photoionization rate of $1.2 \times 10^3 \text{ cm}^{-3}\text{sec}^{-1}$, the observed electron density at the peak ($9 \times 10^4 \text{ electrons/cm}^3$) requires an effective recombination coefficient of $1.5 \times 10^{-7} \text{ cm}^3\text{sec}^{-1}$. This corresponds to the value anticipated for O₂⁺ ions (Biondi, 1964), and Donahue (1966) concludes that O₂⁺ ions are therefore responsible for the observed maximum. He also demonstrates that the suppression of an F2 peak can readily occur if the rate coefficient for the reaction between O⁺ and CO₂ to form CO and O₂⁺ is $1.2 \times 10^{-9} \text{ cm}^3\text{sec}^{-1}$ (Feshenfeld, et al., 1966). In that case, the O/CO₂ abundance ratio must only remain less than 10^2 up to the altitude at which diffusive loss of O⁺ ions becomes important.

Stewart (1967) also favors the F1 interpretation. By applying a criterion derived by Yonezawa (1965), he has shown that, in the Martian atmosphere, the boundary between ionospheric regions governed by attachment-type and recombination-type electron loss probably occurs well above the observed ionization maximum. Therefore, the ionosphere can be described by a Chapman function, with electron-ion diffusion being unimportant in the vicinity of the peak. Stewart (1967) has argued that only slight CO_2 dissociation is present and therefore, that O_2^+ rather than O^+ is the dominant ion responsible for the observed maximum. He finds that the temperature of the Martian exosphere varies from $\sim 180^\circ\text{K}$ to 550°K depending on the point in the solar sunspot cycle, and that the upper atmospheric temperatures for low solar heating flux are consistent with the Mariner IV observations provided that the ionosphere is an F1 layer in which molecular ions (O_2^+) dominate.

The F1 interpretation was not ruled out by Chamberlain and McElroy (1966). Since it requires less extreme conditions in the lower atmosphere than does the F2 model, and less extreme assumptions about reaction rates than does the E model, the F1 interpretation for the ionosphere of Mars seems to be the most acceptable. No detailed calculations, however, have been performed to confirm the existence of the required neutral particle density at the ionospheric level.

DETERMINATION OF ATMOSPHERIC STRUCTURE

From the preceding discussion, the strong dependence of the type of ionosphere observed on Mars upon the structure of the lower Martian atmosphere is evident. Existing models for the lower atmosphere demonstrate the total unacceptability of the F2 interpretation, and favor an E-type ionosphere. The E-model, however, has been ruled out by the recent experimental determination of a critically important reaction rate. Thus, the F1 interpretation seems to be the only plausible explanation of the observed ionosphere, but the considerable reinforcement of this viewpoint, which would result from the actual construction of a consistent lower atmospheric model, is lacking. The present research is designed to determine whether a physically sound model for the lower Martian atmosphere can indeed produce the conditions required for production of an F1 ionospheric layer at an altitude of 125 km.

Evaluation of Model I of Prabhakara and Hogan (1965)

In the calculations of Prabhakara and Hogan (1965), various assumptions were made which limit the acceptability of their results as realistic representations of conditions in the lower Martian atmosphere at the time and place of Mariner IV occultation. Some of these assumptions involve parameters for

variation, such as surface temperature, surface pressure, and atmospheric composition, while others, such as the adoption of the Lorentz line shape and the neglect of non-local thermodynamic equilibrium effects, concern the basic physics employed. It is unlikely that any of these assumptions would drastically influence the results; the atmospheric structures obtained by Prabhakara and Hogan must be reasonable, though not necessarily realistic. It is possible that the cumulative effect of these assumptions could produce overestimates of the atmospheric density at the ionospheric level, and thus lead to the false conclusion that the Martian ionosphere is of the E-type.

In their Model I (Figure 3), Prabhakara and Hogan (1965) adopted a ground temperature of 230°K , characteristic of the daily mean ground temperature near the Martian equator. Figure 1 (Mintz, 1961) suggests that a more representative value for the surface temperature at the occultation point on Mars (55°S) on an early winter afternoon would be $\sim 180^{\circ}\text{K}$. Although this value is based on a somewhat subjective analysis by Mintz (1961), it is probably a better estimate of the actual ground temperature at the point of occultation than is the arbitrarily selected value used by Prabhakara and Hogan. Any significant reduction of surface temperature in a model atmosphere where the structure is governed by radiative transfer will result in a general lowering of temperatures throughout the model up to great heights above the surface.

The surface pressure and atmospheric composition adopted by Prabhakara and Hogan in the construction of their Model I can now be replaced by more realistic estimates of these parameters. The ambient surface pressure on Mars has been found to lie within the 4 mb to 7 mb range by the Mariner IV experimenters (Kliore, et al., 1965) and within the 5 mb - 13 mb range by the spectroscopists who prefer a value of 6 mb (Belton and Hunten, 1966). Thus, it is likely that the atmospheric pressure at the surface of Mars is somewhat lower than the 10 mb value adopted by Prabhakara and Hogan. Moreover, the same observations show that the Martian atmosphere contains a much larger fraction of CO₂ than the 44% assumed by Prabhakara and Hogan, with a 100% CO₂ composition being allowed as a real possibility (Belton and Hunten, 1966).

Since the available evidence now indicates that the ambient temperature and pressure at the surface of Mars near the occultation point were somewhat lower, and the mean molecular weight of the atmosphere somewhat higher than the values adopted in the Prabhakara and Hogan model, it follows that the actual scale height in the lower atmosphere was probably significantly smaller than the model scale height at corresponding levels. For a temperature of 230°K and a mean molecular weight of 35.1 g/mole (corresponding to a 44% CO₂ - 56% N₂ mixture), a model scale height at the surface of ~ 14.4 km is obtained. However, for a temperature of 180°K and a mean molecular weight

of 44 g/mole (corresponding to pure CO₂), a scale height of ~ 9 km near the surface results, in close agreement with the value of 8 km - 10 km measured by Mariner IV (Kliore, et al., 1965) for the lower regions of the Martian atmosphere. This reduction of scale height, coupled with a moderately smaller surface pressure, would result in smaller number densities throughout the region of the atmosphere of interest, with the cumulative effect of the reduced scale height producing significantly lower number densities in the upper layers of the model. Thus, it appears that updating the adopted input parameters to correspond more closely to the lower atmospheric conditions at occultation would favor the F1 ionospheric interpretation by producing a generally colder, heavier model atmosphere, with a decrease in atmospheric density at higher levels from the values previously obtained by Prabhakara and Hogan (1965).

Another assumption, made by Prabhakara and Hogan (1965) in their treatment of the radiative transfer problem, probably results in overestimates of temperatures in all of their models. In their study, vibrational relaxation of CO₂ was not considered, and local thermodynamic equilibrium (LTE) conditions were assumed to be present throughout the atmosphere, both in the $1\mu - 6\mu$ near infrared bands and in the 15μ far infrared band of CO₂. A discussion of the breakdown of LTE in the vibration - rotation bands of CO₂ is given in Appendix B, and a method derived by Prabhakara and Hogan (1966) for treating the radiative

transfer problem under non-LTE conditions is described in Appendix C. As shown in Appendix C, if a strong source is present to supply energy directly to the kinetic mode in an atmospheric region where the band responsible for the radiative structure of the atmosphere (15μ CO_2 band) undergoes relaxation, large heating of the atmosphere with a consequent elevation of the temperature structure will result locally. However, as also shown in Appendix C, if no external heat source exists, the atmosphere will eventually revert to LTE conditions, regardless of the collision frequency.

As illustrated in Figure 4, Prabhakara and Hogan (1965) concluded that, under LTE conditions, the deposition of solar energy in the Martian atmosphere could raise the temperatures in the upper levels by as much as 20°K above the values obtained from basic radiative - convective considerations. Therefore, one might expect the temperature profiles obtained by Prabhakara and Hogan to considerably underestimate the temperatures in the higher Martian atmosphere where LTE breaks down (above ~ 65 km in their Model I). However, the solar energy input at levels above ~ 20 km in the models of Prabhakara and Hogan is due almost entirely to absorption in the $1\mu - 6\mu$ near infrared bands of CO_2 , and these bands, like the 15μ band, undergo relaxation at low pressures. If the solar energy in these bands does not pass into the kinetic mode, as was implicitly assumed in the study of Prabhakara and Hogan

(1965), but is scattered instead, then it cannot influence the temperature structure. In this case, only relatively weak sources and sinks of energy will remain outside of the 15μ CO_2 band, and the atmospheric temperature structure should not depart substantially from that obtained under LTE conditions. Moreover, if the near infrared energy is scattered rather than absorbed, the thermal structures presented by Prabhakara and Hogan probably constitute overestimates, rather than underestimates, of the atmospheric temperatures. From these considerations, it would not be unreasonable to conclude that the temperature near the top of their Model I is too warm by $\sim 20^\circ\text{K}$, and that temperatures would decrease to a value of $\sim 140^\circ\text{K}$ in this model, if the near infrared solar energy source were discounted.

It should also be pointed out that the mean solar energy absorbed in the Prabhakara and Hogan models was calculated for equatorial equinox, rather than for the high-latitude, winter conditions encountered in the Mariner IV occultation. The larger mean zenith angle and shorter sunlit portion of the day appropriate to the occultation point on Mars imply a smaller solar energy input than would be present at equinox near the Martian equator. Modification of the solar energy input in the models of Prabhakara and Hogan to more closely represent occultation conditions would therefore have a further tendency to produce lower atmospheric temperatures.

An additional assumption made by Prabhakara and Hogan (1965) which may significantly influence the temperature structures obtained, concerns the evaluation of their atmospheric transmission functions in the near and far infrared CO₂ bands. The neglect of Doppler broadening of the spectral lines results in underestimation of the line widths by several orders of magnitude in the upper portions of their models. As a result, the opacity of the higher atmospheric layers has been greatly underestimated, so that the temperatures in the upper portions of their models may have been underestimated also.

Plass and Fivel (1953), from their study of the relative importance of Lorentz and Doppler broadening effects on the radiative transfer in the terrestrial atmosphere, concluded that the Doppler effect can be neglected for both strong and weak lines up to the 50 km altitude, where the ambient pressure is $\sim .9$ mb, but that for lines of intermediate intensity, this effect may become important at lower levels. Elsasser (1960) suggested that the neglect of Doppler broadening for all lines may be a reasonable approximation up to ~ 40 km in the Earth's atmosphere, where the pressure is ~ 3 mb. Young (1964) has found the conclusions of Plass and Fivel (1953) for the strong and weak lines to be valid; however, he claims that the importance of lines of intermediate strength cannot be neglected, and that use of the Lorentz line shape at pressures lower than ~ 20 mb can introduce appreciable errors.

Following the arguments of Plass and Fivel (1953) and Elsasser (1960), Prabhakara and Hogan (1965) had reasoned that the pressure in the Martian atmosphere at which Doppler broadening becomes important is $\sim 6 \times 10^{-3}$ mb. In view of the conclusions of Young (1964), however, it appears that this broadening mechanism becomes important at higher pressures (lower atmospheric levels). In any case, if meaningful temperature profiles, determined by radiative transfer, are to be obtained up to the level of the ionosphere on Mars, then the great increase in the opacity of the upper layers which would result from consideration of the Doppler broadening mechanism must be taken into account.

Evaluation of the results of Prabhakara and Hogan (1965), particularly their Model I, leads to the conclusion that, although the thermal structures they obtained are not unreasonable, changes in various input parameters and consideration of the important effects of Doppler line broadening and vibrational relaxation of CO_2 would, nevertheless, produce more meaningful atmospheric models. Furthermore, it would seem that these revisions could quite conceivably create a cooler, more compressed atmospheric structure, with significantly lower densities at higher levels, and thus increase the likelihood that the ionosphere observed on Mars by Mariner IV is of the F1-type.

Present Method

In view of the numerous shortcomings of existing theoretical models, discussed in previous sections, the present study is undertaken to obtain a better understanding of the conditions in the lower Martian atmosphere, at the time and place of Mariner IV occultation.

The present determination of the atmospheric structure on Mars is based upon a steady state solution of the equation of radiative transfer, allowing for vibrational relaxation of the radiating gas, and for the absorption of solar energy in the atmosphere. Possible relaxation of the vibration - rotation near infrared bands of CO_2 in which solar energy is absorbed is considered here, and atmospheric transmission functions in the near and far infrared bands of CO_2 are calculated using a modified version of the Elsasser band model, taking both Lorentz and Doppler broadening of the spectral lines into account. Moreover, the required input data are chosen from the most recent estimates of the surface parameters and atmospheric composition available at this time.

Radiative transfer.

The physical theory related to the present construction of atmospheric models from radiative transfer considerations is developed in the Appendix. In Appendix A, a formal solution of the equation of radiative transfer is presented for boundary

conditions which are meaningful for studies of planetary atmospheres. In Appendix B, vibrational relaxation of the CO_2 molecule, and the relevance of this phenomenon to the problem of atmospheric radiative transfer is discussed. In Appendix C, radiative transfer under LTE and non-LTE conditions is considered, and convenient expressions are obtained for the atmospheric source function and the energy balance relationship, applicable whether or not the gas is relaxing (Prabhakara and Hogan, 1966). In Appendix D, the method of evaluating the atmospheric transmission functions required for solution of the radiative transfer equation is described in detail.

As shown in Appendix A, the radiative transfer equation can be applied to studies of a plane parallel atmosphere of finite thickness, if appropriate boundary conditions are specified. The transfer equation then has a solution in terms of the upward and downward directed specific intensities; these can be evaluated at any point in the atmosphere, for any prescribed atmospheric structure, provided the emission of the gas can be related to local conditions, and the transmission of the gas can be calculated for an arbitrary atmospheric path. With a knowledge of the upward and downward intensities at every level and the transmission characteristics of the gas, the amount of atmospheric radiation absorbed per unit volume at every level in the atmosphere can be obtained. The atmospheric radiation absorbed at any level, plus the solar radiation deposited at that level, must, under steady state conditions, be balanced by

the local emission of the gas. By relating the emission of the gas to the temperature (taking vibrational relaxation into account, if necessary), a new temperature estimate at every level in the atmosphere can be obtained. The resulting thermal structure will produce the emission required to balance the total absorbed energy per unit volume, calculated from radiative transfer considerations for the old atmospheric structure. Repetition of this procedure will eventually result in a convergent solution for temperature as a function of height in the atmosphere.

With the boundary conditions discussed in Appendix A of zero downward flux of infrared energy at the top of the atmosphere z_T and a blackbody surface at the ground z_g , the upward and downward intensities at level z_1 are, from equations (A.24) and (A.25),

$$I^\uparrow(\nu, \theta, z_1) = B(\nu, z_g) \mathcal{C}(\nu, \theta, z_1 - z_g) + \int_{z_g}^{z_1} J(\nu, z) \frac{\partial \mathcal{C}(\nu, \theta, z_1 - z)}{\partial z} dz, \quad (1)$$

and

$$I^\downarrow(\nu, \theta, z_1) = \int_{z_1}^{z_T} J(\nu, z) \frac{\partial \mathcal{C}(\nu, \theta, z - z_1)}{\partial z} dz. \quad (2)$$

The meaning of the various symbols in equations (1) and (2) is given in Appendix A.

Consider a thin slab of the atmosphere of geometric thickness δz centered at the level z_1 (Figure 9). The energy originating at levels below $z_1 - (\delta z/2)$ which is absorbed by the slab per unit time, $A^\uparrow(\delta z)$, will be given by

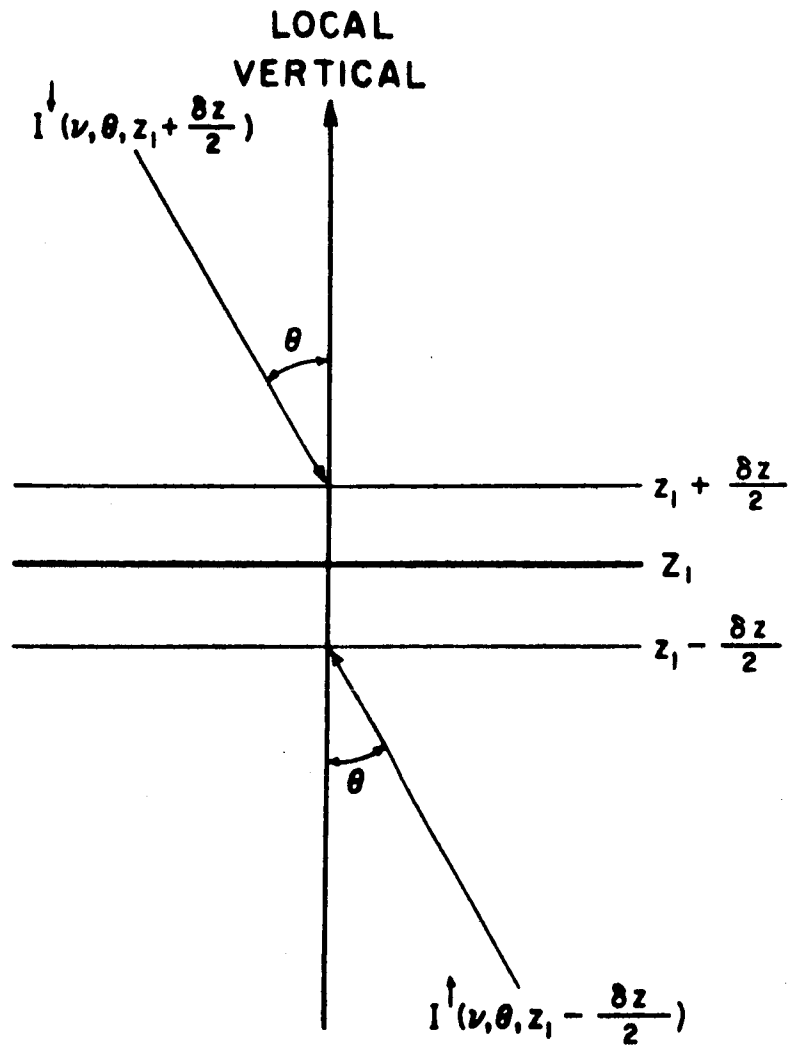


Figure 9. Schematic diagram

$$A^\uparrow(\delta z) = \iint_{\nu, \omega} I^\uparrow(\nu, \theta, z_1 - (\delta z/2)) \times (1 - \tau(\nu, \theta, \delta z)) d\omega d\nu, \quad (3)$$

where $\tau(\nu, \theta, \delta z)$ is the transmission of the slab at frequency ν and zenith angle θ , and where the frequency integration is performed over the 15μ CO_2 band, and the angular integration is performed over the lower hemisphere. A similar expression for the downward travelling radiation absorbed by the slab is

$$A^\downarrow(\delta z) = \iint_{\nu, \omega} I^\downarrow(\nu, \theta, z_1 + (\delta z/2)) \times (1 - \tau(\nu, \theta, \delta z)) d\omega d\nu, \quad (4)$$

where the angular integration is over the upper hemisphere.

The total energy emitted by the slab per unit time under conditions of local thermodynamic equilibrium $R(\delta z)$, is a function of the mean temperature of the slab, here taken to be the temperature at level z_1 :

$$R(\delta z) = \iint_{\nu, \omega} B(\nu, z_1) \times (1 - \tau(\nu, \theta, \delta z)) d\omega d\nu, \quad (5)$$

where the integration with respect to solid angle is performed over the entire sphere.

The mean solar energy absorbed per unit time by the slab $Q(\delta z)$ in the $1\mu - 6\mu$ near infrared bands of CO_2 may be expressed as

$$Q(\delta z) = \frac{1}{\pi} \frac{\Phi'}{\Phi' + \lambda'(z)} \iint_{\nu, \Omega} Q(\nu, z_T) \times \left(\tau(\nu, \theta, z_T - (z_1 + (\delta z/2))) - \tau(\nu, \theta, z_T - (z_1 - (\delta z/2))) \right) d\Omega d\nu \quad (6)$$

where $\lambda'(z)$ and Φ' are a mean relaxation time and a mean radiative lifetime, respectively, for the $1\mu - 6\mu$ bands

(Appendix B), $Q(\nu, z_T)$ is the solar energy of frequency ν incident per unit area per unit time at the top of the atmosphere, frequency integration is performed over the $1\mu - 6\mu$ infrared bands and integration over hour angle Ω is made between noon and sunset. The hour angle Ω and zenith angle Θ are related by the expression

$$\cos \Theta = \sin(l) \sin(d) + \cos(l) \cos(d) \cos \Omega \quad (7)$$

where l is the latitude (55° S) and d is the solar declination (15.3° N). The near infrared solar flux at the top of the Martian atmosphere $Q(\nu, z_T)$ was obtained from the Smithsonian Meteorological Tables (compiled by List, 1963) by multiplying the values tabulated there for Earth by the appropriate factor (0.432) to compensate for the difference in the mean distances of the Earth and Mars from the sun.

Under steady state conditions, the total energy of solar and terrestrial origin absorbed by the slab must be balanced by the total energy emitted. From the considerations of Appendix C, we are able to relate the emission of the gas under non-LTE conditions to the LTE emission (equation (C.8)). Also, we are able to represent the non-LTE effect in the 15μ CO_2 band as a factor amplifying the solar energy absorbed (equation (C.11)). In view of expressions (3), (4) and (5) above, equations (C.8) and (C.11) were rewritten as

$$J(\nu, z_1) = B(\nu, z_1) \left(1 - \frac{\lambda(z_1) Q(\delta z)}{\Phi R(\delta z)} \right) \quad (8)$$

and

$$Q(\delta z) \left(1 + \frac{\lambda(z_1)}{\Phi} \right) + A^\uparrow(\delta z) + A^\downarrow(\delta z) = R(\delta z) \quad (9)$$

From a simultaneous solution of (8) and (9), the temperature structure of the atmosphere was obtained as follows. An arbitrary initial atmospheric structure was specified, and the atmosphere was assumed to be in LTE (i.e. $J(\nu, z_1) = B(\nu, z_1)$) throughout. For this structure, $A^\uparrow(\delta z)$, $A^\downarrow(\delta z)$ and $Q(\delta z)$ were calculated from equations (3), (4) and (6) and $R(\delta z)$ obtained from (9). Since $R(\delta z)$ is directly related to the Planck emission $B(\nu, z_1)$, which, in turn, is a unique function of the temperature at level z_1 , the height distribution of $R(\delta z)$ determines a new distribution of temperature. The inversion of $R(\delta z)$ to obtain a temperature was performed using a standard numerical technique, the Newton-Raphson method. This second temperature structure was then used to evaluate the source function $J(\nu, z_1)$ from equation (8), and the values of $J(\nu, z_1)$ so obtained were used to solve equation (9) for a third atmospheric structure. This procedure was continued until an equilibrium thermal structure was obtained satisfying the convergence criterion that the temperature at any level varies by no more than 0.1°K in two successive iterations. In this manner, a temperature, pressure and density stratification of the atmosphere consistent with the source functions and absorbed solar energy was obtained.

Convection.

In the course of these thermal calculations, whenever the lapse rate of temperature obtained exceeded the adiabatic lapse rate (g/c_p , evaluated for the acceleration due to gravity on Mars and the chosen composition), it was replaced by the adiabatic

lapse rate and the calculation continued. As pointed out by Arking (1962), this procedure for treating convection near the planetary surface amounts to assuming maximum efficiency for convective heat transfer. The resulting temperature profile is somewhat artificial at the tropopause, since the discontinuity of temperature obtained there would be removed in the atmosphere by the penetration of convection into the stable region above. It is also artificial immediately adjacent to the ground where, in the atmosphere, the decrease in the efficiency of convective heat transfer with height tends to produce a superadiabatic gradient. Arking (1962) concludes from mixing length theory that the effect near the ground is not serious since the temperature gradient approaches the adiabatic gradient a very small distance above the ground, so that the temperature obtained near and at the ground by assuming exactly adiabatic conditions should be correct to within a few degrees. He also indicates that if the region of transition from convective to radiative regimes is optically thin, so that the radiative flux entering the radiative region originates primarily below the transition region, then it is not necessary to know the temperature near the tropopause accurately to determine the radiative structure above. If this transition region is optically thick, however, the situation becomes more complicated. Since no means are available, in the absence of observations, for determining the thickness of this transition region in the atmosphere of Mars, it becomes necessary to ignore the effects of penetration convection and to determine the boundary between convective and radiative regions by the above procedure.

Acceptability of method.

The general accuracy of this procedure for the construction of a model atmosphere with a structure governed by radiative transfer in the 15μ CO_2 band, was demonstrated by Prabhakara and Hogan (1966), who used this method in their study of the equilibrium temperature distribution in the Earth's mesosphere and lower thermosphere. In Figure 10, from Prabhakara and Hogan, (1966), a comparison is made between observed summer and winter temperature profiles at

Fort Churchill and White Sands, and three thermal structures calculated by the same basic method as outlined above.

Prabhakara and Hogan (1966) determined profiles of temperature in the Earth's atmosphere for three different values of the relaxation time in the 15μ CO_2 band: 10^{-6} sec, 5×10^{-6} sec and 1.5×10^{-5} sec. Solar heating in the ultraviolet and visible by O_2 and photochemically produced O_3 was considered in their study, rather than the near infrared heating important in the present study of the Martian atmosphere. As can be seen from Figure 10, the profiles they obtained are in good general agreement with the observed temperature profiles. At higher levels, the value of λ used exerts an important influence on the temperature, due to the sizable amount of solar energy absorbed there by O_2 . Were this source of energy at higher levels weaker, the particular value of λ chosen would have a smaller effect on the temperature structure. In any case,

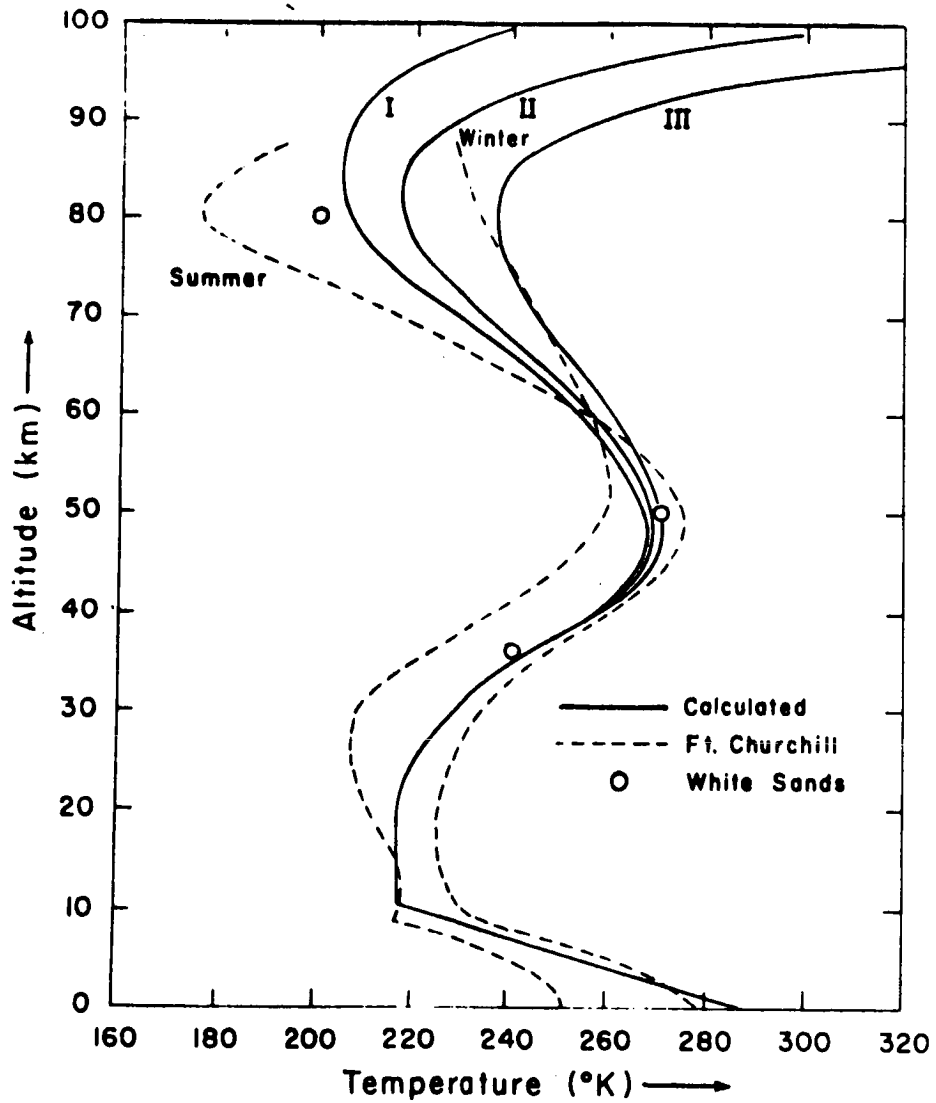


Figure 10. Comparison of calculated temperatures with observations at Ft. Churchill and White Sands. I: $\lambda_0 = 10^{-6}$ sec; II: $\lambda_0 = 5 \times 10^{-5}$ sec; III: $\lambda_0 = 1.5 \times 10^{-5}$ sec. (After Prabhakara and Hogan, 1966).

discrepancies between observed and calculated temperatures at higher levels can be easily accounted for by the fact that important physical processes such as dynamical heating and cooling and OH airglow emission were not considered. The overall ability of this procedure to accurately reproduce the observed temperature structure in the Earth's atmosphere renders it acceptable as a method for the construction of model atmospheres for Mars also.

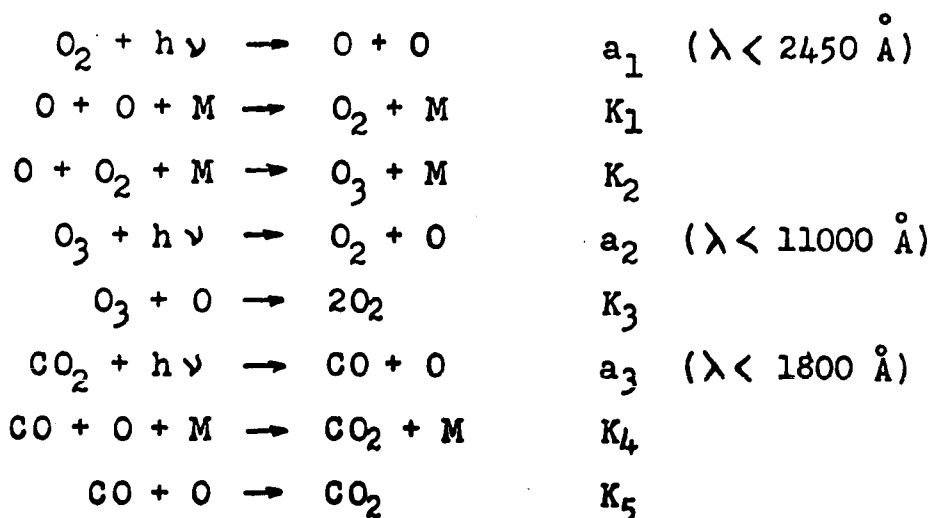
Photochemistry.

As is well known, CO_2 , the principal constituent of the Martian atmosphere, is dissociated by solar ultraviolet radiation into CO and O, and, as a result of various recombination processes, O_2 and O_3 may be produced. This photochemical activity results in a decrease in the concentration of the constituent which is largely responsible for the thermal structure of the lower atmosphere. It also results in the deposition of solar ultraviolet and visible radiation in the higher atmospheric layers. Thus, it is important to assess the influence of CO_2 photochemistry on the atmospheric structure.

In the calculation of a thermal structure by the method outlined above, the composition of the atmosphere was assumed to be uniform with height. The possible effects of CO_2 photochemistry on this basic structure were estimated, however, from a separate calculation, for each thermal model, of a photochemical equilibrium distribution of CO_2 and its

dissociation products. Estimates of the solar heating produced by this photochemical activity were obtained simultaneously with the distribution of the gases. Ideally, the structures of temperature and composition should be made totally consistent with each other by iteration. However, the distribution of gases in the Martian atmosphere is not determined by photochemical activity alone. Certainly, both eddy mixing and diffusive separation of gases in the gravitational field of the planet exert important effects on the local composition. Therefore, rigorous computation of consistent profiles of temperature and photochemical equilibrium composition is of little more than academic interest, and therefore such an iterative calculation was not performed.

The photochemistry of CO_2 in the Martian atmosphere has been discussed by Marmo and Warneck (1961). The following eight reactions involving photodissociation and molecular collisional recombination were considered in their study:



Here a_1 , a_2 and a_3 are the photodissociative production rates, the number of quanta absorbed per molecule per unit time by O_2 , O_3 , and CO_2 , respectively.

The assumption of photochemical equilibrium at every level in the atmosphere leads to the relations:

$$-a_3 n_{CO_2} + (K_4 n_M + K_5) n_{CO} n_O = 0 \quad (10)$$

$$-a_1 n_{O_2} + K_1 n_O^2 n_M - K_2 n_{O_2} n_O n_M + a_2 n_{O_3} + 2K_3 n_{O_3} n_O = 0 \quad (11)$$

$$K_2 n_O n_{O_2} n_M - a_2 n_{O_3} - K_3 n_{O_3} n_O = 0 \quad (12)$$

Furthermore, it can be seen that the total number of O atoms at any level contained in the O, O_2 and O_3 forms must be equal to the total number of O atoms released by CO_2 dissociation. For every molecule of CO_2 dissociated, one O atom is liberated, so that the total number of O atoms released in this way must be equal to the number of CO molecules produced. Thus, at any time

$$n_{CO} = n_O + 2n_{O_2} + 3n_{O_3} \quad (13)$$

Similarly, the total number of CO_2 molecules present at any level must be equal to the total number available $n_{CO_2}(0)$, less the number of CO molecules produced by dissociation:

$$n_{CO_2} = n_{CO_2}(0) - n_{CO} \quad (14)$$

Equations (10), (11), (12), (13) and (14) represent five relationships between five unknown quantities, n_O , n_{O_2} , n_{O_3} , n_{CO} and n_{CO_2} , so that a simultaneous solution for these quantities

is possible. By a succession of substitutions and rearrangements an expression for the number density of atomic oxygen n_0 in terms of known quantities can be derived:

$$n_0^4 + An_0^3 + Bn_0^2 + Cn_0 + D = 0 \quad (15)$$

where

$$A = \frac{a_3 n_M (K_2 K_3 - 2K_1 K_3 - 3K_1 K_2 n_M) - (K_4 n_M + K_5) (a_1 K_3 + 2a_2 K_1 n_M)}{E}$$

$$B = \frac{-a_3 (K_2 K_3 n_{CO_2}(o) n_M + 2a_2 K_1 n_M + a_1 K_3) - (K_4 n_M + K_5) a_1 a_2}{E}$$

$$C = \frac{a_3 (a_1 K_3 n_{CO_2}(o) - a_1 a_2)}{E}$$

$$D = \frac{a_1 a_2 a_3 n_{CO_2}(o)}{E}$$

and

$$E = n_M (K_4 n_M + K_5) (K_2 K_3 - 2K_1 K_3 - 3K_1 K_2 n_M) .$$

This quartic algebraic equation may be solved analytically or numerically for n_0 .

With a knowledge of n_0 , the O_3 number density can be evaluated from

$$n_{O_3} = \frac{K_1 K_2 n_0^3 n_M^2}{a_1 (a_2 + K_3 n_0) - K_2 K_3 n_0^2 n_M} \quad (16)$$

and, with a knowledge of n_0 and n_{O_3} , the O_2 number density can be calculated from

$$n_{O_2} = \frac{(a_3 + K_3 n_0) n_{O_3}}{K_2 n_0 n_M} \quad (17)$$

Finally, the number densities of CO and CO₂ can be obtained from equations (13) and (14).

The photodissociation rates (a_i 's) required for the evaluation of the above quantities may be expressed at any level z_1 as

$$a_i(z_1) = \int \left(\sigma_i(\nu) F(\nu, z_T) \exp \left(-\sec \theta \sum_{j=1}^3 \sigma_j(\nu) \int_{z_1}^{z_T} n_j(z) dz \right) \right) d\nu \quad (18)$$

where $\sigma_i(\nu)$ is the dissociation cross section of the i^{th} constituent at frequency ν , and $F(\nu, z_T)$ is the incident photon flux per unit frequency at the top of the Martian atmosphere. Frequency integration is carried out over the range in which the dissociation cross section of the i^{th} constituent has non-zero values.

The mean solar energy absorbed in the layer δz by the dissociation of CO₂, O₂ and O₃ may be expressed as

$$Q'(\delta z) = \frac{1}{\pi} \iint_{\nu \Omega} Q'(\nu, z_T) \left[\exp \left(-\sec \theta \sum_{j=1}^3 \sigma_j(\nu) \int_{z_1 + (\delta z/2)}^{z_T} n_j(z) dz \right) - \exp \left(-\sec \theta \sum_{j=1}^3 \sigma_j(\nu) \int_{z_1 - (\delta z/2)}^{z_T} n_j(z) dz \right) \right] d\Omega d\nu \quad (19)$$

where $Q'(\nu, z_T)$ is the solar energy of frequency ν incident at the top of the atmosphere, frequency integration is performed over the relevant ultraviolet and visible spectral regions, and integration over hour angle Ω is made between noon and sunset, as in equation (6). The relationship between the energy flux and photon flux at the top of the atmosphere is given by

$$F'(\nu, z_T) = (h\nu)^{-1} Q'(\nu, z_T) \quad (20)$$

In the present photochemical calculations, the spectral distribution of solar energy was obtained from several sources. At wavelengths shorter than 1800 \AA an energy distribution from Hinteregger, et al. (1965) was adopted, while between 1800 \AA and 2600 \AA , values of the solar flux were taken from Detwiler, et al. (1961). For wavelengths between 2600 \AA and 7000 \AA , the solar energies were obtained from the Handbook of Geophysics (compiled by Gast, 1957). The values of the solar flux given by these sources apply at the distance of the Earth from the sun. To compensate for the greater Mars - sun distance, they were multiplied by the appropriate reduction factor.

The dissociation cross sections σ_1 for O_2 , σ_2 for O_3 , and σ_3 for CO_2 , are also required for these calculations. For wavelengths less than 1700 \AA , σ_1 and σ_3 were taken from Nicolet (1960). Values of σ_1 between 1700 \AA and 2200 \AA were taken from Watanabe (1958) and for wavelengths greater than 2200 \AA from London, et al. (1962). Estimates of σ_2 between 2300 \AA and 3000 \AA and in the Chappuis bands in the visible were obtained from Vigroux (1952) while for wavelengths shorter than 2300 \AA , the values of Inn and Tanaka (1953) were used.

The reaction rates K_1 and K_2 were taken from Kaufman and Kelso (1961) and K_3 was taken from Campbell and Nudelman (1960). A value of K_4 suggested by Bates and Witherspoon (1952) was used, and K_5 was assumed to be zero. The values adopted for the reaction rates are

$$\begin{aligned}
 K_1 &= 3.0 \times 10^{-33} \text{ cm}^6 \text{ mol}^{-2} \text{ sec}^{-1} \\
 K_2 &= 1.2 \times 10^{-34} \text{ cm}^6 \text{ mol}^{-2} \text{ sec}^{-1} \\
 K_3 &= 9.0 \times 10^{-12} \exp(-2133/T) \text{ cm}^3 \text{ mol}^{-1} \text{ sec}^{-1} \\
 K_4 &= 5.0 \times 10^{-38} T^{1/2} \text{ cm}^6 \text{ mol}^{-2} \text{ sec}^{-1}
 \end{aligned}$$

Using these values of solar flux, dissociation cross sections and reaction rates, height distributions of CO_2 , CO , O , O_2 and O_3 were calculated for each of the thermal models of the lower atmosphere as follows. For the equilibrium temperature structure given by a particular model, the photodissociation rates (a_i 's) in the uppermost layer of the atmosphere were evaluated from equation (18). Next, equation (15) was solved numerically for n_0 , using the Newton-Raphson method of convergence, and the number densities n_{O_3} , n_{O_2} , n_{CO} and n_{CO_2} were determined from equations (16), (17), (13) and (14). These number densities were then used to determine new values of the dissociation rates for the top layer, and the cycle was continued until a convergent solution for the concentration of each gas in this layer was obtained. The solar energy absorbed in the uppermost layer was then calculated from equation (19), for this photochemical equilibrium distribution of gases. The calculation then proceeded to the layer immediately below, and the entire sequence was repeated.

Height distributions of composition and short-wave solar heating, consistent with the temperature structures calculated earlier, were obtained in this manner for each model. The validity of the temperature structures was examined in view of these photochemical considerations. The estimated effects of

photochemistry, eddy mixing and gravitational separation on the atmospheric models is discussed in the presentation of the results.

Numerical procedure.

In the evaluation of the mean rate of solar energy absorption in a given atmospheric layer $Q(\nu, z)$ and $Q'(\nu, z)$ from equations (6) and (19), integration over hour angle from noon to sunset was approximated by a summation over nine equal hour angle intervals, each with a characteristic zenith angle. The sunset hour angle Ω_s was calculated from equation (7). At sunset the zenith angle θ is $\pi/2$, so that, from (7)

$$\Omega_s = \arccos \left(-\tan(l) \tan(d) \right) . \quad (21)$$

For the Mariner coordinates Ω_s is $\sim 67^\circ$ so that each hour angle interval is $\sim 7.5^\circ$. The factor $1/\pi$ which precedes the integrals in these equations is required to obtain the mean value of the solar energy input over the total day ($\Omega = 2\pi$).

In the evaluation of absorption and emission in the 15μ CO_2 bands from equations (3), (4) and (5), cylindrical symmetry about the vertical was assumed. Integration over solid angle may then be replaced by integration over zenith angle, if the factor $d\Omega$ on the right hand side of these equations is replaced by the factor $2\pi \sin\theta d\theta$. θ -integration is performed from $\pi/2$ to π in equation (3), from 0 to $\pi/2$ in equation (4) and from 0 to $\pi/2$ in equation (5), where an additional factor of 2 must be included to take into account the fact that the layer radiates

over a sphere. In these integrations, nine angular steps of 10° each were used.

To test the sensitivity of the results to the height resolution of the models, calculations were performed using various layer thicknesses, ranging from 1 km to 10 km. Also, in some cases, the layer thickness was varied with altitude, with very thin layers (0.1 km) adjacent to the ground. No significant differences in the calculated temperature structures were observed as the height grid was varied within the 0.1 km to 10 km range. However, it was found that, since most of the numerical computation is involved with the evaluation of the required arrays of far infrared transmission functions, the time required by the computer to establish a convergent temperature structure increases approximately as the square of the number of layers. Use of layers of less than 1 km thickness was found to be uneconomical, while use of very thick layers resulted in the loss of interesting detail (such as the convective layer). A compromise was therefore made, with layers of 2 km, 3 km and 4 km thickness being used. Most of the models presented in the results (Models I thru VII) were calculated with a height scheme consisting of fifteen 2 km layers between the surface and 30 km altitude, ten 3 km layers between 30 km and 60 km altitudes, and ten 4 km layers between 60 km and 100 km altitudes. Some, however, (Models VIII and IX) were obtained for sixty uniform layers of 2 km thickness between the surface and the 120 km level.

An investigation was also undertaken to determine the effect on the calculated temperature distributions of refinement of the spectral intervals in the 15μ region. The strongest portion of this region (700 cm^{-1} to 600 cm^{-1}) was divided first into two 50 cm^{-1} wavenumber intervals, then into five 20 cm^{-1} wavenumber intervals. For each case an equilibrium structure was obtained for the lower 100 km of the Earth's atmosphere. The two temperature profiles which resulted differed by, at most, 3°K within the height range of the model, and both were in good agreement with normally observed temperature distributions (Figure 10). It was therefore deemed acceptable to use the broader spectral intervals in the present thermal calculations for the Martian atmosphere, in the interest of economy of computer time. In Table D.I of Appendix D, two groups of band parameters derived from the transmission tables of Stull, et al. (1963) are presented for the 15μ CO_2 bands. The second group, corresponding to broader spectral intervals, was adopted for the calculation of the necessary transmission functions in this study.

Results and Discussion

Lower atmosphere.

In all, nine basic models of the lower Martian atmosphere were constructed. The values of surface temperature and pressure and atmospheric composition adopted in each of these models are listed in Table III. Surface temperatures within the range 150°K to 220°K and surface pressures within the range 4 mb to 8 mb were considered. In five of the models, the atmosphere was assumed to be composed entirely of CO₂, while in the remaining four, an 80% CO₂ - 20% N₂ mixture was adopted.

The height distributions of temperature obtained for these cases are shown in Figures 11, 12 and 13. In these figures, the computed temperature structures are compared with those given previously by Johnson (1965) and Prabhakara and Hogan (1965). The temperature structures obtained for Models VIII and IX were found to be nearly identical (within 1°K at all levels), and in Figure 13, only one curve, that of Model VIII is shown to represent both models.

It is immediately apparent from Figures 11, 12 and 13, that while all of the model atmospheres obtained here are significantly warmer than the model of Johnson (1965), they are significantly colder than Model I of Prabhakara and Hogan (1965). Only Model IV of the present study attains a temperature slightly in excess of the Prabhakara and Hogan model

TABLE III

BASIC CHARACTERISTICS OF MODEL MARTIAN ATMOSPHERES

Model	Surface Temperature	Surface Pressure	Surface Number Density	Composition	
	(°K)	(mb)	(10^{17} mol/cm ³)	(%CO ₂)	(%N ₂)
I	160	4	1.81	100	0
II	180	5	2.01	100	0
III	200	6	2.17	100	0
IV	220	7	2.31	100	0
V	150	4	1.93	80	20
VI	175	5	2.07	80	20
VII	200	6.3	2.28	80	20
VIII	180	8	3.22	100	0
IX	180	8	3.22	80	20

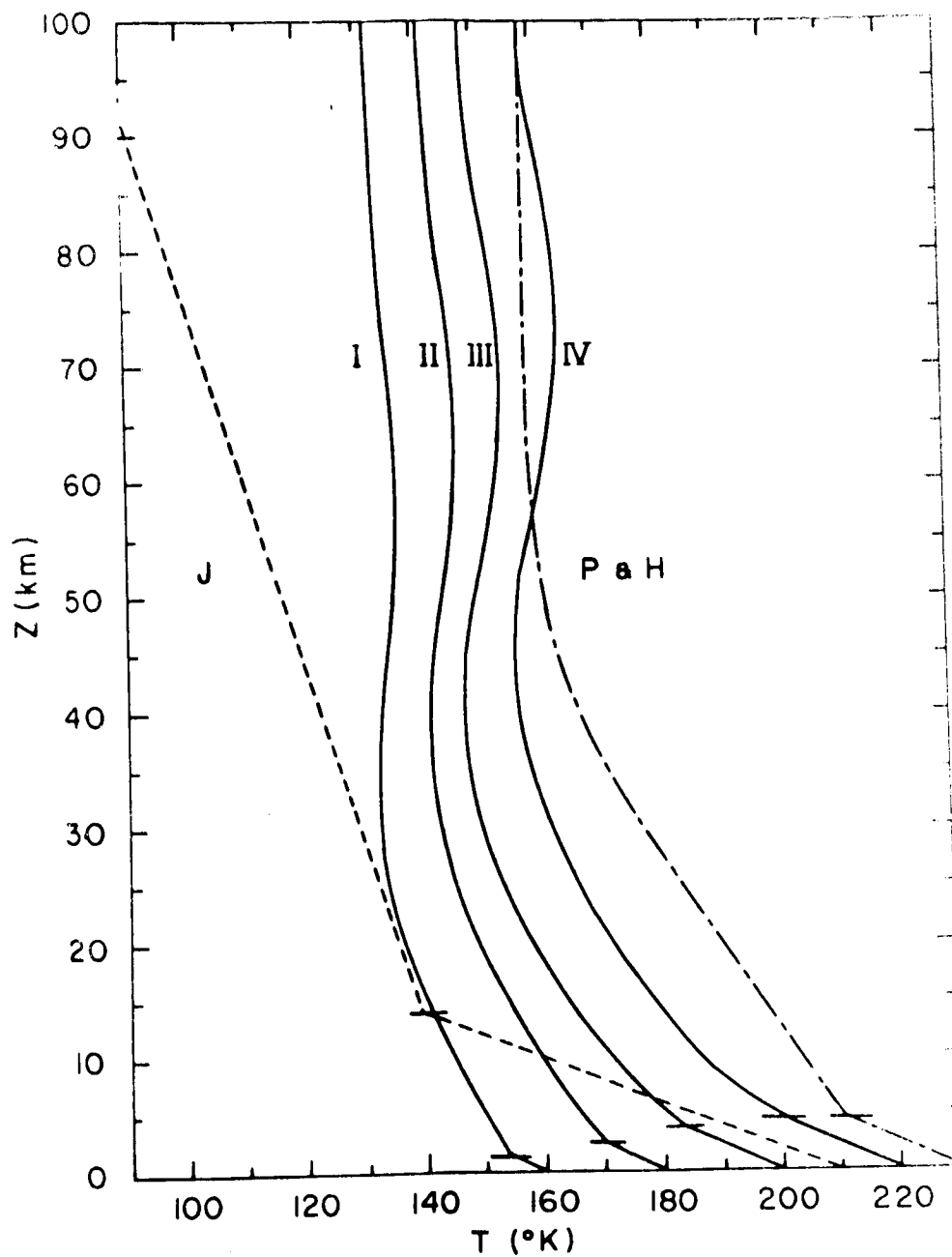


Figure 11. Martian lower atmosphere: Models I thru IV (100% CO₂). J: Johnson (1965); P&H: Prabhakara and Hogan (1965).

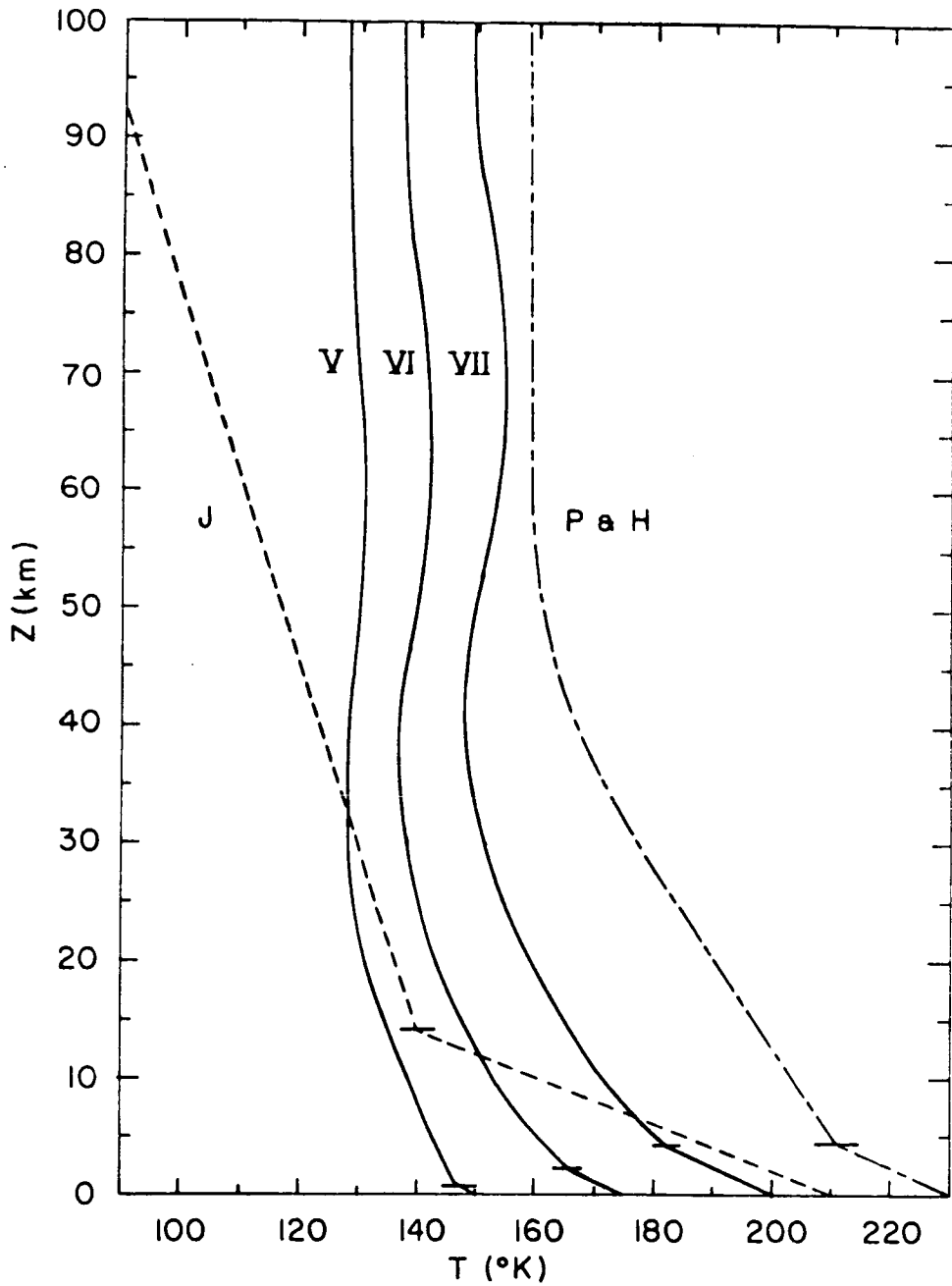


Figure 12. Martian lower atmosphere: Models V thru VII (80% CO₂ - 20% N₂). J: Johnson (1965); P&H: Prabhakara and Hogan (1965).

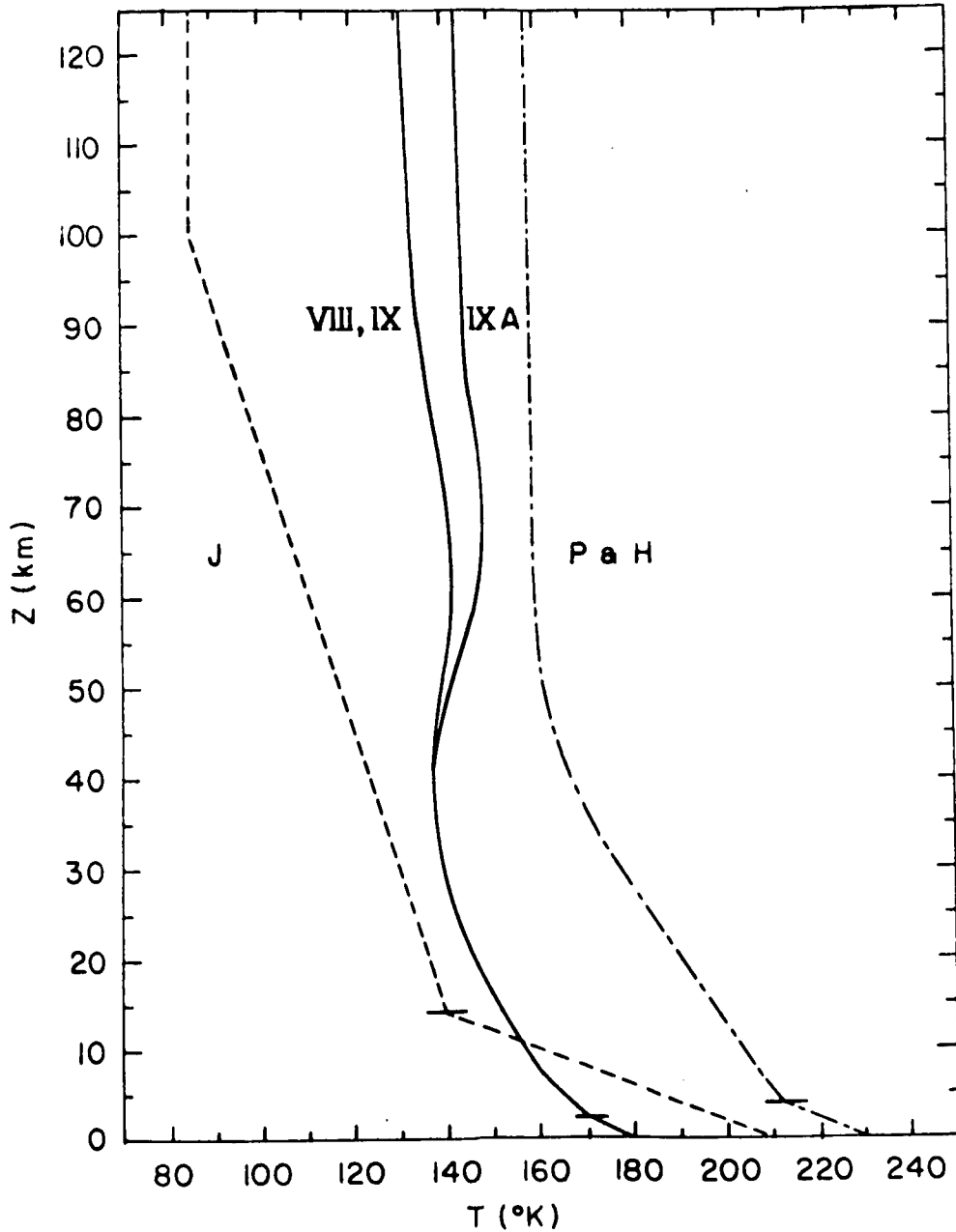


Figure 13. Martian lower atmosphere: Models VIII (100% CO_2), IX (80% CO_2 - 20% N_2), and IX A. J: Johnson (1965); P&H: Prabhakara and Hogan (1965).

(by $\sim 5^\circ\text{K}$), and this occurs only within a limited altitude span. On the other hand, the present models are colder than the Johnson (1965) model only near the surface, with much warmer temperatures (by at least 40°K) in the upper layers.

Models I, II, III, IV and VIII were constructed for an atmospheric composition of pure CO_2 , while Models V, VI, VII and IX were based upon an 80% CO_2 - 20% N_2 mixture. By examining these nine basic models, as depicted in Figures 11, 12 and 13, the effects of changes in the input parameters (surface temperature, surface pressure and composition) on the atmospheric structure can be estimated.

From both Figures 11 and 12, it can be seen that an increase in surface temperature results in a general elevation of atmospheric temperatures throughout the model. Also, this increase in atmospheric temperatures with the temperature of the ground is less pronounced in the higher layers of the atmosphere. In Figure 11, a 60°K increase in surface temperature from 160°K (Model I) to 220°K (Model IV) produces a rise of less than 30°K in the temperature at the 100 km level (131.6°K to 158.0°K). In Figure 12, a rise of 50°K in the ground temperature from 150°K (Model V) to 200°K (Model VII) is accompanied by an increase of less than 25°K near 100 km (127.9°K to 149.2°K). Thus, the range of temperature in the upper layers of both of these groups of models is less than one-half of the range in ground temperature.

It can also be seen from Figures 11 and 12, that the tropopause height increases in a linear fashion with the temperature of the ground. For the coldest value of surface temperature considered, 150°K (Model V, Figure 12) the tropopause level is found at ~ 0.5 km, while for the warmest surface temperature, 220°K (Model IV, Figure 11), the tropopause is located at ~ 4.5 km. Also, if a reasonable extrapolation is allowed, the calculations suggest that for a surface temperature below $\sim 140^\circ\text{K}$, no convective region would appear. The results seem to indicate, therefore, that the height of the tropopause on Mars (h_T) varies approximately according to the relationship

$$h_T = 4.5 (T_g - 140) / 80$$

where T_g is the surface temperature in °K and h_T is expressed in kilometers. The tropopause heights shown for the nine models follow this relationship fairly well, falling in every case within 0.25 km of the predicted level. It should be pointed out, however, that, due to the use of rather thick (2 km) height intervals in the construction of these models, the exact location of the tropopause is somewhat uncertain, and, therefore, the height of the tropopause shown in the figures represents to some degree an artistic interpolation on the part of the author. Nevertheless, in all the cases considered here, the tropopause level appears far below the 14 km height suggested by Johnson (1965). As can be inferred from the figures, radiative transfer is able to rapidly stabilize the

lower layers of the CO₂-rich Martian atmosphere, and as a result, only a thin convective region can develop. From radiative transfer, which was not considered in his study, the thick convective layer proposed by Johnson appears unjustifiable.

Comparison of Models II and VIII demonstrates the effect of variation of surface pressure from 5 mb to 8 mb when surface temperature (180°K) and composition (pure CO₂) are held fixed. An increase in surface pressure by 3 mb (60%) causes a slight reduction in temperature throughout the range of the models, with a maximum decrease of $\sim 3^\circ\text{K}$ near the 100 km level.

The similarity between Models VIII and IX shows that the variation of CO₂ concentration from 80% to 100% for a fixed surface temperature (180°K) and surface pressure (8 mb) has a very small influence on the thermal structure.

The real significance of these temperature profiles, however, lies in the number densities they produce at higher levels. The temperature, pressure and number density (on the basis of no photodissociation) obtained at the 100 km level in each model is given in Table IV, with corresponding values from Johnson (1965) and Prabhakara and Hogan (1965). As indicated in Table IV, the smallest number density obtained in any of the models at 100 km is larger by a factor of 3 or 4 than that obtained by Johnson. Also, the largest number density obtained at 100 km is more than an order of magnitude smaller than the relevant model of Prabhakara and Hogan indicates.

TABLE IV

TEMPERATURE, PRESSURE AND NUMBER DENSITY AT 100 KM

Model	T_{100} (°K)	P_{100} (mb)	n_{100}^* (mol/cm ³)
I	131.6	2.5×10^{-6}	1.4×10^{11}
II	141.3	9.0×10^{-6}	4.6×10^{11}
III	147.7	2.0×10^{-5}	9.9×10^{11}
IV	158.0	5.5×10^{-5}	2.5×10^{12}
V	127.9	4.4×10^{-6}	2.5×10^{11}
VI	137.0	1.0×10^{-5}	5.5×10^{11}
VII	149.2	2.9×10^{-5}	1.4×10^{12}
VIII	133.4	1.1×10^{-5}	5.7×10^{11}
IX	134.0	2.0×10^{-5}	1.1×10^{12}
Prabhakara and Hogan (1965)	158.5	1.2×10^{-3}	5.3×10^{13}
Johnson (1965)	85	$\sim 5 \times 10^{-7}$	$\sim 4 \times 10^{10}$

*

On the basis of a homogeneous atmosphere.

In the present models for a homogeneous atmosphere, a range in number density of 1.4×10^{11} mol/cm³ to 2.5×10^{12} mol/cm³ was obtained at the 100 km level, as compared to a value of $\sim 4 \times 10^{10}$ mol/cm³ given by Johnson and a value of 5.3×10^{13} mol/cm³ given by Prabhakara and Hogan. In Models VIII and IX, calculations were carried to the 120 km levels, with number densities of 2.9×10^{10} mol/cm³ and 6.5×10^{10} mol/cm³ being obtained at that level, respectively.

For a fixed composition the number density in the upper layers increases as the surface temperature is increased (Models I thru IV, V thru VII). Increasing surface pressure, with ground temperature and composition held fixed (Models II and VIII), has little effect on the number densities at higher levels, since the larger density at the ground is offset by a faster decrease in density with height in the cooler atmosphere produced. An increase in the CO₂ concentration, with surface pressure and temperature held fixed (Models VIII and IX) produces lower number densities in the upper layers, although the temperature distribution remains essentially the same, due to the decrease in scale height with the larger molecular weight.

An interesting feature appearing in all of the models examined is the blunt temperature maximum in the 65 km - 75 km region of the atmosphere. Such a maximum might be expected to result from the absorption of solar energy at these levels. This interpretation is not correct, however, as can be seen

from Figure 14. Model II A in this figure shows the thermal structure obtained for the same basic conditions adopted in Model II, in the absence of solar energy absorption in the atmosphere. Since a temperature maximum is obtained near 65 km in this model also, it must be a feature produced in some way by radiative transfer in the $15\ \mu$ CO_2 bands. The possibility of obtaining positive gradients of temperature under radiative equilibrium conditions in a non-grey atmosphere in the absence of solar heating has been noted by Goody (1964).

Analysis of the energetics involved in the determination of the atmospheric structure at these levels reveals the cause of this temperature maximum. The total $15\ \mu$ energy absorbed by each atmospheric layer per unit time was divided into two classifications: indirect radiation, originating in other atmospheric layers, and direct radiation, emanating from the planetary surface. Each of these classifications was further subdivided for examination according to spectral intervals. Thus, the energies of "atmospheric" and "surface" origin absorbed by each atmospheric layer in each of the chosen spectral intervals were obtained. It was found that an important contribution to the total $15\ \mu$ energy absorbed per unit time in the atmospheric layers between \sim 60 km and 70 km is the absorption of radiation directly from the surface in the weak intervals of the $15\ \mu$ CO_2 region.

Energy balance in the $15\ \mu$ region requires that the total $15\ \mu$ energy absorbed per layer be balanced by the total $15\ \mu$

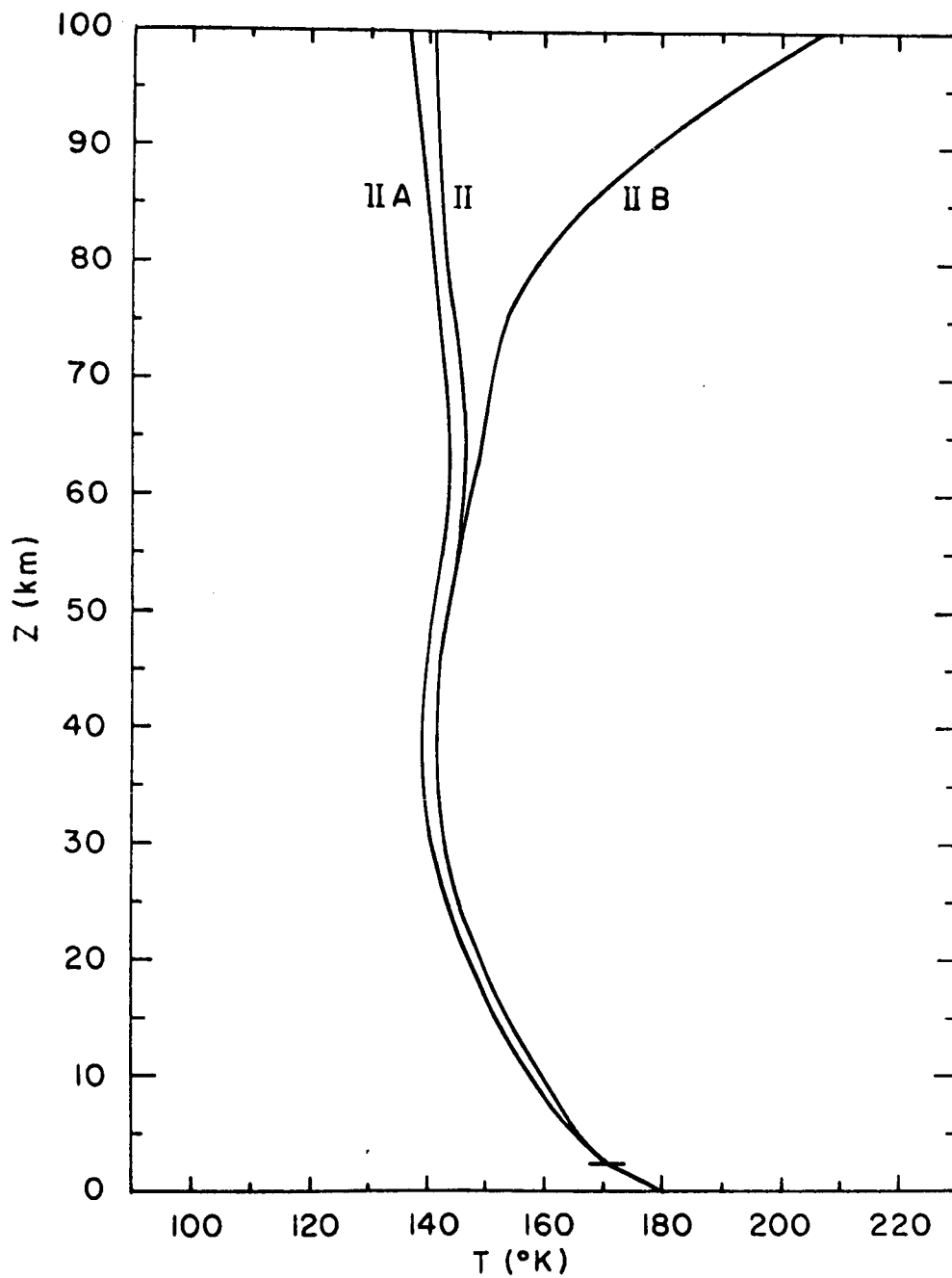


Figure 1/4. Martian lower atmosphere: Models II, II A and II B.

emission. Ordinarily, the largest contributions to both absorption and emission of energy in an atmospheric layer would be from the strongest spectral intervals near the center of the 15μ region. However, an increase, by some means, of the relative contribution of the weak intervals at the edges of the 15μ region to the total absorption of 15μ energy must be accompanied, under balance conditions, by a general increase in the 15μ emission, most of which will be accomplished by more intense radiative cooling in the strong central portion of this region. Thus, a rise in temperature must occur.

At levels in the present models, where the relative contribution of surface energy in the weak spectral intervals increases with height (between 20 km and 60 km in Model II A), the total 15μ energy absorbed per layer decreases less rapidly with height than does the opacity in the strong intervals near the center of the 15μ region. At higher levels, where the relative importance of the surface energy in the weak intervals decreases again (above \sim 65 km in Model II A), the total 15μ energy absorbed per layer decreases more rapidly with height than does the layer opacity near the band center. As a result, a temperature maximum is produced (between 60 km and 65 km in Model II A).

The absorption of a relatively large amount of surface radiation in the weaker portions of the 15μ region in the higher layers of these models is a result of the Doppler broadening mechanism. In the Martian atmosphere where very low pressures are encountered, the fractional absorption of

individual layers lies along the Doppler plateau (represented by the lowest line in the network of Figure D.VIII, Appendix D) throughout a considerable height range. Within this range, only small decreases in layer opacity with height occur, since fractional absorption varies slowly with pressure and path when the center of the Doppler broadened lines becomes saturated. By examining the fractional absorption per layer as a function of altitude, it can be seen that the Doppler plateau is reached at quite different levels by different spectral intervals, due to the large variation of mean line intensity from one spectral interval to another (Table D.I), with weak intervals attaining Doppler saturation at much lower levels than strong intervals. As a consequence of this Doppler effect, the overall decrease of layer opacity with height is more rapid in the lower atmospheric layers for strong intervals than for weak intervals. Since the opacity in the weak intervals increases relative to that of the strong intervals with height, and since the freely transmitted radiative flux from the surface in the weak intervals is larger than the strong-interval flux of atmospheric origin, the importance of weak-interval surface energy absorption increases with height relative to that of the strong-interval atmospheric energy absorption. In the vicinity of 60 km - 70 km in these models, absorbed energies of both types are of about equal weight.

Thus, the temperature maxima appearing in these models are a consequence of the Doppler broadening mechanism and the

non-grey representation of the 15μ CO_2 bands used in the present study. Such temperature maxima did not appear in the models of Prabhakara and Hogan (1965) since these authors did not consider the Doppler broadening effects. It can be seen from Figures 11 and 12 that the maxima appears at higher levels and becomes more pronounced as surface temperature is increased. The upward shift is a consequence of the rise in density at these levels which accompanies the increase in atmospheric temperatures, while the greater amplitude is due to the larger weak-interval radiative fluxes from the warmer surface.

This discussion is not intended to demonstrate that this temperature maximum is a real feature of the Martian atmosphere, but rather that a tendency toward such a maximum exists when non-grey radiative transfer by Doppler broadened lines is treated. For the particular band model and input parameters adopted in the present study, this temperature maximum is produced. Refinement of the spectral intervals, or a different choice of band parameters might remove this feature, but the latent tendency toward its appearance would still be present. Were the relative contribution of surface emission in the weak intervals of the 15μ region to the total absorbed 15μ energy decreased by some means, the general radiative structure of the atmosphere would nevertheless be preserved, with a lowering of atmospheric temperatures in the upper portions of all these models, by $\sim 5^\circ\text{K}$ in the colder cases to $\sim 10^\circ\text{K}$ in the warmer ones. A small reduction in the number densities at higher levels would follow.

In all of the nine basic models, a value of 10^{-6} sec at a pressure of one atmosphere was adopted for λ , the vibrational relaxation time in the 15μ CO_2 band. The value of Φ , the radiative lifetime in this band is $\sim 4.12 \times 10^{-1}$ sec (Appendix B). Moreover, in these basic models, the $1\mu - 6\mu$ near infrared CO_2 bands where solar energy is absorbed were assumed to relax in the same manner as the 15μ region. A mean relaxation time λ' and mean radiative lifetime Φ' were defined for the near infrared bands (equation 6) and, in the nine basic models, the ratio λ'/Φ' was assumed to be the same as the ratio λ/Φ in the 15μ fundamental. As can be seen from equations (6) and (9), when near and far infrared bands relax in the same way (i.e. $\lambda'/\Phi' = \lambda/\Phi$), the solar energy source term in the balance relationship (9) takes the same form as if no relaxation were present; all of the involved solar energy may be thought of as being absorbed and the atmosphere may be thought of as radiating with the Planck intensity. Since, as noted in Appendix B, it is likely that the $1\mu - 6\mu$ bands relax at higher pressures than the 15μ band (i.e. $\lambda/\Phi < \lambda'/\Phi'$), the assumption that $\lambda'/\Phi' = \lambda/\Phi$ probably results in an overestimate of the importance of solar energy in determining the temperature structure.

The influence of the absorption of solar energy on the models can be seen from a comparison of Models II and IIA (Figure 14). As mentioned above, an alternate model was constructed for the same conditions as Model II, except that no solar energy input into the atmosphere was considered. The resulting Model II A is found to be colder throughout, but by a

very small amount, with a maximum decrease in temperature of $\sim 4^\circ\text{K}$ in the upper layers. This slight decrease in atmospheric temperatures when solar energy is removed altogether implies that, even if near infrared scattering becomes important at levels far below that altitude at which the 15μ band relaxes, the atmospheric temperature profile for a given model could not fall below this "no solar energy" limit.

Also shown in Figure 14 is the temperature profile which would result for the same basic conditions as were adopted in Model II if, however, solar energy is not scattered, and only the 15μ band relaxes, with a lifetime of 10^{-6} seconds. As can be seen from Model II B, under these circumstances, above 55 km, where relaxation in the 15μ band occurs, temperatures rise to a value in excess of 200°K near the 100 km level. Were a value larger than 10^{-6} sec used for the 15μ relaxation time, non-LTE conditions would be reached at a lower altitude and even larger temperatures in the upper layers would result. Since relaxation certainly occurs in the near infrared bands, Model II B is of limited usefulness to the present study. However, it might be used for purposes of comparison to measure the effects of an external heat source, supplying energy directly to the kinetic mode, on the atmospheric structure under non-LTE conditions.

A case was also considered in which the near infrared bands were assumed to relax at higher levels than the 15μ band (i.e. $\lambda/\phi > \lambda'/\phi'$). For the same conditions as were adopted in Model IX, Model IX A was constructed, using a value of 10^{-5} sec

for λ and a value of 10^{-6} sec for λ' . As indicated by Figure 13, the thermal structure in this model becomes warmer than the Model IX structure in the upper layers, with temperatures rising from the Model IX values above ~ 40 km toward a maximum differential of $\sim 10^\circ\text{K}$ (144.3°K vs. 134.0°K) at the top of the model. The ratio $(1+\lambda/\phi)/(1+\lambda'/\phi')$ approaches a constant value of 10 at higher levels in Model IX A, as opposed to a value of unity in Model IX. Thus, more weight (10x) is given to the solar energy absorption in Model IX A and the balance temperature is increased accordingly. The solar energy source term, in equation (9), $Q(\delta z)(1+\lambda(z_1)/\phi)$, although uniformly larger in the upper layers of Model IX A than at corresponding levels in Model IX, nevertheless decreases with height in the same manner as does the term representing 15μ absorption ($A^\uparrow(\delta z) + A^\downarrow(\delta z)$). (Both terms are of approximately the same size in Model IX A, but the former is 10x smaller than the latter in Model IX.) Therefore, the temperature does not increase markedly with height in Model IX A but approaches a fairly constant value, slightly in excess of the Model IX temperatures. Because of the warmer temperatures, a slight increase in density at the 100 km level from 1.1×10^{12} mol/cm³ in Model IX to 1.5×10^{12} mol/cm³ in Model IX A results.

The relative values of the relaxation times adopted for Model IX A place undue emphasis on the importance of solar energy absorption. Nevertheless, no great increase in temperature due to this effect is observed. It should be emphasized that, since the relaxation time is probably longer in the near

than in the far infrared bands, the profiles obtained for the nine basic models are probably accurate representations of the thermal structure for the surface pressure, surface temperature and composition assumed in each case, regardless of the exact value of the relaxation time in the 15μ band.

For each of the nine basic thermal models obtained, a photochemical equilibrium distribution of the atmospheric gases was computed, using the values of the solar flux, photodissociation cross-sections and recombination rates referred to previously. A consistent distribution of the solar energy absorbed in the photodissociation processes involved was calculated simultaneously. In all nine cases, almost identical distributions of gases were obtained, with, however, slight upward or downward displacements in the level of maximum photochemical activity, due to vertical shifts in density levels caused by the variation in atmospheric temperatures and assumed composition from model to model. Due to the extreme similarity in all of the resulting chemical structures, only one is shown (Figure 15), that corresponding to thermal Model IX.

As illustrated in Figure 15, CO_2 , the principal constituent in the lower atmosphere is highly dissociated above ~ 75 km where the region of maximum photochemical activity appears. The abundances of CO and O at higher levels are equal, and both decrease with altitude with the scale height of CO_2 . As a result of a three-body O recombination process, a layer of O_2 is formed, with a maximum concentration of $\sim 4 \times 10^{12}$ mol/cm³ near 75 km. The importance of the formation of O_2 from the

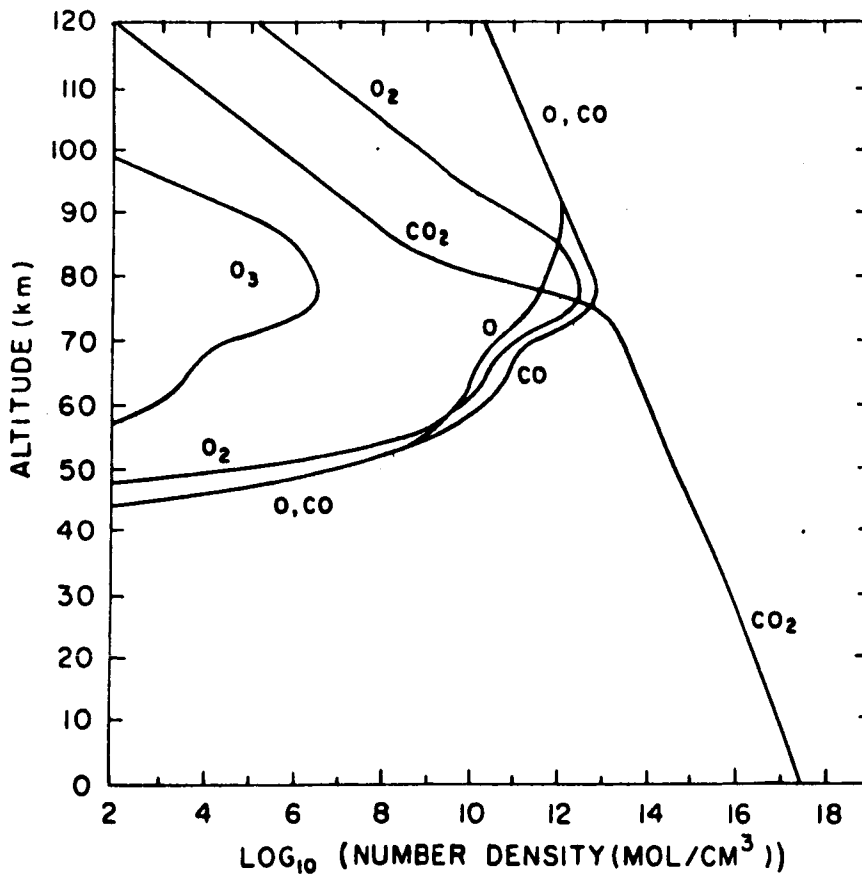


Figure 15. Photochemical equilibrium distribution of gases corresponding to thermal model IX.

dissociation of CO_2 in a planetary atmosphere was first stressed by Chamberlain (1962). Since O_2 absorbs strongly in the same region of the ultraviolet where CO_2 absorption occurs, the presence of an O_2 layer such as that in Figure 15 serves to shield the CO_2 at lower levels from dissociating solar energy. This effect is seen in the large decrease in the concentration of CO_2 between 75 km and 80 km, the region in which the O_2 opacity below 1880 \AA becomes quite large. The total amount of O_2 contained in this layer is $\sim 3.8 \times 10^{18} \text{ mol/cm}^2$ or $\sim 14 \text{ cm-atm}$, well below the 70 cm-atm upper limit suggested by the observations of Kaplan, Münch and Spinrad (1964).

Another three-body recombination reaction of O_2 and O results in the production of a subdued O_3 layer which also peaks in the vicinity of 75 km in this model, with a maximum concentration of $\sim 4 \times 10^6 \text{ mol/cm}^3$. The O_3/O_2 ratio near the maxima in the concentrations of these gases is thus $\sim 10^{-6}$, approximately the same as the value of this ratio near the O_3 maximum in the Earth's atmosphere. The total amount of O_3 present is only $\sim 3.4 \times 10^{12} \text{ mol/cm}^2$ or $\sim 1.25 \times 10^{-5} \text{ cm-atm}$. The influence of this O_3 layer on the concentrations of the other gases present and on the energy balance of the atmosphere is therefore negligible.

The high degree of CO_2 dissociation in the upper layers of this model is a direct result of the choice of K_4 , the rate for the three-body recombination of CO with O . The ratio of CO_2 to O_2 in the upper atmospheric layers is proportional to $(K_4 a_1 / K_1 a_3)$. Although a_1 , a_3 and K_1 are known within narrow

limits, the reaction rate K_4 is not well known. Barth (1964) has suggested a value for K_4 of $\sim 1.4 \times 10^{-34}$ cm⁶/sec, larger by more than two orders of magnitude than the value used in the present study. If Barth's value is correct, the CO₂ profile in Figure 15 would be shifted toward higher number densities by more than two orders of magnitude, so that the concentrations of CO₂ and O₂ in the upper layers would be of about the same order. CO₂ would nevertheless be strongly dissociated, since even the much larger value of K_4 given by Barth (1964) suggests that the CO molecule is stable against oxidation.

Evaluation of the solar ultraviolet energy absorbed per layer in establishing the distribution of gases shown in Figure 15 indicates that above the 75 km level, this energy source, if 100% efficient, would be much larger than the 1 μ - 6 μ infrared energy source corresponding to the same distribution. Below 75 km the near infrared energy source would strongly predominate, however. Since the concentration of CO₂ above \sim 75 km is sharply reduced by photodissociation, which results simultaneously in the deposition of a sizable amount of solar energy in the upper atmosphere, a temperature increase in the layers immediately above the region of maximum photochemical activity near 75 km would be expected from considerations of photochemical equilibrium and radiative transfer alone. However, if the photochemical equilibrium distribution of gases shown in Figure 15 were correct, with CO₂ highly dissociated, then other mechanisms, the ground state transition $O(^3P_1) \rightarrow O(^3P_2)$ in atomic oxygen,

radiation from the first vibrational and rotational levels of CO and the heat conduction process would assume the role of CO₂ radiative transfer in establishing a balance with the absorbed solar energy and determining the atmospheric temperature structure. These three processes, all of a thermostatic nature, would prevent the buildup of any large temperature gradients above ~ 75 km, so that even if photochemical equilibrium were a reasonable assumption, the temperature profiles given for Models I thru IX (Figures 11, 12 and 13) would remain basically correct, with the possibility of a slight warming in the upper layers.

The assumption that the atmospheric gases on Mars are present in a photochemical equilibrium distribution is highly questionable, however. The photodissociation lifetime of a CO₂ molecule in the upper atmosphere of Mars is of the order of one month, while the corresponding lifetime for O₂ is of the order of several days. One is forced to conclude, therefore, that turbulent mixing and/or molecular diffusion will greatly influence the distribution of gases. Stewart (1967), for a photochemical model very similar to that shown in Figure 15, has compared the photochemical lifetimes of the various constituents with their diffusion times. The diffusion time is the time required for the molecules of a particular species to diffuse through a distance equal to the scale height of the constituent. Stewart finds that the photochemical lifetimes for CO₂ and CO are greater than the diffusion time nearly everywhere, so that the photochemical equilibrium number densities of these

constituents are probably greatly in error. Also, at levels above and below the region of maximum photochemical activity, the profile of O is governed by diffusion, while the O₂ concentration is generally determined by photochemical activity except at levels below the maximum. Any removal of O₂ by downward diffusion, however, will result in a lowering of the level at which CO₂ becomes strongly dissociated. Stewart points out that, as a result of simple consideration of the interaction of photochemical and diffusive processes, and acceptance of the value of the reaction rate K_4 given by Barth (1964), it is necessary to conclude that CO₂ is dissociated to a point at which the total CO₂ amount remaining is less than the amount observed. A possible explanation of this discrepancy between theory and observation is based upon the experimental evidence of Harteck, et al. (1966), who suggest that CO may be rapidly oxidized in the presence of trace quantities of hydrogen compounds. If the water vapor observed on Mars is responsible for such oxidation of CO, then turbulent mixing must be present up to the levels where CO is produced, so that CO can gain access to the lower atmospheric layers, where the abundance of H₂O is relatively high. If this oxidation mechanism is correct, then the turbopause on Mars must be at least as high as the region of photochemical activity. (i.e. at levels above ~ 75 km).

While it is fairly certain that the photochemical equilibrium distribution of gases shown in Figure 15 is not a correct representation of the actual distribution of gases in the Martian atmosphere, no means is available at present for making

a more accurate determination of the chemical structure, due to uncertainties with regard to the principal recombination reactions involved, and the relative importance of eddy and molecular diffusion in the region of photochemical activity.

It is possible, however, to set reasonable upper and lower limits to the total number density at higher levels, based on the photochemical equilibrium distribution, for each model considered. The effect of strong eddy mixing in the upper layers would be an upward transport of CO_2 compensated by a downward flux of CO and O . Such a rearrangement of the constituents would imply that the total number density near the top of the models in the presence of strong mixing would be the same as indicated by the $\text{O} - \text{CO}$ curve (Figure 15) which, under photochemical equilibrium conditions, falls off with the scale height of CO_2 . On the other hand, molecular diffusion under the influence of Martian gravity would tend to increase the concentrations of all constituents at higher levels over the values indicated in Figure 15, with each gas being distributed according to its own scale height above the turbopause. Since the concentrations of the lighter dissociation products O and CO would decrease more slowly with altitude than is indicated by photochemical considerations, one would expect these gases to rapidly become more abundant than the $\text{O} - \text{CO}$ profile in Figure 15 indicates. A reasonable upper limit to the total number density at levels some distance above the region of maximum

photochemical activity would be given by the diffusive profile for O.

The total number density determined from basic thermal considerations alone, neglecting photochemistry, mixing and molecular diffusion may, therefore, be thought of as a lower limit to the actual number density at higher levels, while the diffusive O profile above the level of maximum O concentration may be considered an upper limit. An estimated lower limit to the neutral particle number density at ionospheric levels in Models I thru VII was obtained as follows. The temperature at the top of each of these thermal models was adopted as characteristic of the mean temperature between the 100 km level and the level of the ionosphere (124 km). Using this temperature, an estimate of the mean scale height for CO₂ (or a CO₂ - N₂ mixture), in this region of the atmosphere was obtained for each model, and the 100 km number density was extrapolated to the ionospheric level. The lower limit to the number density just below ionospheric levels (at 120 km) has already been cited for Models VIII and IX, so that a similar extrapolation yields the number densities for these models at the ion peak. The upper limit to the neutral particle density in the ionosphere was obtained by extrapolating the O concentration from the level of the O maximum to the 124 km level, using a characteristic scale height for O determined from the basic thermal structure for each model. The upper and lower limits to the total

neutral number density at 124 km obtained in this way are listed in Table V.

If the computed thermal structures for the nine basic models (Figures 11, 12 and 13) are accepted, then the lower limits given in Table V for the neutral particle density at the level of the ionosphere in each model is indeed a lower limit. No physical process can produce a number density smaller than this value for the given thermal structure. The thermal profiles depicted in the figures may, however, constitute slight overestimates (by $\sim 5^\circ\text{K}$) of the true radiative equilibrium temperatures in the upper atmosphere for each case, due to overemphasis of both solar energy input and absorption of weak-interval surface radiation in the higher layers of the models. If, in fact, solar radiation has negligible influence on the atmospheric temperature structure below ionospheric levels, and if the temperature maximum indicated in the figures is not a real feature of the Martian atmosphere, then both the lower and upper limits to the neutral ionospheric number density given in Table V would be reduced by $\sim 50\%$.

If one accepts a surface temperature in the range 180°K to 200°K , a surface pressure in the range 5 mb to 8 mb and a composition of 80% to 100% CO_2 as an accurate description of the basic conditions in the lower Martian atmosphere at the time and place of Mariner IV occultation, then these considerations indicate that the neutral number density in the observed ionosphere

TABLE V

ESTIMATED RANGE OF NEUTRAL NUMBER DENSITY AT IONOSPHERIC LEVEL

Model	Lower Limit (mol/cm ³)	Upper Limit (mol/cm ³)
I	3.6x10 ⁹	1.3x10 ¹¹
II	1.6x10 ¹⁰	2.3x10 ¹¹
III	3.9x10 ¹⁰	3.4x10 ¹¹
IV	1.2x10 ¹¹	5.0x10 ¹¹
V	7.6x10 ⁹	1.7x10 ¹¹
VI	2.3x10 ¹⁰	2.5x10 ¹¹
VII	7.2x10 ¹⁰	4.2x10 ¹¹
VIII	1.6x10 ¹⁰	2.4x10 ¹¹
IX	3.7x10 ¹⁰	2.9x10 ¹¹

was between $\sim 10^{10}$ mol/cm³ and $\sim 10^{11}$ mol/cm³. The smaller value is representative of mixed conditions, with CO₂ the most abundant gas at ionospheric levels, and the larger value is characteristic of a gravitationally separated upper atmosphere, with O the principal constituent in the ionosphere. All of the values within this range are much larger than the 2×10^9 mol/cm³ proposed by Johnson (1965) and more than an order of magnitude smaller than the 5×10^{12} mol/cm³ obtained by Chamberlain and McElroy (1966), using the lower atmospheric model of Prabhakara and Hogan (1965). On these grounds, the ionospheric models proposed by these authors cannot be correct.

Ionosphere.

In view of the results of the photochemical and radiative transfer calculations described above, it appears that the most abundant gas at ionospheric levels on Mars must be either CO₂ or O, the former if mixing governs the distribution of gases and the latter if the constituents are gravitationally separated at that level. Moreover, indications are that the total number density at the height of the ionosphere, if the turbopause is located near ionospheric levels would be $\sim 10^{10}$ mol/cm³, while if the turbopause is found nearer the region of maximum photochemical activity, the total number density in the ionosphere would be $\sim 10^{11}$ mol/cm³. In the present section, an attempt is made to determine the principal constituent, main ionic reactions and atmospheric conditions at the level of the ionosphere on Mars.

Suppose that O is the main constituent at and above the ionospheric level on Mars, and is distributed with its own scale height. Then O^+ will be the principal ion formed by the ionizing EUV solar radiation, with a maximum number density of O^+ occurring at the level where the neutral O density $n(O)$ is given by

$$n(O) = \frac{\cos \Theta}{\sigma(O) H(O)} \quad (23)$$

where Θ is the solar zenith angle, $\sigma(O)$ is the mean photoionization cross section for O, and $H(O)$ is the scale height for O at the ion peak. The value of Θ corresponding to Mariner IV immersion is $\sim 70^\circ$, the mean photoionization cross section for O is $\sim 10^{-17} \text{ cm}^2$ (Hinteregger, et al., 1965), and if the thermal models calculated in the present study are accurate, the scale height of O at ionospheric levels is $\sim 20 \text{ km}$. Thus we obtain a value of $\sim 2 \times 10^{10} \text{ mol/cm}^3$ for the O density at the level where a maximum in O^+ production occurs. The rate of formation of O^+ ions at the maximum is given by

$$Q(O^+) = F \sigma(O) n(O) \exp(-1) \quad (24)$$

max

where F is the total ionizing flux at the top of the atmosphere, $\sim 10^{10} \text{ photons/cm}^2 \text{ sec}$ (Hinteregger, et al., 1965). The value of $Q(O^+)$ at the ion peak is therefore $\sim 7.4 \times 10^2 \text{ ion pairs/cm}^3 \text{ sec}$, and if a balance between local production and loss of ions is assumed,

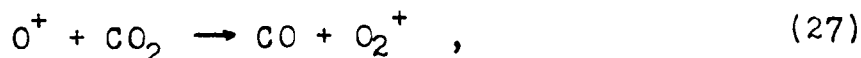
$$Q(O^+) - \alpha n^2(e) = 0 \quad (25)$$

where α is an effective recombination coefficient for electrons

with ions. Since a maximum ion number density of $\sim 9 \times 10^4$ electrons/cm³ was observed by Mariner IV, an estimate of about 9.1×10^{-8} cm³sec⁻¹ for α is obtained from this balance relationship. Such a value is characteristic of the dissociative recombination coefficient for the reaction



(Biondi, 1964), and suggests that a faster reaction rapidly transforms the EUV produced O^+ into O_2^+ . Since it is well known that an abundance of CO_2 is present in the Martian atmosphere, a likely mechanism for this transformation is



for which a rate coefficient of 1.2×10^{-9} cm³sec⁻¹ has been proposed (Feshenfeld, et al., 1966).

At higher levels, where the atmosphere is optically thin in the ionizing frequencies, the ion production rate is given by

$$Q(\text{O}^+) = F \sigma(\text{O})n(\text{O}) , \quad (28)$$

or, from the above values of F and $\sigma(\text{O})$,

$$Q(\text{O}^+) \approx 10^{-7} n(\text{O}) . \quad (29)$$

On the other hand, the loss rate of O^+ from reaction (27) is

$$L(\text{O}^+) = 1.2 \times 10^{-9} n(\text{O}^+) n(\text{CO}_2) . \quad (30)$$

A balance between production and loss of O^+ ions implies that

$$10^{-7} n(O) = 1.2 \times 10^{-9} n(O^+) n(CO_2) \quad , \quad (31)$$

so that

$$n(O^+) \approx 10^2 \frac{n(O)}{n(CO_2)} \quad . \quad (32)$$

The suppression of a diffusion controlled F2 ion peak to a non-detectable level ($n(O^+)$ less than $\sim 10^4$ mol/cm³) requires that the abundance of CO₂ remain large enough to rapidly remove O⁺ ions via reaction (27). From expression (32), if $n(O^+)$ is to remain less than $\sim 10^4$, the inequality

$$\frac{n(O)}{n(CO_2)} < 10^2 \quad (33)$$

must hold, up to the level at which diffusion becomes the dominant mechanism for O⁺ removal.

At levels in the atmosphere where local loss of O⁺ ions is governed by ambipolar diffusion, the loss rate $L(O^+)$ may be written

$$L(O^+) = n(O^+) \frac{D(O^+, O)}{H(O)^2} \quad , \quad (34)$$

where $D(O^+, O)$ is the ambipolar diffusion coefficient for O⁺ ions in atomic oxygen, inversely proportional to $n(O)$. The level at which diffusive loss of O⁺ is equal to the loss via reaction (27) is reached at the point where

$$1.2 \times 10^{-9} n(CO_2) = \frac{D(O^+, O)}{H(O)^2} \quad . \quad (35)$$

Donahue (1966) finds that if $H(O)$ is ~ 50 km at this level

($T \sim 360^\circ\text{K}$), then the CO_2 concentration is related to the $n(\text{O})$ concentration via equation (35) by

$$n(\text{CO}_2) = 3 \times 10^{14} / n(\text{O}) \quad , \quad (36)$$

at the level where ambipolar diffusion becomes important.

Since inequality (33) must hold at this level also, simultaneous solution of (33) and (36) results in a value for $n(\text{CO}_2)$ of 2×10^6 and a value for $n(\text{O})$ of less than $\sim 2 \times 10^8$ mol/cm³ at the diffusion level. Such a value for O requires a decrease of two orders of magnitude (4.5 scale heights) in $n(\text{O})$ between the ion peak and the diffusion level. Due to the smaller scale height of CO_2 (2.75 CO_2 scale heights per O scale height), a decrease of $n(\text{CO}_2)$ by more than six orders of magnitude (12.4 scale heights) between ion maximum and diffusion level is implied. Thus a number density of CO_2 of $\sim 2 \times 10^6$ mol/cm³ at the diffusion level demands a number density of $\sim 5 \times 10^{11}$ at the ion peak. Such a value is larger by an order of magnitude than the number of O atoms initially assumed to be present as the main neutral constituent near the ion peak. Thus, an irreconcilible contradiction arises from the assumption of a predominately O - O^+ - O_2^+ ionosphere. The concentration of CO_2 required at higher levels to suppress an F2 peak, implies that CO_2 must be present near the ion peak in an abundance greater by far than that of O required to produce the peak.

Suppose, on the other hand, that CO_2 is the dominant constituent at 124 km, but that at higher levels diffusive

separation occurs and O rapidly predominates. Then the main ion produced at 124 km would be CO_2^+ . The mean ionization cross-section for CO_2 is slightly larger ($\sim 2x$) than the cross-section for O (Hinteregger, et al., 1965), but the smaller scale height (by a factor of ~ 2.75) implies (from the CO_2 analogy of equation (23)) that the maximum production of CO_2^+ ions would occur where the neutral density of CO_2 is $\sim 2.3 \times 10^{10}$ mol/cm³. The maximum rate of CO_2^+ ion production would be (from the CO_2 analogy to equation (24)) $\sim 1.7 \times 10^3$ ion pairs/cm³ sec. A balance between production and loss of CO_2^+ ions (via the CO_2 analogy of equation (25)) results in an estimate of the effective recombination coefficient for CO_2^+ ions of $\sim 2.1 \times 10^{-7}$ cm³ sec⁻¹. Such a value is slightly smaller than the $3.8 \pm 0.5 \times 10^{-7}$ cm³/sec estimated by Weller and Biondi (1967) for dissociative recombination of CO_2^+ ions with electrons. Nevertheless, it suggests that this may be the chief mechanism for ion removal. It is only reasonable to expect that, even if CO_2 is the main constituent in the ionosphere, at higher levels O will eventually predominate and O^+ will be the dominant ion formed. The same conditions must therefore be met for the suppression of the F2 ion peak as described previously, leading to the conclusion that at the level where the CO_2 number density is $\sim 2 \times 10^6$, the number density of O atoms must be less than $\sim 2 \times 10^8$. In this case, a decrease by a factor of 10^4 (9 scale heights) in CO_2 concentration must occur between ion peak and diffusion level, corresponding to a decrease in the O concentration by a factor of 2.6×10^1 (3.27 scale heights). Thus, the O number density

at the ion peak would be at most 4.5×10^9 mol/cm³, well below the CO₂ number density initially assumed to be present at that level, so that, with this interpretation, no contradiction arises.

A simple exercise demonstrates the ability of this interpretation to produce the ionospheric profile observed (Figure 8). It was assumed that the concentration of CO₂ at the ion peak was 2×10^{10} mol/cm³, that the O concentration at this level is 10x smaller (2×10^9 mol/cm³), and that both constituents are distributed according to their own scale heights above the peak. It was further assumed that both constituents are ionized by a solar flux of 10^{10} photons/cm² sec, CO₂ with a cross-section of 2×10^{-17} cm² and O with a cross-section of 10^{-17} cm². Dissociative recombination was assumed to proceed for CO₂⁺ and O₂⁺ with the rates of Weller and Biondi (1967) and Biondi (1964). CO₂⁺, O₂⁺ and total ion number densities were calculated at unit scale heights above the peak. The resulting neutral particle and ion densities are listed in Table VI. It can be seen that the total ion number density at the peak is quite close to the observed value, with approximately two-thirds of the ions at the peak CO₂⁺ and one-third O₂⁺; at higher levels, the ratio O₂⁺/CO₂⁺ increases, and at a level six CO₂ scale heights above the peak, this ratio is ~ 3 . By relating the CO₂ scale height intervals to altitude above the ion peak (124 km), it is possible to fit these total ion number densities to the observed electron profile (Figure 8). A reasonable fit is obtained using the tabulated values, if a scale height gradient of 1 km/scale

TABLE VI

IONOSPHERIC MODEL

Height Above Ion Peak [*]	Number Density (cm^{-3})				Electrons
	CO_2	CO_2^+	O	O_2^+	
0	2.0(10)**	6.5(4)	2.0(9)	2.7(4)	9.2(4)
1	7.4(9)	5.3(4)	1.4(9)	3.0(4)	8.3(4)
2	2.7(9)	3.6(4)	9.7(8)	2.8(4)	6.4(4)
3	9.8(8)	2.4(4)	6.7(8)	2.6(4)	5.0(4)
4	3.6(8)	1.4(4)	4.7(8)	2.2(4)	3.6(4)
5	1.4(8)	0.9(4)	3.2(8)	1.8(4)	2.7(4)
6	5.0(7)	0.6(4)	2.2(8)	1.4(4)	2.0(4)

Height [*] Above Ion Peak	Estimated Altitude (km)	Estimated Temperature (°K)
0	124	140
1	131	160
2	139	180
3	148	200
4	158	220
5	169	240
6	181	260

* measured in scale heights of CO_2

** powers of 10 are enclosed in parentheses, e.g.,
2.0(10) = 2.0×10^{-1} .

height CO_2 is used above the ion peak. This scale height gradient is consistent with the thermospheric model of Chamberlain and McElroy (1966). The altitude and temperature corresponding to each ion density level for this fit are also given in Table VI.

SUMMARY

The present construction of model atmospheres for Mars from detailed considerations of radiative transfer demonstrates that the low atmospheric temperatures proposed in order to identify the observed ionosphere as an F2 layer (Johnson, 1965; Fjeldbo, et al., 1966,a,b) cannot be attained if the physics of the atmosphere is properly taken into account. The present calculations also indicate that, if values of the basic atmospheric parameters more representative of the time and place of Mariner IV occultation are adopted, and if vibrational relaxation of CO₂ and Doppler broadening of the spectral lines are considered, then the Martian atmosphere is probably significantly colder than was shown by Model I of Prabhakara and Hogan (1965). Thus, the E-layer interpretation of Chamberlain and McElroy (1966) which was based upon this earlier model of the lower Martian atmosphere has no solid foundation.

For lower atmospheric conditions suggested by theory and observations, it is found, from considerations of photochemical, mixing and molecular diffusion processes in the light of the thermal structures obtained, that probable lower and upper limits to the neutral number density in the observed Martian ionosphere are $\sim 10^{10}$ mol/cm³ and $\sim 10^{11}$ mol/cm³ respectively, the former, CO₂, being attained if mixing extends to near-ionospheric levels, and the latter, O, being reached if gravitational separation predominates above the photochemically active region.

For the calculated thermal structures, at a zenith angle of $\sim 70^\circ$, the maximum rate of production of either CO_2^+ or O^+ ions occurs at the level where the neutral particle number density is $\sim 2 \times 10^{10} \text{ mol/cm}^3$. The effective recombination rate required to produce the observed electron number density maximum is $\sim 10^{-7} \text{ cm}^3/\text{sec}$, characteristic of dissociative recombination of O_2^+ , or possibly, CO_2^+ . The interpretation of an $\text{O} - \text{O}^+ - \text{O}_2^+$ ionosphere requires that CO_2 be the main constituent near the ion peak, in order to account for the suppression of a diffusion-controlled ion peak at higher levels, and thus involves a contradiction. On the other hand, the assumption that CO_2 and CO_2^+ are the main neutral and ionized constituents near the ion peak results in no apparent contradiction. In this case, the criterion for suppression of an F2 peak at higher levels requires that the O concentration near the ion peak be at least an order of magnitude smaller than the local CO_2 concentration.

Calculations from simple ionospheric theory of the CO_2^+ and O_2^+ abundances at and near the ion peak at 124 km, assuming neutral densities of $2 \times 10^{10} \text{ mol/cm}^3$ CO_2 and $2 \times 10^9 \text{ mol/cm}^3$ O at the peak, show that, although the concentration of O is only one-tenth of that of CO_2 at 124 km, nevertheless O_2^+ ions constitute about one-third of the total ion population at that level, due to the slower recombination rate for these ions. At a level three CO_2 scale heights ($\sim 25 \text{ km}$) above the peak, CO_2^+ and O_2^+ ions are equally plentiful, while at higher levels where the CO_2 concentration falls off, O_2^+ , and eventually O^+ , becomes the dominant ion.

The probable structure of the Martian atmosphere and ionosphere at the time and place of occultation indicated by the present investigation may be described as follows. The surface temperature was within the range 180°K to 200°K, the surface pressure was between 5 mb and 8 mb, and the composition of the atmosphere was 80% to 100% CO₂. The tropopause level lay between 2 km and 3.5 km above the surface of Mars, with temperatures decreasing at higher levels to values of 140°K - 150°K, 135°K - 145°K, and 130°K - 140°K at 50 km, 100 km, and 125 km respectively. The atmosphere is mixed up to near-ionospheric levels, but at and above the observed ion maximum molecular diffusion under the influence of Martian gravity is likely to predominate. There is little dissociation of CO₂ below ionospheric levels. The observed ion peak on Mars is an F₁-layer, with dissociative recombination of molecular ions the chief mechanism for electron removal. The neutral particle density at the ion peak, mainly due to CO₂, is 2×10^{10} mol/cm³. Two-thirds of the ion population at the peak is CO₂⁺, one-third is O₂⁺. A few CO₂ scale heights above the peak, O₂⁺ becomes the dominant ion, and at still greater altitudes, O⁺ ions must predominate. A gradient in scale height (temperature) of about 1 km/CO₂ scale height exists above the ion peak. It is possible, and, indeed, likely, that a true thermospheric structure, such as found by Chamberlain and McElroy (1966) and Stewart (1967), is present in the upper atmosphere of Mars.

The above description is consistent with the Mariner IV results as well as with recent spectroscopic evidence. In addition, it is in agreement with careful studies which indicate the presence of a warm thermosphere on Mars.

APPENDIX A
THE EQUATION OF RADIATIVE TRANSFER

The basic equation describing the transfer of radiation through a plane parallel atmosphere, Schwarzschild's equation, may be written

$$\mu \frac{dI(\nu, \mu, \tau^*)}{d\tau^*} = I(\nu, \mu, \tau^*) - J(\nu, \tau^*) \quad (\text{A.1})$$

where $I(\nu, \mu, \tau^*)$ is the specific intensity of the radiation

$J(\nu, \tau^*)$ is the source function

ν is the frequency of the radiation

$\mu = \cos \theta$

θ is the zenith angle

τ^* is the optical depth ($d\tau^* = -n(z)k(\nu, z)dz$)

$k(\nu, z)$ is the absorption coefficient

$n(z)$ is the number density of absorbing molecules

z is the geometric height above the planetary surface.

If suitable boundary conditions are specified, the equation of radiative transfer (A.1) can be solved by standard methods for the upward and downward directed specific intensities at optical depth τ^* , $I^\uparrow(\nu, \mu, \tau^*)$ and $I^\downarrow(\nu, \mu, \tau^*)$ respectively. Physically meaningful boundary conditions for a planetary atmosphere require that the downward intensity at the top of the atmosphere ($\tau^* = 0$) be zero,

$$I^\downarrow(\nu, \mu, 0) = 0 \quad , \quad (\text{A.2})$$

and that the upward directed intensity at the lower boundary ($\tau^* = \tau_g^*$) be the blackbody intensity of the planetary surface,

$$I^\uparrow(\nu, \mu, \tau^*_g) = B(\nu, \tau^*_g) \quad . \quad (A.3)$$

One method of solution of equation (A.1), involving Green's functions, proceeds as follows.

Equation (A.1), an inhomogeneous, linear, first order differential equation, has a solution since the corresponding homogeneous equation,

$$\mu \frac{dI(\nu, \mu, \tau^*)}{d\tau^*} - I(\nu, \mu, \tau^*) = 0 \quad , \quad (A.4)$$

has a solution. The solution of (A.4) for the upward intensity is of the general form

$$I^\uparrow(\nu, \mu, \tau^*) = C' \exp(\tau^*/\mu) \quad (A.5)$$

where C' is an arbitrary constant. Then the solution of (A.1) may be expressed as

$$I^\uparrow(\nu, \mu, \tau^*) = C'' \psi(\tau^*) + \int_{\tau^*}^{\tau^*_g} H(\tau^*, t) r(t) dt \quad (A.6)$$

where C'' is a constant to be determined by the lower boundary condition, and $\psi(\tau^*)$ is the solution of (A.4),

$$\psi(\tau^*) = C' \exp(\tau^*/\mu) \quad . \quad (A.7)$$

Also, $r(t)$ is the inhomogeneous term in the transfer equation,

$$r(t) = -J(\nu, t)/\mu \quad , \quad (A.8)$$

and $H(\tau^*, t)$ is the one-sided Green's function, here given by

$$H(\tau^*, t) = -\psi(\tau^*)/\psi(t) = -\exp(-(t-\tau^*)/\mu) \quad . \quad (A.9)$$

Substituting equations (A.7), (A.8) and (A.9) into (A.6), we obtain

$$I^\uparrow(\nu, \mu, \tau^*) = C' C'' \exp(\tau^*/\mu) + \int_{\tau^*}^{\tau^*_g} J(\nu, t) \exp(-(t-\tau^*)/\mu) \frac{dt}{\mu} \quad (A.10)$$

Applying the lower boundary condition (A.3) we have

$$I^\uparrow(\nu, \mu, \tau_g^*) = C' C'' \exp(\tau_g^*/\mu) = B(\nu, \tau_g^*) \quad , \quad (A.11)$$

so that

$$C' C'' = B(\nu, \tau_g^*) \exp(-\tau_g^*/\mu) \quad . \quad (A.12)$$

Substituting from expression (A.12) for $C' C''$ in (A.10), the relation for the upward directed specific intensity becomes

$$I^\uparrow(\nu, \mu, \tau^*) = B(\nu, \tau_g^*) \exp\left(-(\tau_g^* - \tau^*)/\mu\right) + \int_{\tau^*}^{\tau_g^*} J(\nu, t) \exp\left(-(t - \tau^*)/\mu\right) \frac{dt}{\mu} \quad . \quad (A.13)$$

By a similar sequence of operations, we derive the expression for the downward directed specific intensity. The solution of (A.14) for $I^\downarrow(\nu, \mu, \tau^*)$ is of the same form as given by (A.5). Then the general solution of (A.1) will be of the type

$$I^\downarrow(\nu, \mu, \tau^*) = C'' \psi(\tau^*) + \int_0^{\tau^*} H(\tau^*, t) r(t) dt \quad (A.14)$$

where C'' is a constant to be determined by the upper boundary condition, $\psi(\tau^*)$ is given by (A.7), and $r(t)$ is given by (A.8). $H(\tau^*, t)$ is here given by (A.9). Substituting from (A.7), (A.8) and (A.9) into (A.14), we obtain

$$I^\downarrow(\nu, \mu, \tau^*) = C' C'' \exp(\tau^*/\mu) + \int_0^{\tau^*} J(\nu, t) \exp\left(-(t - \tau^*)/\mu\right) \frac{dt}{\mu} \quad (A.15)$$

At the upper boundary, (A.2) applies, so that

$$I^\downarrow(\nu, \mu, 0) = C' C'' = 0 \quad . \quad (A.16)$$

Hence, expression (A.15) for the downward directed specific intensity becomes

$$I^\downarrow(\nu, \mu, \tau^*) = \int_0^{\tau^*} J(\nu, t) \exp\left(-\frac{(t-\tau^*)}{\mu}\right) \frac{dt}{\mu} \quad . \quad (\text{A.17})$$

For θ between $-\frac{\pi}{2}$ and $+\frac{\pi}{2}$, μ has a positive value, so that upward directed intensities will be regarded as positive. For θ between $\frac{\pi}{2}$ and $-\frac{\pi}{2}$, μ is negative, and the downward directed intensities will therefore be negative.

The upward and downward specific intensities may be written in terms of the atmospheric transmission function τ . The transmission of the atmosphere at frequency ν and zenith angle arc $\cos \mu$ between optical depths τ^* and t is

$$\tau(\nu, \mu, t-\tau^*) = e^{-\frac{(t-\tau^*)}{\mu}} \quad . \quad (\text{A.18})$$

Hence,

$$\frac{\partial \tau(\nu, \mu, t-\tau^*)}{\partial t} = -\frac{1}{\mu} e^{-\frac{(t-\tau^*)}{\mu}} \quad , \quad (\text{A.19})$$

and equations (A.13) and (A.17) may be written

$$I^\uparrow(\nu, \mu, \tau^*) = B(\nu, \tau_g^*) \tau(\nu, \mu, \tau_g^* - \tau^*) - \int_{\tau^*}^{\tau_g^*} J(\nu, t) \frac{\partial \tau(\nu, \mu, \tau^* - t)}{\partial t} dt \quad , \quad (\text{A.20})$$

and

$$I^\downarrow(\nu, \mu, \tau^*) = - \int_0^{\tau^*} J(\nu, t) \frac{\partial \tau(\nu, \mu, \tau^* - t)}{\partial t} dt \quad , \quad (\text{A.21})$$

respectively.

For the present problem, the specific intensities were expressed in terms of θ and z , rather than in terms of μ and τ^* . The relationship between τ^* and z is given by

$$\tau^*(z) = \int_z^{z_T} n(\xi) k(\nu, \xi) d\xi \quad , \quad (\text{A.22})$$

where z_T is the top of the atmosphere. (The actual height z_T chosen for the upper boundary is arbitrary, provided no significant contribution to the net flux of infrared energy originates above this level.) The maximum value of τ^* in the atmosphere occurs at the lower boundary z_g

$$\tau_g^*(z_g) = \int_{z_g}^{z_T} n(\xi)k(\nu, \xi) d\xi \quad . \quad (\text{A.23})$$

With these considerations, the specific intensities (A.20) and (A.21) may be written

$$I^\uparrow(\nu, \theta, z) = B(\nu, z_g) \tau(\nu, \theta, z-z_g) + \int_{z_g}^z J(\nu, \xi) \frac{\partial \tau(\nu, \theta, z-\xi)}{\partial \xi} d\xi \quad (\text{A.24})$$

and

$$I^\downarrow(\nu, \theta, z) = \int_z^{z_T} J(\nu, \xi) \frac{\partial \tau(\nu, \theta, \xi-z)}{\partial \xi} d\xi \quad , \quad (\text{A.25})$$

corresponding to solutions of the transfer equation (A.1) in the form

$$\frac{dI(\nu, \theta, z)}{ds} = -n(z)k(\nu, z)I(\nu, \theta, z) + n(z)k(\nu, z)J(\nu, z) \quad (\text{A.26})$$

where $ds = \sec dz$.

APPENDIX B

VIBRATIONAL RELAXATION OF THE CARBON DIOXIDE MOLECULE

An individual molecule may possess four modes of internal energy: translational, vibrational, rotational and electronic. Only the first three of these energy modes will be considered here. Because of the relatively large energies involved in electronic transitions, thermal radiation from excited electronic levels is not, in general, important in planetary atmospheres.

The translational or kinetic mode of molecular energy is unquantized; a molecule may possess any amount of kinetic energy and may freely exchange this energy in collisions with other molecules. (A molecular collision, by definition, involves an interchange of kinetic energy.) Since there is a rapid adjustment to equilibrium (Boltzmann's law) in this mode, the molecular velocity distribution is continuous and Maxwellian in nature up to very great heights in a planetary atmosphere (Spitzer, 1952). The mean translational energy of the molecules is an observable quantity and therefore the temperature of a gas is usually defined as the kinetic temperature or that associated with the molecular velocities.

The vibrational and rotational internal energy modes are quantized; only discrete energy levels are possible and a number of rotational energy levels are associated with each vibrational level. Thus, a given vibrational transition can occur in combination with any one of a number of rotational transitions.

The probability of energy transfer between vibration - rotation and translation during a collision is less than one, and a number of collisions f normally occurs before an energy exchange between vibrational - rotational and translational modes takes place. If the collision rate in the gas is f_c , then the relaxation time λ , or mean time for loss or gain of energy by the vibration - rotation modes by collision is given by

$$\lambda = \frac{f}{f_c} \quad (\text{B.1})$$

where λ is a function of the pressure p and the temperature. Since the collision frequency is directly proportional to the pressure, at a given temperature

$$\lambda = \left(\frac{p_0}{p} \right) \lambda_0 \quad (\text{B.2})$$

where λ_0 is the relaxation time at a reference pressure p_0 . The pressure variation of λ is the one of importance, since pressure varies by many orders of magnitude in a planetary atmosphere, while temperatures are ordinarily confined to a relatively narrow range.

In addition to excitation and deexcitation by collisional processes, transitions between vibrational or rotational levels may result from the absorption or emission of a quantum of radiant energy. Any excited molecule has a (statistical) natural lifetime for spontaneous deexcitation by a radiative transition. Curtis and Goody (1956) have shown that, if the Planck function does not vary much within a vibration - rotation band, a

radiative lifetime for such a band may be expressed as

$$\Phi^{-1} = 8\pi \left(\frac{\nu_0}{c}\right)^2 \int k_\nu d\nu \quad (\text{B.3})$$

where Φ is the radiative lifetime, ν_0 is the central frequency of the band, c is the velocity of light and $\int k_\nu d\nu$ is the band intensity or integrated absorption.

When pressure is high and collisions are frequent there is a rapid exchange of energy between vibration - rotation and translation, and the energy levels of the vibrational and rotational states are populated in a Boltzmann distribution due to collisions. Under these circumstances, the vibrational or rotational temperature is equal to the kinetic temperature. The gas is said to be in a state of local thermodynamic equilibrium (LTE) and it radiates according to Kirchhoff's and Planck's law. Due to the frequent collisions, there is strong coupling between matter and the radiation field.

As pressure decreases, collisions become less frequent and the transfer of energy between vibration - rotation and translation becomes less rapid. The relaxation time increases and eventually becomes longer than the radiative lifetime. When this occurs, the energy involved in deexcitations will be lost to the radiation field. Moreover, when a photon with a frequency lying within the range of the relaxing band is absorbed by a molecule, it will on the average be reemitted without passing into the kinetic energy of the gas or translational mode. Under these conditions, the gas is said to undergo "relaxation" and the

atmosphere is said to be "scattering". Collisions are insufficient to maintain the vibration - rotation energy levels in a Boltzmann distribution in the presence of the radiation field. The radiation field will then determine the populations of these energy levels, and the coupling between matter and radiation will be weak. The gas no longer obeys Kirchhoff's or Planck's laws and is said to be in a state of non-local thermodynamic equilibrium (non-LTE). Therefore, at low pressures, one cannot properly relate the temperature of the gas to the vibrational - rotational energy levels without considering the relaxation process.

The 15μ vibration - rotation band of CO_2 is certainly the most important band for the transfer of infrared radiation in the lower atmosphere of Mars. Vibrational relaxation in this band must be taken into account in any radiative transfer study since it occurs at altitudes where CO_2 is present in abundant quantities. The level of vibrational relaxation in the 15μ CO_2 band depends simply on the adopted values of the relaxation time and radiative lifetime.

Rotational relaxation of CO_2 will be of no importance in this study. The energies involved in transitions between rotational energy levels is comparatively small, so that the probability of a rotation - translation transfer of energy in collisions is much greater than the probability of a vibration - translation interchange. The rotational relaxation time will therefore be many orders of magnitude smaller than the

vibrational relaxation time (Lambert, 1962), and rotational relaxation could occur only at very high altitudes (low pressures) where CO_2 is likely to be dissociated.

The 15μ vibration - rotation band of CO_2 is composed of a fundamental (ν_2 or "bending" mode of vibration) at 667.40 cm^{-1} and thirteen overtone and combination bands. The fundamental is by far the most intense of these bands, accounting for about 90 percent of the overall 15μ band intensity (Yamamoto and Sasamori, 1958; Madden, 1961). The band intensities of the sub-bands in the 15μ region are much smaller (Young, 1964). According to equation (B.3), therefore, the radiative lifetimes of the sub-bands are considerably longer than the lifetime of the fundamental. Unfortunately, no estimates of the relaxation times of the CO_2 sub-bands near 15μ have appeared in the literature. If however, the relaxation time of these bands is of the same order as the relaxation time of the fundamental (Young, 1964), they will relax at much higher levels, due to their longer radiative lifetimes. One might then assume that these subsidiary bands are in LTE in the lower region of the Martian atmosphere.

Since the contributions of the overtone and combination bands to the infrared energy flux are proportional to their intensities, their influence on the infrared transfer is small compared to the influence of the fundamental. Therefore, it is assumed in the present study, that the sub-bands relax in the same manner as the fundamental. The radiative lifetime and

relaxation time for the 15μ fundamental is used throughout the 15μ region. This assumption permits an enormous simplification of the computational procedure involved in calculating a temperature structure from energy balance considerations.

According to Madden (1961) the band intensity of the 15μ CO_2 fundamental is $194 \text{ cm}^{-2} \text{ atm}^{-1}$. Using this value for the intensity, one obtains a radiative lifetime of 4.12×10^{-1} sec. Experimental determinations of the vibrational relaxation time for the fundamental (Herzfeld and Litovitz, 1959; Lambert, 1962; Marriott, 1966) give estimates ranging from 10^{-5} sec to 10^{-6} sec at a pressure of one atmosphere. Vibrational relaxation in the 15μ CO_2 band should then occur at an altitude where the pressure is between $\sim 2.5 \times 10^{-2}$ mb and 2.5×10^{-3} mb.

The $1\mu - 6\mu$ near infrared CO_2 bands also undergo vibrational relaxation at low pressures. These bands are important for the absorption of solar energy, and this absorption could become large at high levels where the lines are unsaturated. However, a study of solar heating in the Earth's atmosphere by Mc Clatchey (1966) has shown that vibrational relaxation in these bands probably occurs far below the levels at which the stronger lines become unsaturated, so that the solar heating rates due to these bands are probably very small throughout the Earth's atmosphere. The same arguments would apply to Mars, and solar near infrared heating in the Martian atmosphere must be small also. According to Mc Clatchey (1966), relaxation of the intense ν_3 band of CO_2 near 4.3μ begins to exert a strong damping effect on the

heating in this band at pressures between 10^{-1} mb and 10^{-2} mb, and at lower pressures, almost complete scattering of solar energy occurs.

Thus, the near infrared bands relax at higher pressures than does the 15μ CO_2 band, and their influence on the temperature structure should be of little consequence. In order to assess their effect on the equilibrium distribution of temperature, however, a mean relaxation time λ' and radiative lifetime Φ' may be assigned to these bands as parameters for variation. The fraction of the interacting solar energy in these bands which is not scattered, but which passes into the kinetic mode and appears as local atmospheric heating will then be given by $(1 + \frac{\lambda'(z)}{\Phi'})^{-1}$ where, as in the case of the 15μ band, the relaxation time is inversely proportional to pressure.

APPENDIX C

RADIATIVE TRANSFER UNDER LTE AND NON-LTE CONDITIONS

The integral form of the transfer equation (A.26)

$$\iint \frac{dI(\nu, \theta, z)}{ds} d\nu d\omega = - \iint I(\nu, \theta, z) n(z) k(\nu, z) d\nu d\omega + \iint J(\nu, z) n(z) k(\nu, z) d\nu d\omega, \quad (C.1)$$

where ω is solid angle ($d\omega = 2\pi \sin\theta d\theta$), relates the divergence of the net flux of infrared radiation to the difference between the absorbed and emitted energies per unit volume at any level z . Here, frequency integration is performed over the transferring band(s) and integration with respect to solid angle ω is performed over both hemispheres.

If local dynamical or chemical sources and sinks of energy are absent, and if no radiation is absorbed at frequencies beyond the range of the integration in (C.1), radiative equilibrium conditions require that the infrared flux divergence be zero, so that there is a balance between absorbed and emitted infrared energies

$$- \iint I(\nu, \theta, z) n(z) k(\nu, z) d\nu d\omega + \iint J(\nu, z) n(z) k(\nu, z) d\nu d\omega = 0 \quad (C.2)$$

Since $I(\nu, \theta, z)$ is itself a function of $J(\nu, z)$ ((A.24) and (A.25)), expression (A.28) is an integro-differential equation for $J(\nu, z)$, which may be used to determine an equilibrium atmospheric structure, provided a relationship can be established between $J(\nu, z)$ and the local atmospheric conditions (including the local radiative field). In order to obtain a unique thermal

structure, however, the surface temperature T_g (which determines $B(\nu, z_g)$) and a form for the transmission function $\mathcal{T}(\nu, \theta, |z - \xi|)$ must be specified. The form and method of evaluation of the infrared transmission function is described in Appendix D.

If sources and sinks of energy outside of the range of the frequency integration in (C.1) are present, then, under radiative equilibrium conditions, the local infrared flux divergence must be equal to the local energy gain or loss $Q(z)$ from these sources and sinks:

$$\iint \frac{dI(\nu, \theta, z)}{ds} d\nu d\omega = Q(z) \quad . \quad (C.3)$$

We then have

$$Q(z) + \iint I(\nu, \theta, z) n(z) k(\nu, z) d\nu d\omega - \iint J(\nu, z) n(z) k(\nu, z) d\nu d\omega = 0 \quad , \quad (C.4)$$

which, with the above considerations, may be solved for a unique atmospheric structure also, if $Q(z)$ is known.

The relationship between $J(\nu, z)$ and the local conditions in the atmosphere varies with the collision frequency. In regions where collisions are frequent, $J(\nu, z)$ will simply be the "Planck" emission, expressed in terms of the gas temperature, and given by the relationship.

$$J(\nu, z) = B(\nu, T(z)) = \frac{2h\nu^3}{c^2 (\exp(h\nu/KT(z)) - 1)} \quad , \quad (C.5)$$

where h is Planck's constant, K is Boltzmann's constant and c is the velocity of light. As discussed in Appendix B, in low pressure regions where "relaxation" processes occur, molecular

collisions are too infrequent to maintain a Boltzmann distribution among the vibration - rotation energy levels. The atmosphere in such a region does not, therefore, radiate according to (C.5) and another form is required to properly relate $J(\nu, z)$ to local atmospheric conditions.

In their investigation of the problem of radiative transfer in a vibrationally relaxing gas, Curtis and Goody (1956) derived a general expression for the emission of the gas $J(\nu, z)$ which is applicable under low pressures. They have shown that if $\Delta\nu$, the band width is narrow, so that variation of the Planck function $B(\nu, z)$ over the band is small, then $J(\nu, z)$ will have the same dependence on frequency as $B(\nu, z)$ and will be isotropic. From their equation (10) (in the present notation),

$$J(z) = B(z) + \frac{\lambda}{\Phi} \frac{h(z)}{4\pi \int n(z)k(\nu, z) d\nu} \quad (C.6)$$

where $J(z)$ and $B(z)$ are the values of $J(\nu, z)$ and $B(\nu, z)$ at the band center ($J(\nu, z) \approx J(z)$ and $B(\nu, z) \approx B(z)$), and where

$$h(z) = - \iint \frac{dI(\nu, \theta, z)}{ds} d\nu d\omega \quad ,$$

it follows that the source function is related to the Planck function by

$$J(\nu, z) = B(\nu, z) \left\langle 1 - \frac{\lambda}{\Phi} \frac{\iint \frac{dI(\nu, \theta, z)}{ds} d\nu d\omega}{\iint B(\nu, z) n(z) k(\nu, z) d\nu d\omega} \right\rangle \quad (C.7)$$

This expression gives the nature of the source function in a vibrationally relaxing gas. For λ small (high pressure) this expression for $J(\nu, z)$ reduces to the Planck emission $B(\nu, z)$.

When an energy source or sink $Q(z)$ outside of the range $\Delta\nu$ is

present, in view of equation (C.3), the source function may be expressed as

$$J(\nu, z) = B(\nu, z) \left(1 - \frac{\lambda}{\Phi} \frac{Q(z)}{\iint B(\nu, z) n(z) k(\nu, z) d\nu d\omega} \right) . \quad (C.8)$$

This equation suggests that when the gas is relaxing, it does not radiate with Planck intensity in the band, but only with a fraction of $B(\nu, z)$, the fraction being given by the term in the brackets.

In order to calculate the temperature structure in atmospheric regions where radiative transfer of energy is important, we assume that radiative equilibrium conditions prevail, so that the energy balance described by equation (C.4) holds. Substituting from equation (C.8) in (C.4) we have

$$\begin{aligned} Q(z) + \iint I(\nu, \theta, z) n(z) k(\nu, z) d\nu d\omega & \quad (C.9) \\ = \iint B(\nu, z) \left(1 - \frac{\lambda}{\Phi} \frac{Q(z)}{\iint B(\nu, z) n(z) k(\nu, z) d\nu d\omega} \right) n(z) k(\nu, z) d\nu d\omega \end{aligned}$$

or,

$$\begin{aligned} Q(z) + \iint I(\nu, \theta, z) n(z) k(\nu, z) d\nu d\omega & \\ = \iint B(\nu, z) n(z) k(\nu, z) d\nu d\omega & \quad (C.10) \\ - \frac{\lambda}{\Phi} Q(z) \iint \left(\frac{B(\nu, z) n(z) k(\nu, z)}{\iint B(\nu, z) n(z) k(\nu, z) d\nu d\omega} \right) d\nu d\omega . \end{aligned}$$

Since $\iint B(\nu, z) n(z) k(\nu, z) d\nu d\omega$ is not a function of ν or ω but only of z , it may be extracted from the outer integral in the second term on the right hand side of (C.10), and cancelled with the numerator. Upon rearrangement of the remaining terms, we obtain

$$Q(z) \left(1 + \frac{\lambda}{\phi}\right) + \iint I(\nu, \theta, z) n(z) k(\nu, z) d\nu d\omega \\ = \iint B(\nu, z) n(z) k(\nu, z) d\nu d\omega \quad . \quad (C.11)$$

The factor $(1 + \frac{\lambda}{\phi})$ in the first term on the left hand side of (C.11) may be regarded as a factor amplifying external sources and sinks of energy to take into account the fact that the radiation emanating from a relaxing atmospheric layer is not related directly to or characteristic of the kinetic temperature of the layer alone. With the source function related to the temperature via equation (C.8), it is possible to calculate the radiative equilibrium temperature structure of the atmosphere by a simultaneous solution of (C.8) and (C.11).

The infrared flux divergence $\iint \frac{dI(\nu, \theta, z)}{ds} d\nu d\omega$ (equation (C.1)) determines the rate at which energy is exchanged between the vibrational - rotational energy levels and the radiation field. If these energy levels are perturbed, so that a Boltzmann distribution is no longer present, then the rate of energy transfer between vibrational - rotational and translational modes by collisions is given by (Curtis and Goody, 1956)

$$\frac{dE}{dt} = \frac{\bar{E}}{\lambda} \left(1 - \frac{E}{\bar{E}}\right) \quad , \quad (C.12)$$

where E is the total vibrational energy expressed in quanta per unit volume, and \bar{E} is the value of E under Boltzmann conditions. The "non-Boltzmann" source function $J(\nu, z)$ will then be related to the Planck function by

$$J(\nu, z) = B(\nu, z) \frac{E}{\bar{E}} \quad . \quad (C.13)$$

Equation (C.12) indicates that in high pressure regions, any perturbation in the vibrational populations from a Boltzmann distribution will rapidly decay. When pressure is low, however, significant departures from a Boltzmann distribution may persist indefinitely if, for example, a periodic perturbation such as solar heating is operating. But with cessation of a perturbing influence, the atmosphere will eventually reach a state of LTE, regardless of the collision frequency, as may be inferred also from equation (C.11) if $Q(z)$ is zero.

APPENDIX D
TRANSMISSION FUNCTIONS OF CARBON DIOXIDE

Line shape and mean line absorption.

The width and shape of a spectral line are influenced by three broadening mechanisms: collisional, Doppler and natural broadening. Collisional broadening arises out of molecular interactions while Doppler effects are due to molecular "line-of-sight" velocities. Natural broadening results from radiation damping.

In the case of non-interacting, stationary molecules, spectral lines have a finite width due to the uncertainty principle which predicts an uncertainty ΔE in an energy level. This uncertainty is related to the natural lifetime Φ of the molecule in the excited level by the expression (Goody, 1964)

$$2\pi \Delta E \Phi = h \quad (D.1)$$

where h is Planck's constant. Hence, all spectral lines involving transitions between ground and excited levels will have an uncertainty in frequency $\Delta \nu$, or natural half-width α_N , $(\Delta \nu/2)$, given by

$$\Delta \nu = \Delta E/h \quad , \quad (D.2)$$

or,

$$\alpha_N = \frac{1}{4\pi\Phi} \quad . \quad (D.3)$$

The variation of absorption coefficient within a naturally broadened line may be expressed as (Mitchell and Zemansky, 1934)

$$k(\nu) = \frac{1}{1 + \left(\frac{\nu - \nu_0}{\alpha_N}\right)^2} \quad . \quad (D.4)$$

Thus, natural line broadening is independent of all effects external to the molecule.

Normally, however, natural broadening of spectral lines is negligible in comparison with the Doppler effect, resulting from the thermal motions of the molecules and therefore related to the temperature. The Doppler half-width α_D and line shape are readily derived from kinetic theory (Aller, 1953). The theoretical expression for the Doppler half-width is

$$\alpha_D = \frac{\nu_0}{c} \left(\frac{2KT}{m} \right)^{1/2}, \quad (D.5)$$

where K is Boltzmann's constant and m is the mass of the absorbing molecule. We may therefore express the Doppler half-width as

$$\alpha_D = \alpha_{D_0} \left(\frac{T}{T_0} \right)^{1/2}, \quad (D.6)$$

where α_{D_0} is the value of α_D at reference temperature T_0 . The absorption coefficient within a Doppler broadened line is given by

$$k(\nu) = \frac{S}{\alpha_D \sqrt{\pi}} \exp\left(-\left(\frac{\nu - \nu_0}{\alpha_D}\right)^2\right), \quad (D.7)$$

where S is the integrated line intensity. Doppler broadening produces noticeable effects when absorption or emission of a gas under low pressures such as those encountered in the higher levels of a planetary atmosphere is considered.

When pressures are high, the line shape is determined by collisional broadening. Molecular interactions cause perturbations of the energy levels of the molecules, and, as a result of these perturbations, absorbed or emitted energies are spread

over a finite frequency range. In addition, the line center may be displaced toward lower frequencies by an amount proportional to the total pressure and the line shape may become asymmetrical. The classical theory of line shape and absorption coefficient within a pressure broadened line was developed by Lorentz, who found that

$$k(\nu) = \frac{S\alpha_L}{\pi} \frac{1}{(\nu - \nu_0)^2 + \alpha_L^2}, \quad (D.8)$$

where α_L is the half-width of the line due to collisions. The theoretical evaluation of the Lorentz half-width is difficult, and experimental values are normally used. From kinetic theory, the collision frequency depends upon the ratio p/\sqrt{T} , so that α_L , which is proportional to the collision frequency, is given by

$$\alpha_L = \alpha_{L_0} (T_0/T)^{1/2} (p^*/p_0), \quad (D.9)$$

where α_{L_0} is the measured Lorentz half-width at reference pressure p_0 and temperature T_0 , and p^* is an effective broadening pressure. For collisional broadening of CO_2 lines, p^* may be expressed as

$$p^* = p + .3p_{\text{CO}_2}, \quad (D.10)$$

where p_{CO_2} is the partial pressure of CO_2 . In a pure CO_2 atmosphere, a correction of about 30% to the total pressure is required to properly take into account the more effective self-broadening of CO_2 in computing the Lorentz half-width.

In addition to the Lorentz theory of collisional line shapes a number of alternate theories and modifications have been proposed (cf. Lindholm, 1945; Benedict, et al., 1956). There is nevertheless strong support for use of the basic Lorentz line profile (Curtis and Goody, 1956; Young, 1964), and it appears

that, due to the other inaccuracies involved in a study of this type, it would serve no purpose to consider non-Lorentzian line shapes for collisional broadening in lower layers of an atmosphere.

When all three broadening mechanisms act together, the line absorption coefficient takes the form (Mitchell and Zemansky, 1934)

$$k(\nu) = S \int_{-\infty}^{+\infty} \left(\frac{m}{2\pi KT} \right)^{1/2} \exp\left(-\frac{mU^2}{2KT} \right) \frac{\alpha_L}{\pi} \frac{dU}{(\nu - \nu_0 + U\nu_0/c)^2 + \alpha_L^2} \quad , \quad (D.11)$$

or, in view of (D.5),

$$k(\nu) = S \int_{-\infty}^{+\infty} \left(\frac{\nu_0}{\sqrt{\pi} c \alpha_D} \right) \exp\left(-\frac{\nu_0 U}{c \alpha_D} \right)^2 \frac{\alpha_L}{\pi} \frac{dU}{(\nu - \nu_0 + U\nu_0/c)^2 + \alpha_L^2} \quad , \quad (D.12)$$

where U is the mean molecular velocity. Making the substitutions

$$y = \left(\frac{mU^2}{2KT} \right)^{1/2} \quad , \quad (D.13)$$

$$v = \left(\frac{\nu - \nu_0}{\alpha_D} \right) \quad , \quad (D.14)$$

$$k(0) = \frac{S}{\sqrt{\pi} \alpha_D} \quad , \quad (D.15)$$

and
$$\alpha = \alpha_L / \alpha_D \quad , \quad (D.16)$$

equation (D.12) may be written (Plass and Fivel, 1953)

$$\frac{k(\nu)}{k(0)} = \frac{\alpha}{\pi} \int_{-\infty}^{+\infty} \frac{e^{-y^2}}{\alpha^2 + (v-y)^2} dy \quad . \quad (D.17)$$

Under low pressures, ($\alpha < .5$), Harris (1948) has shown that the right-hand side of (D.17) can be expressed as a Taylor series, $H(\alpha, v)$, so that

$$\frac{k(\nu)}{k(0)} = H(\alpha, v) = H_0(v) + \alpha H_1(v) + \alpha^2 H_2(v) + \dots \quad (D.18)$$

Band models.

Equations (D.20) and (D.21) represent the mean fractional absorption associated with a single spectral line. The calculation of the absorption or transmission over a finite spectral interval is extremely difficult due to the larger number and complex arrangement of the rotational lines in a vibration - rotation band. Various models have been proposed to represent the mean transmission function of the lines in a real band. The "regular" or Elsasser model (Elsasser, 1938, 1942) is based upon the assumption that the lines all have the same intensity and half-width and are uniformly spaced. The "statistical" model (Goody, 1952) assumes a random spacing of the line centers with the intensities represented by a probability function. The "random Elsasser" model of Plass (1958) is somewhat less restrictive, with the spectrum represented by a random distribution of several Elsasser bands, each with its characteristic line intensity and line spacing. Recently, Wyatt, et al. (1962) have introduced the "quasi-random" model, in which a spectral interval of interest is divided into a number of much smaller intervals, each of which contains a random distribution of lines. The lines in each sub-interval are grouped according to intensities, and the contribution to the absorption in the interval from the wings of lines outside of the interval is taken into account. This model is probably the most realistic representation of a spectral band introduced to date.

where the coefficients $H_i(v)$ are tabulated functions. The absorption coefficient within the line is thus given by

$$k(v) = \frac{S}{\sqrt{\pi}\alpha} H(\alpha, v) \quad . \quad (D.19)$$

From this expression for the absorption coefficient, the mean fractional absorption under low pressures for a spectral line, over an interval of width d equal to the mean line spacing, can be expressed as

$$\bar{K} = \frac{\alpha_D}{d} \int_{-d/2\alpha_D}^{+d/2\alpha_D} \left(1 - \exp(-k(v)u) \right) dv \quad (D.20)$$

where u is the optical path. \bar{K} is evaluated numerically by substituting the tabulated functions $H_i(v)$ of Harris (1948) in (D.19) for $k(v)$.

Van der Held (1931) has shown that when pressures are high ($\alpha > 1$), the mean fractional absorption for a spectral line of Lorentz shape is closely approximated by the Ladenburg-Reiche (1913) formula

$$\bar{K} = 1 - \exp\left(-\beta x e^{-x} (I_0(x) + I_1(x))\right) \quad , \quad (D.21)$$

where $I_0(x)$ and $I_1(x)$ are the Bessel functions of order zero and one and of imaginary argument, and where

$$\beta = \frac{2\pi\alpha_L}{d} \quad , \quad (D.22)$$

and

$$x = \frac{Su}{2\pi\alpha_L} \quad . \quad (D.23)$$

For calculations of temperature from energy balance considerations, it can be seen that, if the dominant terms in equation (9) are those representing the energy absorbed and emitted per unit volume in the 15μ CO_2 band, the effects of the local transmission function in this band on the temperature will be minimal, since this function has equal weight in both terms. Due to this compensatory effect, the choice of a particular band model does not critically affect the determination of atmospheric temperature. However, care must certainly be exercised in the choice of a band model when time dependent calculations involving the evaluation of heating rates are performed. For present purposes, the transmission or absorption of a gas can be adequately described by any one of several band models. For a linear, "well behaved" molecule such as CO_2 , line intensities and spacing are fairly uniform, and the Elsasser model closely approximates the true absorption (Howard, et al, 1955).

In the present study, a modified version of the Elsasser model is used. The band of interest is divided into several frequency intervals. The Lorentz half-width and mean line spacing are assumed to be the same throughout the band, while the Doppler half-width and mean line intensity are varied from interval to interval within the band. For such a model, the mean fractional absorption for each spectral interval becomes identical with the mean fractional absorption for an individual spectral line given by equation (D.20) or (D.21).

In a planetary atmosphere, pressure varies by many orders of magnitude in the vertical. Variations of temperature are ordinarily much smaller, but these may also be significant. In using the above band model to evaluate transmission functions over long atmospheric paths, the pressure and temperature variations must be taken into account. Since the band parameters S , α_L and α_D vary with pressure and temperature, equations (D.7) and (D.8) cannot be used to obtain the absorption coefficients for an atmospheric path over which p and T variations are significant.

Curtis (1952) and Godson (1953) derived an approximate method for dealing with variations of pressure along an absorbing path. Their method consists essentially in choosing a weighted value for pressure along the path which, when used to evaluate the fractional absorption from (D.20) or (D.21), results in the same value of \bar{A} as would be obtained by integration of the absorption coefficient over the path. For isothermal paths along which the CO_2 mixing ratio is constant, the weighted pressure given by the Curtis-Godson approximation is simply the average of the pressures at the two end points. The mean temperature for the path may also be taken to be the average of the two end points. Unless large temperature maxima or minima occur in the atmosphere, such a mean value should be fairly characteristic of the temperature along the path.

The Curtis-Godson approximation has been found satisfactory for transmissivity and flux calculations (Godson, 1953; Kaplan, 1959) and also for heating rate calculations (Walshaw and

Rodgers, 1963). It was used in the present study to evaluate the parameter α for any atmospheric path required.

Using the Curtis-Godson approximation together with the band model described above, the transmission functions were evaluated from equations (D.20) and (D.21). In the lower levels of a planetary atmosphere, where the pressure is relatively high, an appropriate form for \bar{A} is the Ladenburg-Reiche expression (D.21). In the higher, more rarified atmospheric regions, equation (D.20), based on Harris (1948), properly represents the true absorption, while at intermediate levels, a suitable interpolation scheme may be employed.

Band parameters.

Stull, et al. (1963) have made a detailed theoretical investigation of the transmission of CO_2 in the spectral region between 1μ and 20μ . They have obtained the absorptive properties of CO_2 for effective broadening pressures ranging from 1 atm to 10^{-2} atm and path lengths from 10^4 cm-atm to 0.2 cm-atm for three temperatures: 200°K, 250°K and 300°K. All contributing spectral lines whose relative intensity is greater than 10^{-8} times that of the strongest line in any particular band were included, and the various isotopes of C and O were taken into account. Transmission functions were calculated using the "quasi-random" band model and assuming a Benedict line shape for refined spectral intervals, as small as 2.5 cm^{-1} . In Figure D.I, the absorption spectrum of CO_2 in the $1\mu - 6\mu$ near infrared

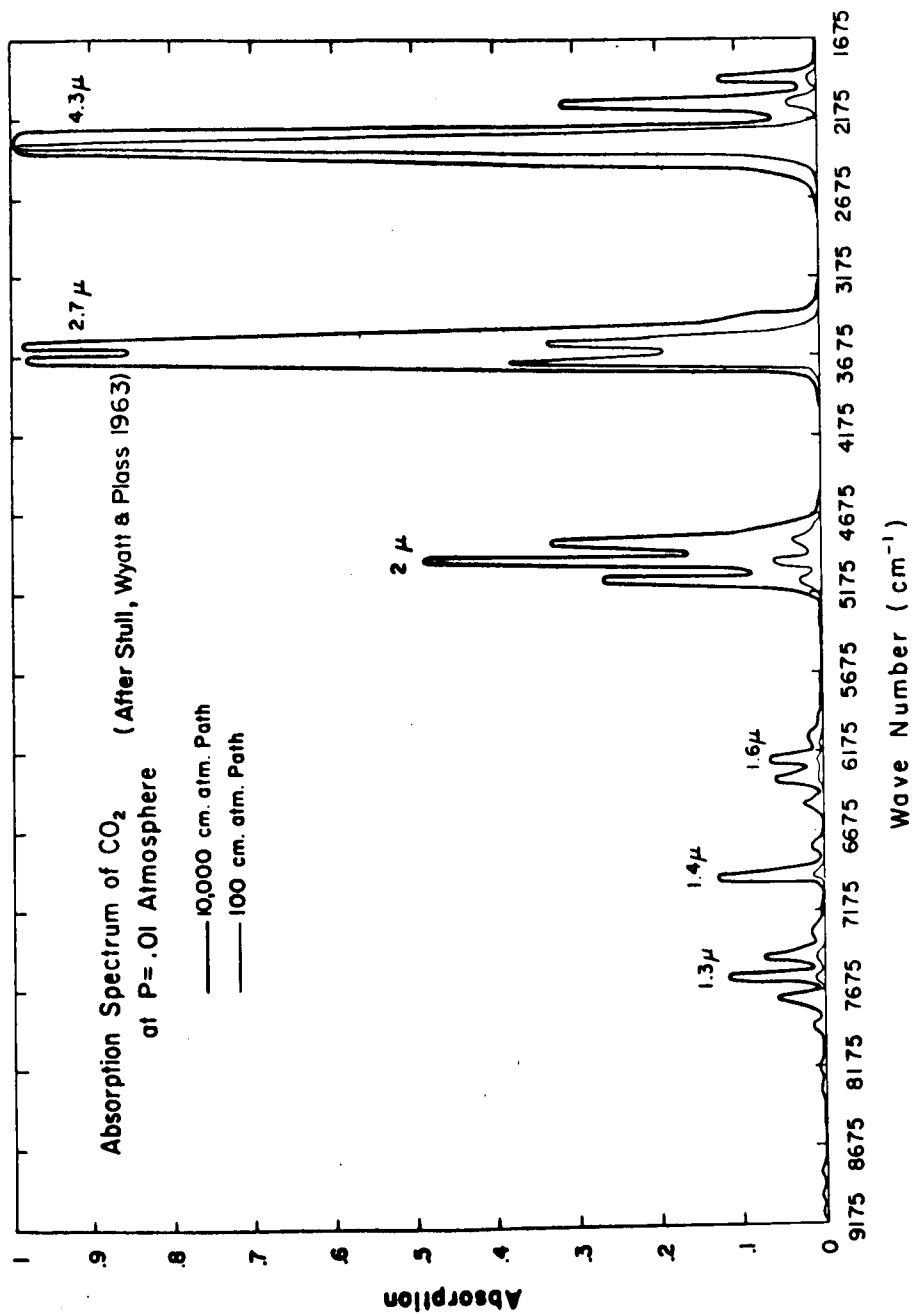


Figure D.I. Near infrared absorption spectrum of CO₂ (After Stull, et al., 1963).

region obtained by Stull, et al. (1963) is shown for optical paths of 10^4 cm-atm and 10^2 cm-atm. Comparison of the theoretical transmissions of Stull, et al. (1963) with the measurements of Burch, et al. (1962) in the strong CO_2 bands at 2.7μ , 4.3μ and 15μ indicates excellent agreement.

Estimates of the band parameters required for the evaluation of the near and far infrared transmission functions of CO_2 were obtained from the transmission tables of Stull, et al. (1963) in the following manner.

For constant values of β (D.22) and constant values of βx (D.23), a log-log plot was made of the Ladenburg-Reiche function

$$f_1(\beta, x) = 1 - \exp\left(-\beta x e^{-x} (I_0(x) + I_1(x))\right) \quad (\text{D.24})$$

against the parameters $\beta^2 x$. Also plotted against $\beta^2 x$ was the function

$$f_2(\beta, x) = 1 - \exp\left(-\left(\frac{2}{\pi} \beta^2 x\right)^{1/2}\right) \quad (\text{D.25})$$

The function $f_1(\beta, x)$ is the exact expression for the mean absorption in a spectral interval given by the statistical model, and the function $f_2(\beta, x)$ is the absorption given by the "strong line" approximation to the statistical model, applicable for large values of βx and small values of β (Plass, 1960). The network for $f_1(\beta, x)$ shown in Figure D.II was thus obtained, with the uppermost line in the network corresponding to $f_2(\beta, x)$. The functions $f_1(\beta, x)$ and

$$f_3(\beta, x) = 1 - \exp(-\beta x) \quad (\text{D.26})$$

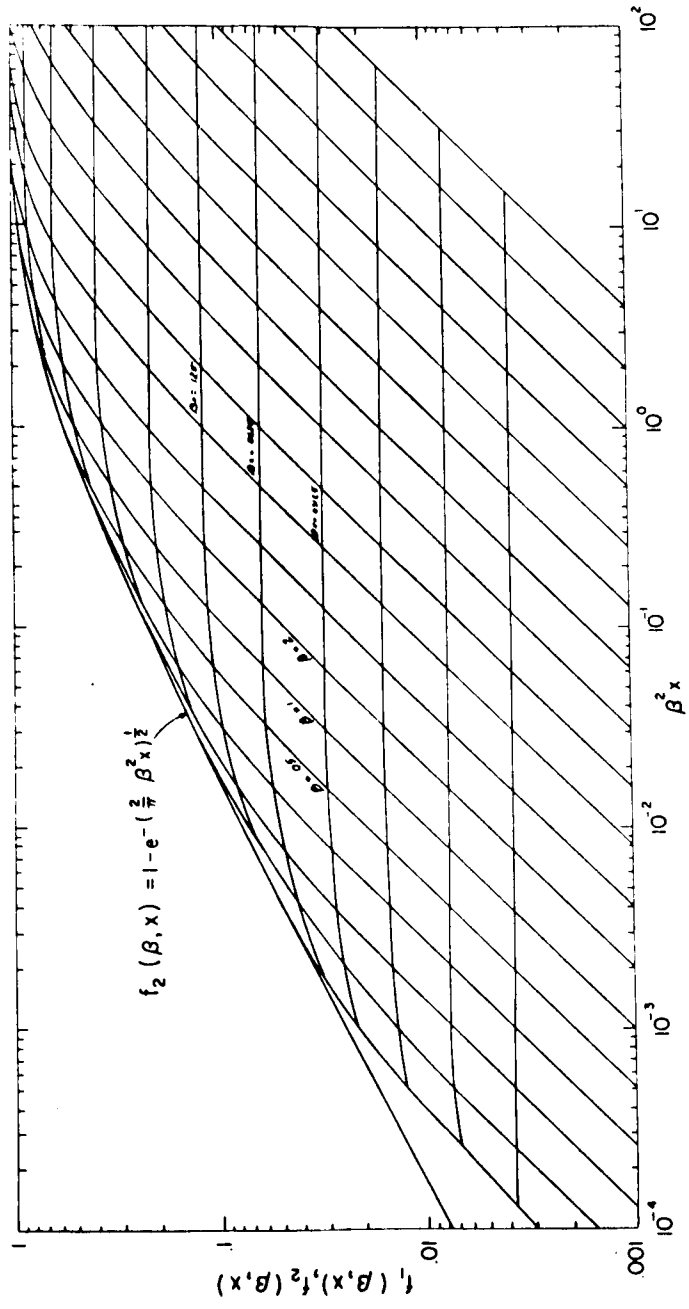


Figure D.II. $f_1(\beta, x)$ vs $\beta^2 x$ for constant values of β and constant values of βx . Also $f_2(\beta, x)$ vs $\beta^2 x$.

were also plotted in log-log fashion against the parameter βx , $f_1(\beta, x)$ at constant values of β (Figure D.III). $f_3(\beta, x)$ represents the mean absorption in a spectral interval as given by the "weak line" approximation, valid when β is large and x is small (Plass, 1960).

From the tables presented by Stull, et al. (1963), the average fractional absorption \bar{A} for a frequency interval of interest was extracted for various path lengths u and pressures p^* at a temperature of 200°K. The mean absorption at constant u and constant p^* was plotted in log-log fashion as a function of the parameter up^* , and the mean absorption at constant p^* was plotted in the same way as a function of u . As an example, plots of \bar{A} at constant u and p^* against up^* and of \bar{A} at constant p^* against u for the far infrared interval between 710 cm^{-1} and 730 cm^{-1} are presented in Figures D.IV and D.V.

The relationships between $\beta^2 x$ and up^* and βx and u are evident from equations (D.22) and (D.23). By superimposing the patterns of mean fractional absorption in a spectral interval from Stull, et al. (1963) (such as Figures D.IV and D.V) on the general patterns for \bar{A} (Figures D.II and D.III), it is possible to obtain a correspondence between $\beta^2 x$ and up^* , βx and u and β and p^* . In spectral intervals where the absorption is strongest, only a "strong line" fit could be obtained, giving the relationship between $\beta^2 x$ and up^* . In weaker intervals, however, it was generally possible to obtain the correspondence between βx and u and β and p^* also. Thus, in some spectral intervals, a consistency check on the estimated values of the band parameters was

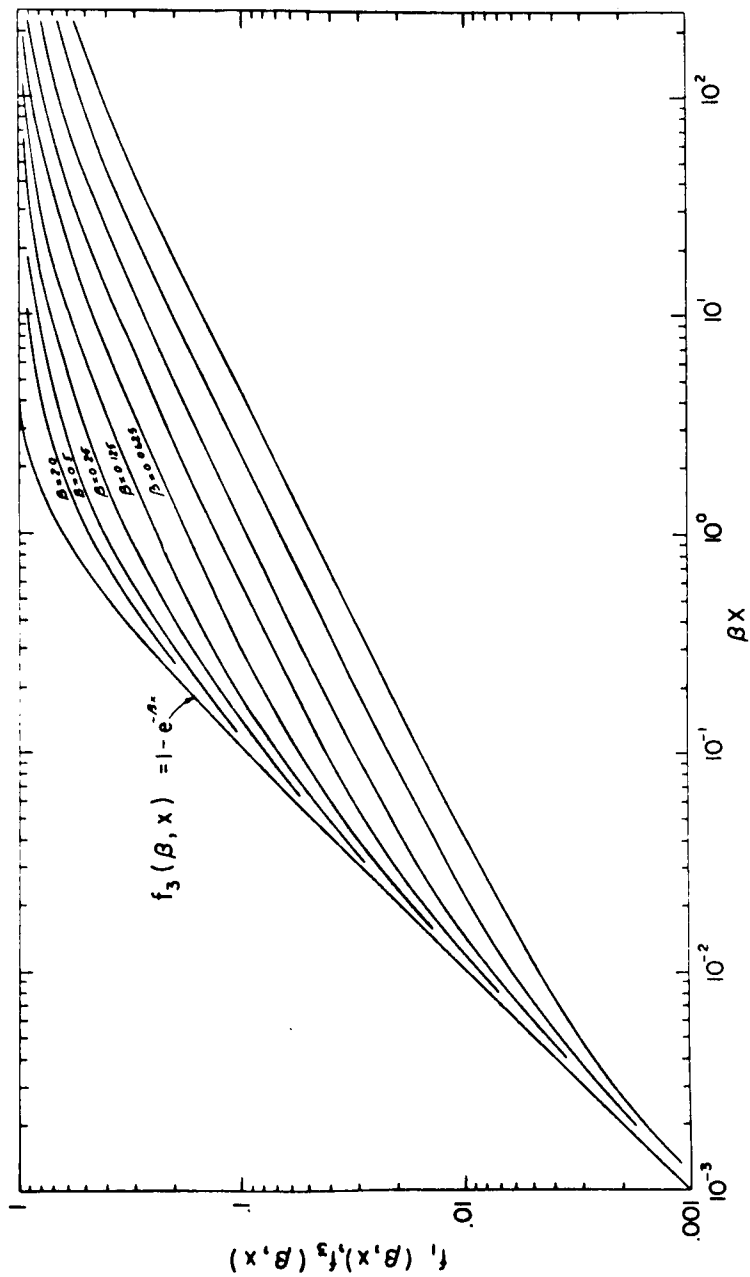


Figure D.III. $f_1(\beta, x)$ vs βx for constant values of β . Also $f_3(\beta, x)$ vs βx .

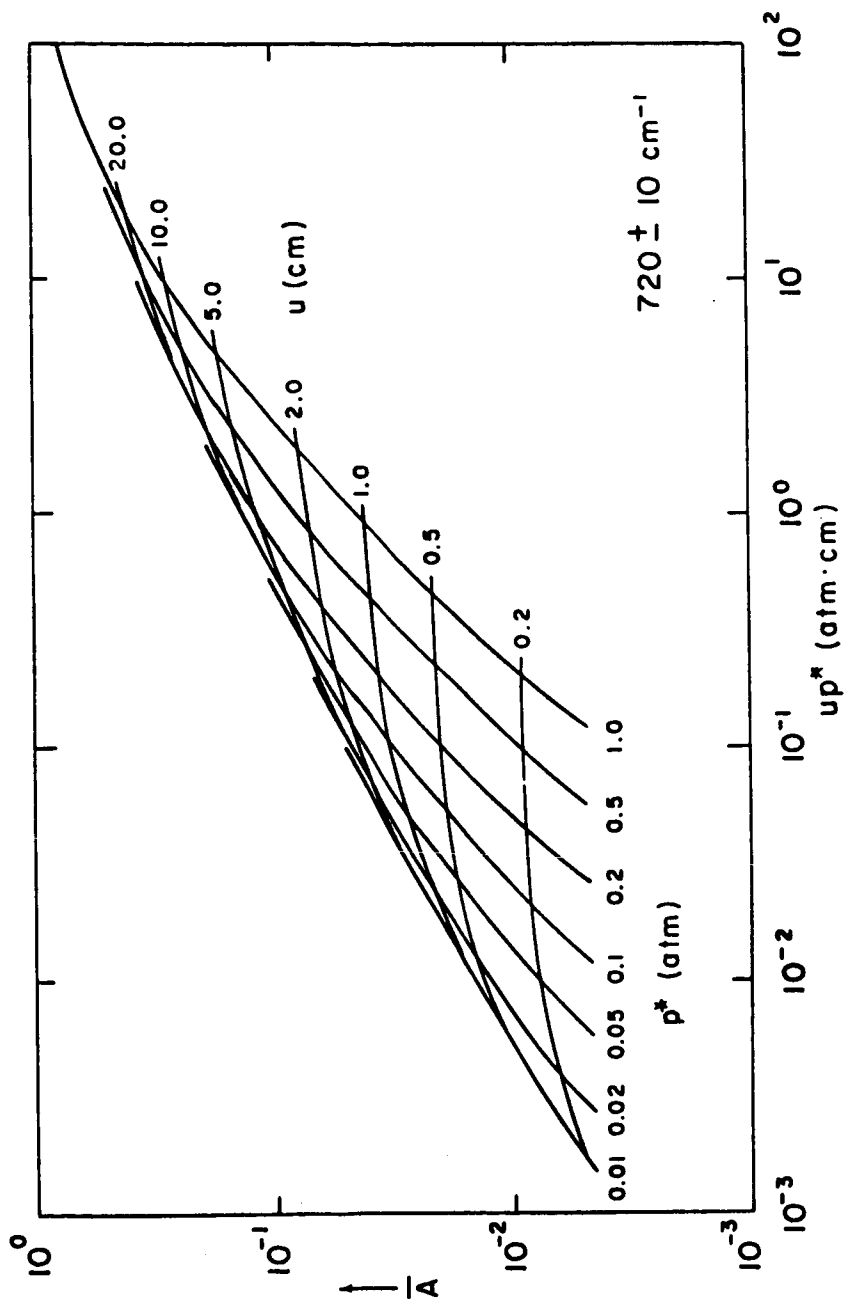


Figure D.IV. \bar{A} vs up^* for constant values of p^* and constant values of u for spectral interval $720 \pm 10 \text{ cm}^{-1}$ (From transmission tables of Stull, et al., 1963).

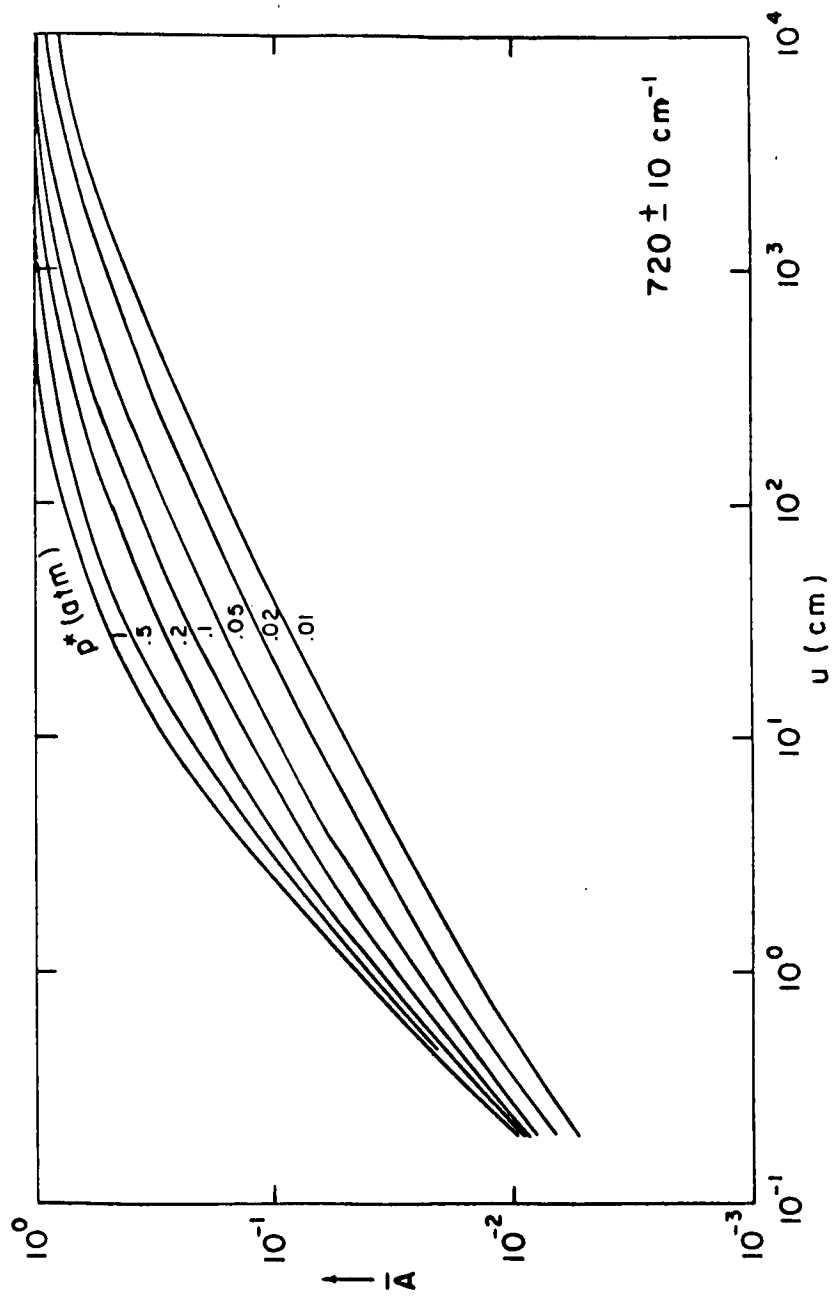


Figure D.V. \bar{A} vs u for constant values of p^* for spectral interval $720 \pm 10 \text{ cm}^{-1}$ (From transmission tables of Stull, et al., 1963).

provided. The ratios

$$\frac{\beta^2 x}{u p^*} = \frac{2\pi\alpha_{L_0} S_0}{d^2} \quad , \quad (D.27)$$

$$\frac{\beta x}{u} = \frac{S_0}{d} \quad , \quad (D.28)$$

$$\frac{\beta}{p^*} = \frac{2\pi\alpha_{L_0}}{d} \quad , \quad (D.29)$$

where the subscript (0) refers to 200°K, may be manipulated to yield values for the parameters

$$C_1 = \frac{S}{2\pi\alpha_{L_0}} \quad , \quad (D.30)$$

$$C_2 = \frac{2\pi\alpha_{L_0}}{d} \quad . \quad (D.31)$$

(Thus $x = C_1 u/p^*$ and $\beta = C_2 p^*$.) The preliminary estimates of C_1 and C_2 obtained by curve fitting were corrected by trial and error to find the best possible agreement with Stull, et al. (1963). Final estimates of C_1 and C_2 at a temperature of 273.2°K for various spectral intervals in the near and far infrared are listed in Table D.I.

Yamamoto and Sasamori (1958) have used a mean line spacing d of 1.55 cm^{-1} in their calculation of the absorption in the $15 \mu \text{ CO}_2$ band. The mean half-width for pressure broadening in this band α_L has been determined by Kaplan and Eggers (1956) using a curve of growth method as 0.064 cm^{-1} at 1 atm and 298°K. Correcting this estimate of α_L to 273.2°K, a value for C_2 of

TABLE D.I

BAND PARAMETERS C_1 AND C_2 FOR NEAR AND FAR INFRARED CO_2 BANDS

Band	Interval (cm^{-1})	C_1 ($atm\ cm^{-1}$)	C_2 (atm^{-1})
1.3 μ	7775-7725	5.0×10^{-4}	.30
	7725-7675	1.2×10^{-4}	.30
	7675-7625	1.5×10^{-5}	.30
	7625-7575	2.0×10^{-3}	.30
	7575-7525	1.3×10^{-4}	.30
	7525-7475	2.0×10^{-4}	.30
	7475-7425	7.2×10^{-4}	.30
	7425-7375	1.8×10^{-5}	.30
1.4 μ	7025-6975	9.2×10^{-4}	.30
	6975-6925	2.0×10^{-3}	.30
	6925-6875	1.2×10^{-3}	.30
1.6 μ	6575-6525	2.9×10^{-6}	.30
	6525-6475	9.0×10^{-5}	.30
	6475-6425	2.9×10^{-6}	.30
	6425-6375	6.4×10^{-6}	.30
	6375-6325	7.0×10^{-4}	.30
	6325-6275	2.5×10^{-5}	.30
	6275-6225	3.5×10^{-4}	.30
	6225-6175	2.3×10^{-5}	.30
	6175-6125	1.0×10^{-5}	.30
	6125-6075	5.5×10^{-5}	.30
	6075-6025	1.9×10^{-5}	.30
2.0 μ	5200-5150	3.9×10^{-6}	.33
	5150-5100	3.5×10^{-2}	.33
	5100-5050	3.0×10^{-2}	.33
	5050-5000	7.5×10^{-3}	.33
	5000-4950	5.3×10^{-1}	.33
	4950-4900	2.0×10^{-2}	.33
	4900-4850	1.0×10^{-1}	.33
	4850-4800	6.0×10^{-2}	.33
	4800-4750	1.3×10^{-3}	.33
	4750-4700	3.0×10^{-4}	.33
	2.7 μ	3850-3800	1.0×10^{-4}
3800-3750		2.0×10^{-3}	.36
3750-3700		2.7×10^1	.36
3700-3650		5.0×10^0	.36
3650-3600		1.7×10^1	.36

(Continued)

TABLE D.I (Continued)

BAND PARAMETERS C_1 AND C_2 FOR NEAR AND FAR INFRARED CO_2 BANDS

Band	Interval (cm^{-1})	C_1 ($atm\ cm^{-1}$)	C_2 (atm^{-1})
2.7 μ	3600-3550	6.0×10^0	.36
	3550-3500	2.1×10^{-1}	.36
	3500-3450	5.0×10^{-3}	.36
	3450-3425	2.0×10^{-5}	.36
4.3 μ	2470-2450	2.2×10^{-5}	.86
	2450-2430	2.0×10^{-5}	.86
	2430-2410	5.0×10^{-4}	.86
	2410-2390	3.2×10^{-3}	.86
	2390-2370	1.6×10^0	.86
	2370-2350	7.0×10^1	.86
	2350-2300	2.0×10^1	.86
	2300-2250	7.0×10^{-1}	.86
	2250-2200	6.0×10^{-3}	.86
	2200-2150	6.6×10^{-5}	.86
	2150-2100	1.0×10^{-3}	.35
	2100-2050	2.0×10^{-2}	.35
	2050-2000	1.0×10^{-3}	.35
	2000-1950	5.0×10^{-5}	.35
	1950-1900	2.0×10^{-3}	.35
	15 μ	750-730	1.1×10^{-1}
730-710		5.6×10^{-1}	.27
710-690		2.4×10^0	.27
700-680		8.5×10^0	.27
690-670		3.8×10^1	.27
680-660		9.9×10^1	.27
670-650		9.9×10^1	.27
660-640		2.4×10^1	.27
650-630		8.8×10^0	.27
640-620		2.0×10^0	.27
630-610		8.3×10^{-1}	.27
620-600		4.4×10^{-1}	.27
800-750		7.6×10^{-3}	.27
750-700		4.1×10^{-1}	.27
700-650		3.8×10^1	.27
650-600		2.7×10^0	.27
600-550		1.3×10^{-2}	.27

0.27 at this temperature is obtained. Also, the mean line intensity for a chosen interval within the 15μ band can be estimated, in view of this knowledge of α_L , from equation (D.30).

Although they are not directly involved in the calculation of the transmission functions, estimates of S (at 200°K) were obtained and are presented in Table D.II.

No estimates of α_L or d are available for the $1\mu - 6\mu$ near infrared CO_2 bands. However, as can be seen from Table D.I, the estimates of C_2 for the near infrared bands are quite close to that for the 15μ region, the largest discrepancy being found in the 4.3μ band, where C_2 is larger than the 15μ value by a factor slightly greater than three. This implies that both α_L and d are of approximately the same size in both the $1\mu - 6\mu$ region and 15μ region. Then, if the Kaplan and Eggers (1956) value of α_L is adopted in the near infrared bands also, an estimate of d in each near infrared interval can be derived from (D.31) and S can be obtained from (D.30). The values of d and S (at 200°K) resulting for spectral intervals in the $1\mu - 6\mu$ region are given in Table D.II.

The temperature dependence of the mean line intensity for each spectral interval in the 15μ CO_2 band can be taken into account by an exponential term representing the increase of the population of the lower vibrational energy state with temperature (Burch, et al., 1961). This temperature dependence in the $1\mu - 6\mu$ bands is negligible, as is a small effect due to the temperature dependence of the rotational levels associated with each

TABLE D.II

BAND PARAMETERS S, d AND Γ FOR INFRARED CO₂ BANDS

Band	Interval (cm ⁻¹)	S (atm ⁻¹ cm ⁻²)	d (cm ⁻¹)	Γ (°K)
1.3 μ	7775-7725	2.1 x 10 ⁻⁴	1.39	
	7725-7675	5.0 x 10 ⁻⁵	1.39	
	7675-7625	6.3 x 10 ⁻⁶	1.39	
	7625-7575	8.4 x 10 ⁻⁴	1.39	
	7575-7525	5.3 x 10 ⁻⁵	1.39	
	7525-7475	8.4 x 10 ⁻⁵	1.39	
	7475-7425	3.0 x 10 ⁻⁴	1.39	
	7425-7375	7.5 x 10 ⁻⁶	1.39	
1.4 μ	7025-6975	3.8 x 10 ⁻⁴	1.39	
	6975-6925	8.4 x 10 ⁻⁴	1.39	
	6925-6875	5.0 x 10 ⁻⁴	1.39	
1.6 μ	6575-6525	1.2 x 10 ⁻⁶	1.39	
	6525-6475	3.7 x 10 ⁻⁵	1.39	
	6475-6425	1.2 x 10 ⁻⁶	1.39	
	6425-6375	2.7 x 10 ⁻⁶	1.39	
	6375-6325	2.9 x 10 ⁻⁴	1.39	
	6325-6275	1.0 x 10 ⁻⁵	1.39	
	6275-6225	1.5 x 10 ⁻⁴	1.39	
	6225-6175	9.6 x 10 ⁻⁵	1.39	
	6175-6125	4.2 x 10 ⁻⁶	1.39	
	6125-6075	2.3 x 10 ⁻⁵	1.39	
6075-6025	7.9 x 10 ⁻⁶	1.39		
2.0 μ	5200-5150	1.6 x 10 ⁻⁶	1.27	
	5150-5100	1.5 x 10 ⁻²	1.27	
	5100-5050	1.3 x 10 ⁻²	1.27	
	5050-5000	3.1 x 10 ⁻³	1.27	
	5000-4950	2.2 x 10 ⁻¹	1.27	
	4950-4900	8.4 x 10 ⁻³	1.27	
	4900-4850	4.2 x 10 ⁻²	1.27	
	4850-4800	2.5 x 10 ⁻²	1.27	
	4800-4750	5.4 x 10 ⁻⁴	1.27	
4750-4700	1.3 x 10 ⁻⁴	1.27		

(Continued)

TABLE D.II (Continued)

BAND PARAMETERS S , d AND Γ FOR INFRARED CO_2 BANDS

Band	Interval (cm^{-1})	S ($\text{atm}^{-1}\text{cm}^{-2}$)	d (cm^{-1})	Γ ($^{\circ}\text{K}$)
2.7 μ	3850-3800	4.2×10^{-5}	1.15	
	3800-3750	8.4×10^{-4}	1.15	
	3750-3700	1.1×10^1	1.15	
	3700-3650	2.1×10^0	1.15	
	3650-3600	7.1×10^0	1.15	
	3600-3550	2.5×10^0	1.15	
	3550-3500	8.8×10^{-2}	1.15	
	3500-3450	2.1×10^{-3}	1.15	
	3450-3425	8.4×10^{-4}	1.15	
4.3 μ	2470-2450	9.2×10^{-6}	.485	
	2450-2430	8.4×10^{-6}	.485	
	2430-2410	2.1×10^{-4}	.485	
	2410-2390	1.3×10^{-3}	.485	
	2390-2370	6.7×10^{-1}	.485	
	2370-2350	2.9×10^1	.485	
	2350-2300	8.4×10^0	.485	
	2300-2250	2.9×10^{-1}	.485	
	2250-2200	2.5×10^{-3}	.485	
	2200-2150	2.7×10^{-5}	.485	
	2150-2100	4.2×10^{-4}	1.19	
	2100-2050	8.4×10^{-3}	1.19	
	2050-2000	4.2×10^{-2}	1.19	
	2000-1950	2.1×10^{-5}	1.19	
	1950-1900	8.4×10^{-4}	1.19	
15 μ	750-730	4.6×10^{-2}	1.55	
	730-710	2.3×10^{-1}	1.55	
	710-690	1.0×10^0	1.55	
	700-680	3.6×10^0	1.55	
	690-670	1.6×10^1	1.55	
	680-660	4.1×10^1	1.55	
	670-650	4.1×10^1	1.55	
	660-640	1.0×10^0	1.55	
	650-630	3.7×10^0	1.55	
	640-620	8.4×10^{-1}	1.55	
	630-610	3.5×10^{-1}	1.55	
	620-600	1.8×10^{-1}	1.55	

(Continued)

TABLE D.II (Continued)

BAND PARAMETERS S , d AND Γ FOR INFRARED CO_2 BANDS

Band	Intervals (cm^{-1})	S ($\text{atm}^{-1}\text{cm}^{-2}$)	d (cm^{-1})	Γ ($^{\circ}\text{K}$)
15μ	800-750	3.2×10^{-3}	1.55	2.0×10^3
	750-700	1.7×10^{-1}	1.55	1.3×10^3
	700-650	1.6×10^1	1.55	4.0×10^2
	650-600	1.1×10^0	1.55	1.0×10^3
	600-550	5.4×10^{-3}	1.55	2.0×10^3

vibrational state in the 15μ region, which alters the shape of individual bands (Hanel and Bartko, 1964). The mean line intensity in a particular spectral interval of the 15μ band may therefore be expressed as

$$S(T) = S_0 \exp\left(\Gamma \left(T_0^{-1} - T^{-1}\right)\right) , \quad (D.32)$$

where Γ is the coefficient of temperature dependence and S_0 is the mean line intensity at temperature T_0 . Thus, from a knowledge of S at 200°K , S at any other temperature may be computed, if Γ is known.

The parameter Γ in a sub-interval of the 15μ band was obtained from equation (D.32) using the transmission functions of Stull, et al. (1963) at three different temperatures. Obtaining S at 200°K , 250°K and 300°K by the procedure outlined above, values of Γ , representing an empirical fit to equation (D.32) were derived for selected spectral intervals. The estimates obtained for the coefficient of temperature dependence for various 15μ band intervals are given in Table D.II.

Combined with estimates of the other band parameters C_1 , C_2 , d , α_L , α_D and S_0 , the determination of Γ enables us to evaluate the atmospheric transmission functions required for solution of the radiative transfer equation from expressions (D.20) and (D.21). In the weaker bands of the $1\mu - 6\mu$ region, these estimates of the various band parameters lead to precise agreement with the transmission functions of Stull, et al. (1963).

Even in the strongest spectral regions near 4.3μ and 15μ , a comparison of the transmission functions obtained here with those of Stull, et al. indicates close agreement (Figure D.VI).

Numerical evaluation of CO₂ transmission functions.

The determination of atmospheric temperatures by a steady-state, iterative solution of the radiative transfer equation requires the evaluation of tens of thousands of transmission functions. Direct evaluation of \bar{A} making use of equations (D.20) and (D.21) is quite involved, and innumerable repetitions of this procedure are clearly not practical, even making use of the most modern high speed electronic computers. Therefore, a more economical method was developed, utilizing a table-searching and interpolation scheme to obtain the necessary transmission functions.

Using the value of α_D at the center of the 15μ CO₂ band (667.40 cm^{-1}) and at a temperature of 150°K , along with the estimate of d given by Yamamoto and Sasamori (1958), a table of the parameter $(\bar{A} d / \alpha_D)^*$ was constructed, with coordinates α and $2\pi\alpha x$, from equations (D.20) (for $\alpha < 1$) and (D.21) (for $\alpha \geq 1$). Entries were made for values of α ranging from 10^{-6} to 10^2 in order-of-magnitude steps, and for values of $2\pi\alpha x$ ranging from 10^{-1} to 10^9 in steps of tenths of orders-of-magnitude. Thus, this table has dimensions 9×91 , with a total of 819 entries. A plot of these entries is shown in Figure D.VII, where an additional line has been added corresponding to $\alpha = 10^3$.

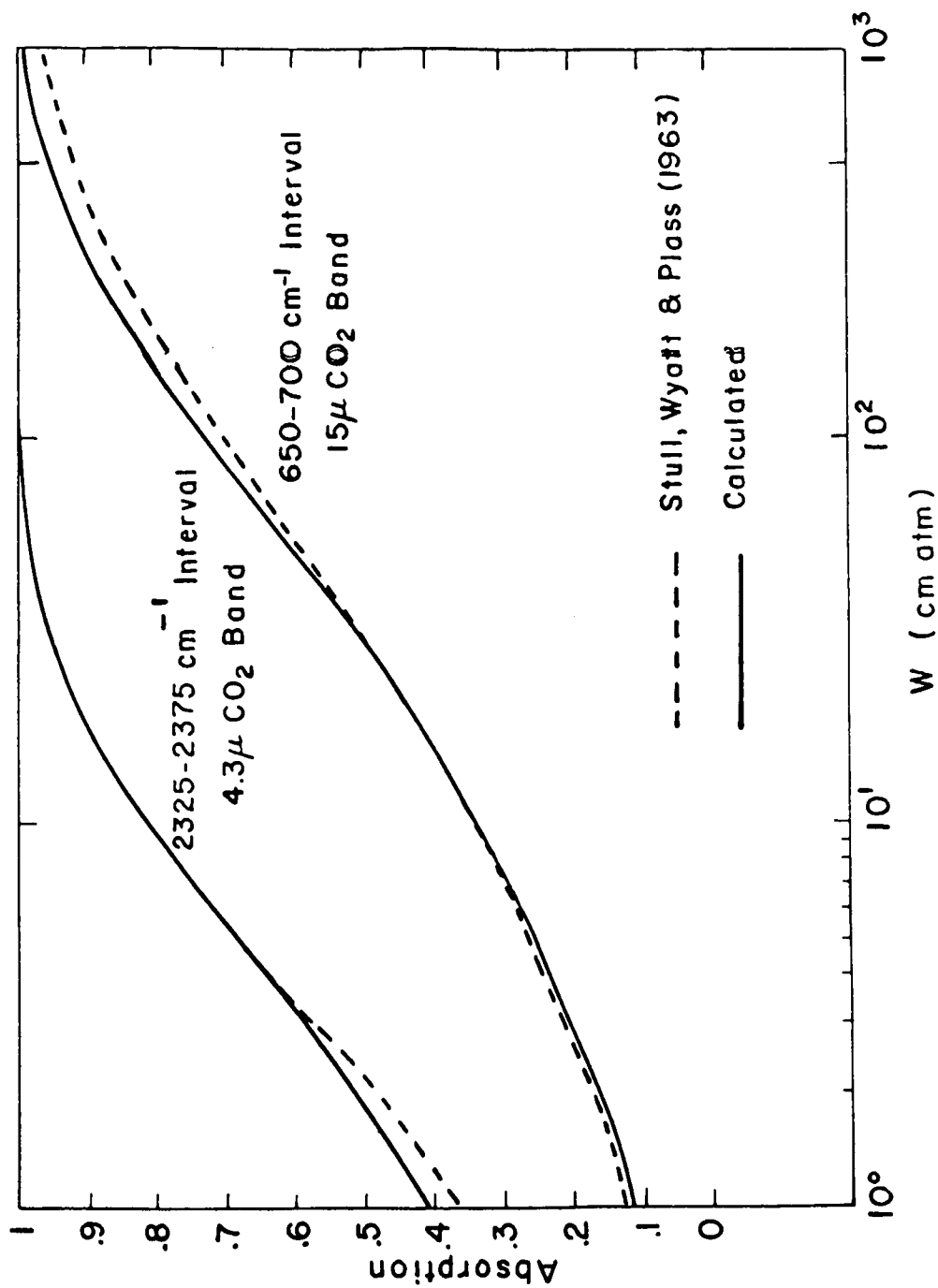


Figure D.VI. Comparison of present calculations of fractional absorption with Stull, et al. (1963).

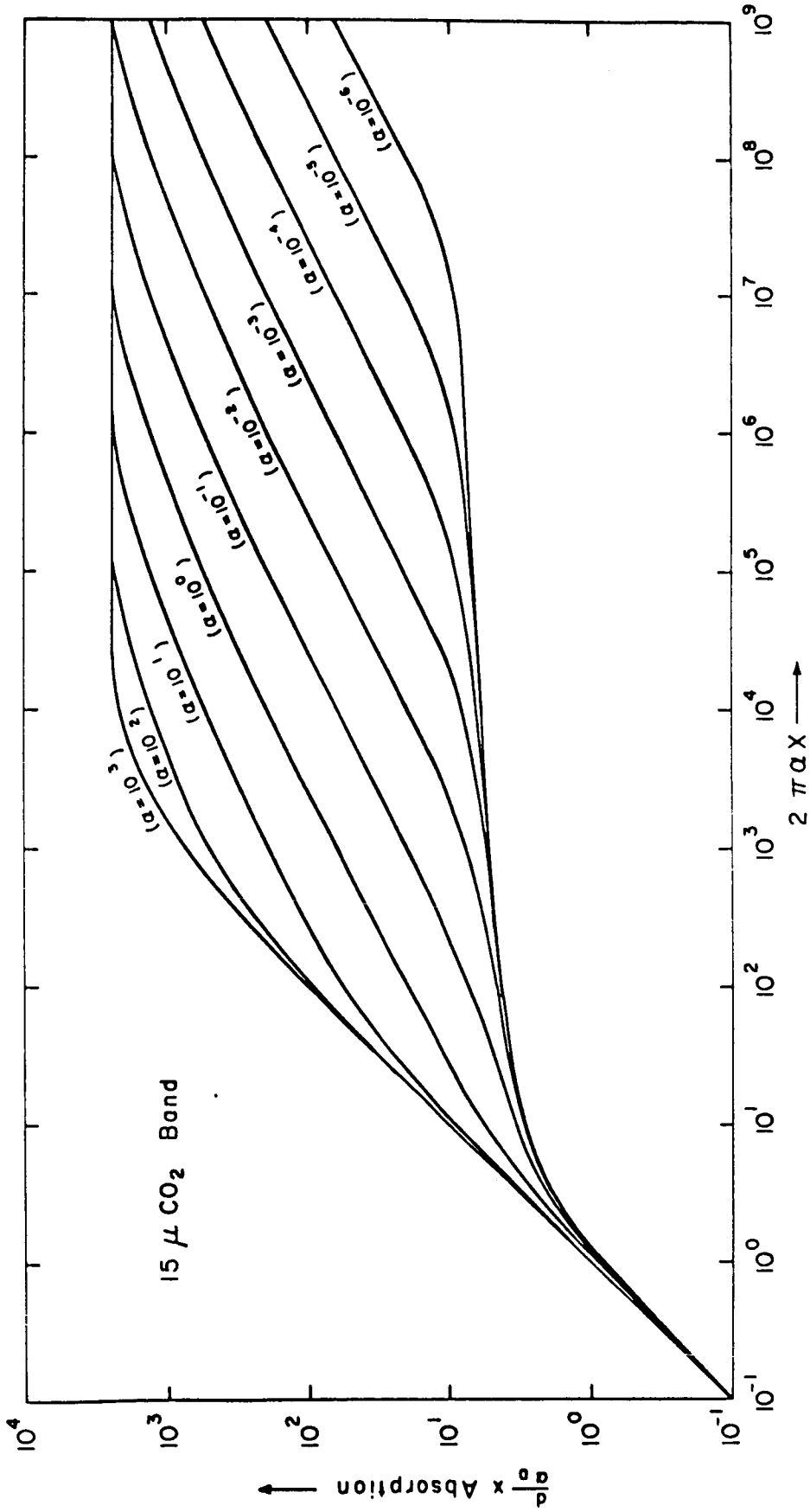


Figure D.VII: Absorption by mixed Doppler and Lorentz lines in the 15 μ CO₂ band. The abscissa $2\pi\alpha x = Su/\alpha_D$, and $d/\alpha_D = 2.46 \times 10^3$.

Figure D.VII represents \bar{A} as a function of α and $2\pi\alpha x$ at 667.40 cm^{-1} and 150°K ; a slightly modified version would be representative of absorption at another wavenumber and/or temperature, with differences occurring toward larger values of $2\pi\alpha x$ (saturation) for a given α . An upward or downward shift in the position of the saturation level (uppermost curve) and in the location of lines of constant α near this level would result from consideration of frequencies and temperatures other than those for which the figure was constructed. All except the uppermost portion of Figure D.VII would, however, remain unchanged, unless drastically different values of frequency and temperature were used. Therefore, a suitable correction scheme was adopted to adjust \bar{A} near the saturation level for frequency and temperature, so that a single table could be used to obtain the absorption for all of the frequency intervals in the 15μ band at any desired temperature.

For a given atmospheric path the parameters $\alpha (= \alpha_L / \alpha_D)$ and $2\pi\alpha x (= Su / \alpha_D)$ were evaluated for a particular frequency interval using the weighting procedure described previously. Then, by logarithmic interpolation on the α coordinate and a linear interpolation on the $2\pi\alpha x$ coordinate, a value of $(\bar{A} d / \alpha_D)^*$ was obtained from the table, where the asterisk corresponds to 667.40 cm^{-1} and 150°K . (This interpolation method was found to reproduce quite accurately the values of $(\bar{A} d / \alpha_D)^*$ computed directly for intermediate values of α and $2\pi\alpha x$ from equations (D.20) and (D.21).) The value of $(\bar{A} d / \alpha_D)^*$ extracted

in this way from the table was then corrected for the variation of α_D with frequency and/or temperature to obtain \bar{A} , making use of the expression

$$\bar{A} = \frac{\alpha_D (\bar{A} d / \alpha_D)^*}{d} \left(1 - \left(\bar{A} d / \alpha_D \right)^* 1.5 \left(\frac{d}{\alpha_D} \right)^*^{-2.5} \left(\left(\frac{d}{\alpha_D} \right)^* - \left(\frac{d}{\alpha_D} \right) \right) \right) \quad (D.33)$$

(This formulation leads to values of \bar{A} in excellent agreement with those calculated directly from (D.20) and (D.21) taking the frequency and temperature dependence of α_D into account.)

A scheme was also devised for making use of the table of $(\bar{A} d / \alpha_D)^*$ to obtain \bar{A} whenever the values of α and $2\uparrow\alpha x$ fall outside of the covered range. In the Martian atmosphere, with a surface pressure near 10 mb, the value of α for any path can never be much greater than 10^0 , and must certainly be less than 10^2 ; it may, on the other hand, become smaller than 10^{-6} . Whenever α is this small, however, the value of $2\uparrow\alpha x$ must be relatively small also. Thus, when $\alpha < 10^{-6}$, $(\bar{A} d / \alpha_D)^*$ for a given $2\uparrow\alpha x$ will be independent of α , and equal to the value of $(\bar{A} d / \alpha_D)^*$ at $\alpha = 10^{-6}$, as indicated by Figure D.VII. When $\alpha < 10^{-6}$, all required values of $(\bar{A} d / \alpha_D)^*$ fall on the lowermost curve in the figure, regardless of the particular value of α , and \bar{A} is determined by $2\uparrow\alpha x$ alone. For some path-lengths in the atmosphere of Mars, the parameter $2\uparrow\alpha x$ lies outside the range of the table also. However, when $2\uparrow\alpha x$ is smaller than 10^{-1} , $(\bar{A} d / \alpha_D)^*$ is equal to $2\uparrow\alpha x$ for all α (Figure D.VII). In addition, whenever $2\uparrow\alpha x$ exceeds 10^9 , α too must be relatively large, so that saturation has been reached

and $(\bar{A} d/\alpha_D)^*$ assumes its maximum value. With these considerations, the tabulated values of $(\bar{A} d/\alpha_D)^*$ could be used to determine \bar{A} for any required path, throughout the entire range of temperature, pressure and optical thickness encountered in the Martian atmosphere, in any chosen spectral interval in the 15μ band.

A similar procedure was used to evaluate \bar{A} for spectral intervals in the $1\mu - 6\mu$ CO_2 bands. Due to its frequency dependence, the Doppler half-width in these bands is larger by nearly an order of magnitude than α_D in the 15μ band. Figure D.VII, therefore, would have to be considerably modified to properly represent \bar{A} in these bands, with saturation occurring at a lower level, and correction of the tabular values of $(\bar{A} d/\alpha_D)^*$, using equation (D.33) would be of doubtful accuracy for some atmospheric paths. Therefore, to avoid the lengthy evaluation of \bar{A} via (D.20) or (D.21), another table of the same dimensions as that described previously was constructed, using the value of α_D near the center of the 1.6μ region (6325 cm^{-1}) at a temperature of 150°K , and the estimated value of d in the 1.6μ band given in Table D.II. Operating on this second table in exactly the same manner as described above, and using the same correction scheme (equation (D.33)), fractional absorption in the desired intervals in the near infrared was obtained.

The near infrared transmission function for various paths obtained from the table were compared with those calculated directly from (D.20) and (D.21) and the agreement was found to

be quite satisfactory. This method of obtaining transmission functions in the $1\mu - 6\mu$ CO_2 bands was used in determining the transmission of near infrared solar energy in the Martian atmosphere.

REFERENCES

- Adams, W.S., and T. Dunham, Jr., 1937: Water vapor lines in the spectrum of Mars. Publications of the Astronomical Society of the Pacific, 49, 209 - 211.
- Adams, W.S., 1941: Some results with the Coude spectrograph of the Mount Wilson Observatory. Astrophys. J., 93, 11 - 23.
- Aller, L.H., 1953: Astrophysics, the Atmospheres of the Sun and Stars. Ronald Press, New York, 412 pp.
- Anderson, H.R., 1965: Mariner IV measurements near Mars: Initial results, Spacecraft description and encounter sequence. Science, 149, 1226 - 1228.
- Arking, A., 1962: Non-grey convective planetary atmospheres. Mem.Soc. Roy. Sci. Liege, 5, 180 - 189.
- Barth, C.A., 1964: Three body reactions. Annales de Géophysique, 20, 182 - 197.
- Bates, D.R., and A.E. Witherspoon, 1952: The photochemistry of some minor constituents of the Earth's atmosphere (CO_2 , CO, CH_4 , N_2O). Monthly Notices Roy. Astronom. Soc., 112, 101 - 124.
- Belton, M.J.S., and D.M. Hunten, 1966: The abundance and temperature of CO_2 in the Martian atmosphere. Astrophys. J., 145, 454 - 467.
- Benedict, W.S., R. Herman, G.E. Moore and S. Silverman, 1956: The strengths, widths and shapes of infrared lines. I. General considerations. Canadian J. Phys., 34, 830 - 849.
- Biondi, M.A., 1964: Electron - ion and ion - ion recombination. Annales de Géophysique, 20, 34 - 46.
- Burch, D.E., D. Gryvnak and D. Williams, 1961: Infrared absorption by carbon dioxide. Ohio State University Research Foundation, Columbus, Ohio, Report SR-2.
- Burch, D.E., D. Gryvnak and D. Williams, 1962: Absorption by carbon dioxide. Infrared absorption by carbon dioxide, water vapor and minor atmospheric constituents, Part B, Report Contract AF19(604) - 2633, Ohio State University.

- Campbell, E.S., and C. Nudelman, 1960: Reaction kinetics, thermodynamics and transport properties in the ozone-oxygen system. Contract AFOSR TN-60-502, New York University.
- Chamberlain, J.W., 1962: Upper atmospheres of the planets. Astrophys. J., 136, 582 - 593.
- Chamberlain, J.W., and D.M. Hunten, 1965: Pressure and CO₂ content of the Martian atmosphere: A critical discussion. Reviews of Geophysics, 3, 299 - 317.
- Chamberlain, J.W., and M.B. McElroy, 1966: Martian atmosphere: The Mariner occultation experiment. Science, 152, 21 - 25.
- Coblentz, W.W., and C.O. Lampland, 1923: Measurements of planetary radiation. Lowell Observatory Bulletin, 3, 91 - 134.
- Coblentz, W.W., and C.O. Lampland, 1927: Further radiometric measurements and temperature estimates of the planet Mars. Scientific Papers of the National Bureau of Standards, 22, 237 - 276.
- Curtis, A.R., 1952: Discussion of Goody's "A statistical model for water-vapor absorption". Quart. J. Roy. Meteorol. Soc., 78, 638 - 640.
- Curtis, A.R., and R.M. Goody, 1956: Thermal radiation in the upper atmosphere. Proc. Roy. Soc., London, A, 236, 193 - 206.
- Danielson, R.E., J.E. Gaustad, M. Schwarzschild, H.F. Weaver and W.J. Woolf, 1964: Mars observations from Stratoscope II. Astronaut. J., 69, 344 - 352.
- Detwiler, C.R., D.L. Garrett, J.D. Purcell and R. Tousey, 1961: The intensity distribution in the ultraviolet solar spectrum. Annales de Géophysique, 17, 263 - 272.
- De Vaucouleurs, G., 1954: Physics of the Planet Mars. Faber and Faber, London, 365 pp.
- Dollfus, A., 1957: Études des planètes par la polarisation de leur lumière. Ann. Astrophys., Supp. 4, 70 - 110.

- Dollfus, A., 1963: Mesure de la quantité de vapeur d'eau contenue dans l'atmosphère de la planète Mars. Comptes Rendus de l'Académie des Sciences, 256, 3009 - 3011.
- Donahue, T.M., 1966: Upper atmosphere and ionosphere of Mars. Science, 152, 763 - 764.
- Dunham, T., Jr., 1952: Spectroscopic observations of the planets at Mount Wilson. The Atmospheres of the Earth and Planets, 2nd Ed., ed. by G.F. Kuiper. University of Chicago Press, 288 - 305.
- Elsasser, W.M., 1938: Mean absorption and equivalent absorption coefficient of a band spectrum. Phys.Rev., 54, 126 - 129.
- Elsasser, W.M., 1942: Heat transfer by infrared radiation in the atmosphere. Harvard Meteorological Studies, 6, Harvard University Press, Cambridge, 107 pp.
- Elsasser, W.M., 1960: Atmospheric radiation tables. Meteorological Monographs, 4, No. 23, American Meteorological Society, Boston, 43 pp.
- Feshenfeld, F.F., A.L. Schmeltekopf and E.E. Ferguson, 1966: Thermal energy ion-neutral reaction rates. III. The measured rate constant for the reaction $O^+(4S) + CO_2(1\Sigma) \rightarrow O_2^+(2II)$. J. Chem. Phys., 44, 3022 - 3024.
- Fjeldbo, G., 1964: Bistatic-radar methods for studying planetary ionospheres and surfaces. Final Report Contract NSF G-21543, SU-SEL-64-025, Stanford Electronics Laboratory, Stanford University, Stanford, California.
- Fjeldbo, G., and V.R. Eshleman, 1965: The bistatic radar - occultation method for the study of planetary atmospheres. J. Geophys. Res., 70, 3217 - 3225.
- Fjeldbo, G., V.R. Eshleman, C.F. Garriott and F.L. Smith, III, 1965: The two-frequency bistatic radar - occultation method for the study of planetary ionospheres. J. Geophys. Res., 70, 3701 - 3710.
- Fjeldbo, G., W.C. Fjeldbo and V.R. Eshleman, 1966a: Models for the atmosphere of Mars based on the Mariner IV occultation experiment. J. Geophys. Res., 71, 2307 - 2316.

- Fjeldbo, G., W.C. Fjeldbo and V.R. Eshleman, 1966b: Atmosphere of Mars; Mariner IV models compared. Science, 153, 1518 - 1522.
- Gast, P.R., 1957: Solar radiation. Handbook of Geophysics, Air Force Cambridge Research Center, MacMillan, New York, 16-14 to 16-32.
- Gifford, F., Jr., 1956: The surface temperature climate of Mars. Astrophys. J., 123, 154 - 161.
- Giordmaine, J.A., L.E. Alsop, C.H. Townes and C.H. Mayer, 1959: Observations of Jupiter and Mars at 3 cm wavelength. Astrophys. J., 64, 332 - 333.
- Godson, W.L., 1953: The evaluation of infrared radiative fluxes due to atmospheric water vapour. Quart. J. Roy. Meteorol. Soc., 79, 367 - 379.
- Goody, R.M., 1952: A statistical model for water-vapour absorption. Quart. J. Roy. Meteorol. Soc., 78, 165 - 169.
- Goody, R.M., 1957: The atmosphere of Mars. Weather, 12, 3 - 15.
- Goody, R.M., 1964: Atmospheric Radiation, I. Clarendon Press, Oxford, 435 pp.
- Grandjean, J., and R.M. Goody, 1955: The concentration of carbon dioxide in the atmosphere of Mars. Astrophys. J., 121, 548 - 552.
- Gray, L.D., 1966: Transmission of the atmosphere of Mars in the region of 2μ . Icarus, 5, 390 - 398.
- Gross, S.H., W.E. McGovern and S.I. Rasool, 1966: The upper atmosphere of Mars. Science, 151, 1216 - 1221.
- Hanel, R.A., and F. Bartko, 1964: Radiative equilibrium in planetary atmospheres. NASA Technical Note NASA TN D-2397, Goddard Space Flight Center, Greenbelt, Maryland.
- Harris, D.L., 1948: On the line-absorption coefficient due to the Doppler effect and damping. Astrophys. J., 108, 112 - 115.

- Harteck, F., R.R. Reeves, Jr., B.A. Thompson and R.J. Waldron, 1966: Radiation equilibrium pertinent to planetary atmospheres. Tellus, 18, 192 - 197.
- Herzfeld, K.F., and T.A. Litovitz, 1959: Absorption and Dispersion of Ultrasonic Waves. Academic Press, New York, 535 pp.
- Hess, S.L., 1950: Some aspects of the meteorology of Mars. J. Meteorol., 7, 1 - 13.
- Hinteregger, H.E., L.A. Hall and G. Schmidtke, 1965: Solar XUV radiation and neutral particle distribution in July 1963 thermosphere. Space Research V, ed. by P. Muller. North-Holland Publishing Co., Amsterdam, 1175 - 1190.
- Howard, J.N., D.L. Burch and D. Williams, 1955: Near infrared transmission through synthetic atmospheres. Geophysical Research Paper No. 40, Air Force Cambridge Research Center, Cambridge, Massachusetts, 145 pp.
- Hunten, D.M., 1967: The ionosphere and upper atmosphere of Mars. The Atmospheres of Venus and Mars, ed. J.C. Brandt and M.B. McElroy. Gordon and Breach.
- Inn, E.C.Y., and Y. Tanaka, 1953: Absorption coefficient of ozone in the ultraviolet and visible regions. J. Opt. Soc. Amer., 43, 870 - 873.
- Johnson, F.S., 1965: Atmosphere of Mars. Science, 150, 1445 - 1448.
- Kaplan, L.D., and D.F. Eggers, 1956: Intensity and line-width of the 15 micron CO_2 band, determined by a curve of growth method. J. Chem. Phys., 25, 876 - 883.
- Kaplan, L.D., 1959: A method for calculation of infrared flux for use in numerical models of atmospheric motion. The Atmosphere and Sea in Motion, ed. by B. Bolin. Oxford University Press, Oxford, 509 pp.
- Kaplan, L.D., G. Münch and H. Spinrad, 1964: An analysis of the spectrum of Mars. Astrophys. J., 139, 1 - 15.
- Kaufman, F., and J.R. Kelso, 1961: The homogeneous recombination of atomic oxygen. Chemical Reactions in the Lower and Upper Atmosphere. Interscience Pub., John Wiley & Sons, New York, 255 - 268.

- Kiess, C.C., C.H. Corliss, H.K. Kiess and E.L. Corliss, 1957: High dispersion spectra of Mars. Astrophys. J., 126, 579 - 584.
- Kliore, A., D.L. Cain, G.S. Levy, V.R. Eshleman, G. Fjeldbo and F.D. Drake, 1965: Mariner IV measurements near Mars: Initial results, Occultation experiment: Results of the first direct measurement of Mars's atmosphere and ionosphere. Science, 149, 1243 - 1248.
- Kuiper, G.P., 1952: Planetary atmospheres and their origin. The Atmospheres of the Earth and Planets, 2nd Ed., ed. by G.P. Kuiper. University of Chicago Press, 308 - 405.
- Kuiper, G.P., 1963: Infrared spectra of planets and cool stars; Introductory report. Mem. Soc. Roy. Sci. Liege, 5, 365 - 391.
- Ladenburg, R., and F. Reiche, 1913: Uber selektive Absorption. Ann. d. Phys., 42, 181.
- Lambert, J.D., 1962: Relaxation in gases. Atomic and Molecular Processes, ed. by D.R. Bates. Academic Press, New York, 904 pp.
- Leighton, R.B., B.C. Murray, R.F. Sharp, J.D. Allen and R.K. Sloan, 1965: Mariner IV photography of Mars: Initial results. Science, 148, 627 - 630.
- Lindholm, E., 1945: Pressure broadening of spectral lines. Ark. Mat. Astron. och. Fys., 32A, No. 17.
- List, R.J., 1963: Smithsonian Meteorological Tables, 6th Ed. Table 131, p. 415.
- London, J., K. Ooyama and C. Prabhakara, 1962: Mesospheric dynamics. Final Report Contract AF 19(604)-5492, New York University.
- Lyot, B., 1929: Recherches sur la polarisation de la lumière des planètes et de quelques substances terrestres. Annales de l'Observatoire de Meudon, VIII, 51 - 62, 147 - 150.
- Madden, R.P., 1961: A high resolution study of the CO₂ absorption spectra between 15 and 18 microns. J. Chem. Phys., 35, 2083 - 2097.

- Marmo, F.F., and P. Warneck, 1961: Planetary Atmosphere Studies, VIII. Technical Report 61-20-N, CC. Corporation, Bedford, Massachusetts.
- Marriott, R., 1964: Molecular collision cross sections and vibrational relaxation in carbon dioxide. Proc. Phys. Soc., 84, 877 - 888.
- Mayer, C.H., T.P. McCullough and R.M. Sloanaker, 1958: Observations of Mars and Juniter at a wavelength of 3.15 cm. Astrophys. J., 127, 11 - 16.
- Mayer, C.H., 1961: Radio emission of the moon and planets. The Solar System, III (Planets and Satellites), ed. by G.P. Kuiper and B.M. Middlehurst. University of Chicago Press, 442 - 472.
- McClatchey, R.A., 1966: The effect of vibrational relaxation on atmospheric heating in the 4.3 micron CO₂ band. Ph.D. Thesis, Dept. of Meteorology, UCLA.
- McElroy, M.B., J. L'Ecuyer and J.W. Chamberlain, 1965: Structure of the Martian upper atmosphere. Astrophys. J., 141, 1523 - 1535.
- McElroy, M.B., 1967: The upper atmosphere of Mars. Astrophys. J., 150, 1125 - 1138.
- Mintz, Y., 1961: The general circulation of planetary atmospheres. The Atmospheres of Mars and Venus, ed. by W.W. Kellogg and C. Sagan. National Academy of Sciences - National Research Council, Washington, D.C., 107 - 146.
- Mitchell, A.C.G., and M.W. Zemansky, 1934: Resonance Radiation and Excited Atoms. Cambridge University Press, 338 pp.
- Nicolet, M., 1960: Effets de l'ultraviolet lointain solaire sur l'atmosphère de la terre et des autres planètes. Mem.Soc. Roy. Sci. Liege, 5, 319 - 368.
- O'Gallagher, J.J., and J.A. Simpson, 1965: Mariner IV measurements near Mars: Initial results, Search for trapped electrons and a magnetic moment at Mars by Mariner IV. Science, 149, 1233 - 1239.
- Ohring, G., 1963: A theoretical estimate of the average vertical distribution of temperature in the Martian atmosphere. Icarus, 1, 328 - 333.

- Pettit, E., and S.B. Nicholson, 1924: Measurements of the radiation from the planet Mars. Popular Astronomy, 32, 601 - 608.
- Flass, G.N., and D.I. Fivel, 1953: Influence of Doppler effect and damping on line-absorption coefficient and atmospheric radiative transfer. Astrophys. J., 117, 225 - 233.
- Flass, G.N., 1958: Models for spectral band absorption. J. Opt. Soc. Amer., 48, 690 - 703.
- Flass, G.N., 1960: Useful representations for measurements of spectral band absorption. J. Opt. Soc. Amer., 50, 868 - 875.
- Prabhakara, C., and J.S. Hogan, 1965: Ozone and carbon dioxide heating in the Martian atmosphere, J. Atmos. Sci., 22, 97 - 109.
- Prabhakara, C., and J.S. Hogan, 1966: Equilibrium temperature structure in the mesosphere and lower thermosphere. New York University, Dept. of Meteorology and Oceanography, Geophysical Sciences Laboratory Report No. TR-66-1, NASA Grant NSG-499.
- Rasool, S.I., 1963: Structure of planetary atmospheres. AIAA J., 1, 6 - 19.
- Richardson, R.S., 1957: Preliminary report on observations of Mars made at Mount Wilson in 1956. Publications of the Astronomical Society of the Pacific, 69, 23 - 30.
- Rishbeth, H., and D.W. Barron, 1960: Equilibrium electron distribution in ionospheric F₂ layer. J. Atmos. Terr. Phys., 18, 234 - 252.
- Sinton, W.M., and J. Strong, 1960: Radiometric observations of Mars. Astrophys. J., 131, 459 - 469.
- Sinton, W.M., 1961: An upper limit to the concentration of CO₂ and N₂O in the Martian atmosphere. Publications of the Astronomical Society of the Pacific, 73, 125 - 128.
- Sinton, W.M., 1963: Recent infrared spectra of Mars and Venus. J. Quant. Spectrosc. Rad. Trans., 3, 551 - 558.

- Smith, E.J., L. Davis, Jr., P.J. Coleman, Jr., and D.E. Jones, 1965: Mariner IV measurements near Mars: Initial results, Magnetic field measurements near Mars. Science, 149, 1241 - 1242.
- Spitzer, L., 1952: The terrestrial atmosphere above 300 km. The Atmospheres of the Earth and Planets, 2nd Ed., ed. by G.P. Kuiper. University of Chicago Press, 211 - 247.
- Stewart, R.W., 1967: Temperature and composition of the Martian atmosphere. Ph.D. Thesis. Columbia University.
- Stull, V.R., P.J. Wyatt, and G.N. Plass, 1963: The infrared absorption of carbon dioxide. Infrared transmission studies, III. Report Contract SSD-TDR-62-127, Space Systems Division, Air Force Systems Command, Los Angeles, California.
- Sytinskaya, N.N., 1962: Sur l'application de la photometrie dans les recherches de la nature de Mars. Mem. Soc. Roy. Sci. Liege, 5, 394 - 401.
- Van Allen, J.A., L.A. Frank, S.M. Krimigis and H.K. Pills, 1965: Mariner IV measurements near Mars: Initial results, Absence of Martian radiation belts and implications thereof. Science, 149, 1228 - 1233.
- Van der Held, E.F.M., 1931: Intensität und natürliche Breite von Spektrallinien. Z. Phys., 70, 508 - 515.
- Vigroux, E., 1952: Contributions to the experimental study of the absorption of ozone. Ann. Phys., 8, 709 - 762.
- Walshaw, C.D., and C.D. Rodgers, 1963: The effect of the Curtis-Godson approximation on the accuracy of radiative heating-rate calculations. Quart. J. Roy. Meteorol. Soc., 89, 122 - 130.
- Watanabe, K., 1958: Ultraviolet absorption processes in the upper atmosphere. Advances in Geophysics, 5. Academic Press, New York, 153 - 221.
- Weller, C.S., and M.A. Biondi, 1967: Measurements of dissociative recombination of CO_2^+ ions with electrons. Phys. Rev. Letters, 19, 59 - 61.

Wyatt, F.J., V.R. Stull and G.N. Plass, 1962: Quasi-random model of band absorption. J. Opt. Soc. Amer., 52, 1209 - 1217.

Yamamoto, G., and T. Sasamori, 1958: Calculations of the absorption of the 15 μ carbon dioxide band. Science Reports, Tohoku University, 5th Series (Geophysics), 10, 37 - 57.

Yonezawa, T., 1965: Theory of formation of the ionosphere. Space Science Reviews, 5, 3 - 56.

Young, C., 1964: A study of the influence of carbon dioxide on infrared radiative transfer in the stratosphere and mesosphere. Tech. Rept. NSF Grant No. G-19131, CRA Project 04682, University of Michigan, Ann Arbor, Michigan.